

Dissertation zur Erlangung des Doktorgrades
der Fakultät für Chemie und Pharmazie
der Ludwig-Maximilians-Universität München

Characterization of the Glia in the Adult
Drosophila Central Nervous System



Malte Christoph Kremer

aus Herrenberg, Baden-Württemberg, Deutschland

2013

Erklärung

Diese Dissertation wurde im Sinne von §7 der Promotionsordnung vom 28. November 2011 von Frau Prof. Dr. Ulrike Gaul der Fakultät für Chemie und Pharmazie am Genzentrum München der Ludwigs-Maximilians-Universität München betreut.

Eidesstattliche Versicherung

Diese Dissertation wurde eigenständig und ohne unerlaubte Hilfe erarbeitet.

München, den 29.07.2013

.....

(Unterschrift des Autors)

Dissertation eingereicht am: 07.08.2013

Erstgutachterin: Prof. Dr. Ulrike Gaul

Zweitgutachter: Prof. Dr. Thomas Misgeld

Tag der mündlichen Prüfung: 17.09.2013

Im Rahmen einer Kooperation mit der Gruppe von Dr. Gerald Rubin und eines Besucherstipendiums wurde ein Teil der experimentellen Arbeit am Forschungscampus *Janelia Farm* (Ashburn, Virginia, USA) des Howard-Hughes-Medical-Institute (HHMI, USA) durchgeführt.

Diese Arbeit wurde im Rahmen des Graduierten-Programms der Max-Planck-Gesellschaft ('International-Max-Planck-Research-School for Molecular and Cellular Life Sciences (IMPRS-LS)') abgeschlossen.

1 Acknowledgement

First and foremost, I would like to thank my supervisor Ulrike Gaul, for support and guidance throughout this project, the persistence to look at the finest details of glial anatomy and the opportunity and support to conduct some of the experiments at the Janelia Farm Research Campus. I am particularly indebted to Gerry Rubin, who hosted my project there. I have fond memories of the exciting atmosphere in his lab and his passion for all aspects of science. I also would like to thank my thesis advisory committee members, Hiromu Tanimoto and Thomas Misgeld, for their enthusiasm and encouragement.

All members of the Gaul and Rubin lab have been greatly supportive in every possible situation, thank you guys. Most of this work would not have been possible without the following people I want to acknowledge: Arnim Jenett for help with the Annotation of Gal4 lines, Christophe Jung for the Definiens analysis and 3D reconstructions, Sara Batelli for sharing the adult homeostasis project, Barret Pfeiffer for uncounted tools, Aljoscha Nern for the key to access the multicolored fly brain, Fulvia Ferrazzi and Ulrich Unnerstall for help with the statistical analysis, Myrto Deligiannaki for access to the developmental RNAi screen data, Florian Simon for help with the characterization of Gal4 lines during development, Sara Batelli and Abbie Casper for critically reading this manuscript and Chris Zugates, Todd Lavery as well as the JFRC FlyFacility and FlyCorp for technical assistance. I also want to thank the VDRC, DGRC and the Developmental Studies Hybridoma Bank as well as the fly community for kindly providing many tools and reagents.

Aside scientific contributions, I want to thank a few people for their moral support, talent to ignite enthusiasm and simply for being good friends. Mountaineers on both sides of the Atlantic Ocean, you opened up a whole new world for me. Sara and Arnim, I could not have thought of better companions to run a project together. Mark and Sofia, as much as I enjoyed your inquisitive minds, I miss them since you guys have left. Deniz for those Gin Tonics on the pavewalk and my dear friends for constantly enabling me to catch a glimpse outside of the box.

ACKNOWLEDGEMENT

My biggest thank you goes to my family. Without your understanding, support, encouragement and trust, this would be a different one.

2 Abstract

The role of glia in nervous system function is still poorly understood. Particularly the functions of glial cells in the homeostasis of the adult central nervous system are largely unknown. Among vertebrates and invertebrates, the major glial subgroups are comparable, making *Drosophila melanogaster* a suitable model system to study glial functions during development and adulthood.

An important prerequisite for functional studies is a comprehensive descriptive analysis of the existing cell types, their development, location, number, and morphology. In the first and second part of this thesis, I report a detailed characterization of glia in the adult central nervous system of *Drosophila*. This was achieved by screening through the Janelia Farm's large collection of synthetic Gal4 lines to identify some 650 glial-specific Gal4 driver lines. Having determined the glial identity of the expressing drivers, I characterized their location, morphology, region-restricted specializations and their relationship to other glia and to neurons.

In the third part of this thesis, I present our preliminary efforts to investigate glial subtype-specific, adult-specific functional differences. In particular, we looked at the glial role in detoxification, nutrients supply, ion and neurotransmitter homeostasis and circadian rhythm. In these experiments we confirmed previously described adult-specific glial function and discovered new glial-subtype-specific functions.

Overall, this thesis provides the first comprehensive description of all the different glia found in the adult fly brain. Additionally, it introduces a system to achieve adult-specific gene knockdown based on which interesting aspects of adult-specific glial cell function in the central nervous system of *Drosophila* could be demonstrated in a preliminary RNAi screen.

3 Zusammenfassung

Das Nervensystem höhere Organismen besteht im Wesentlichen aus Nerven- und Gliazellen. Während die Anatomie und Funktion von Nervenzellen immer besser bekannt und verstanden ist, sind Gliazellen nach wie vor weitestgehend unerforscht. Insbesondere die Funktionen der Gliazellen in erwachsenen Organismen sind dabei weitestgehend unbekannt.

Gliazellen, die in der Fruchtfliege *Drosophila melanogaster* klassifiziert wurden, ähneln den wichtigsten Gliasubtypen in Vertebraten. Es wird daher angenommen, dass sich die Fruchtfliege hervorragend als Modelorganismus eignet um die Funktion von Gliazellen während der Entwicklung und in ausgewachsenen Organismen zu untersuchen. Eine wesentliche Voraussetzung für sämtliche funktionelle Studien bleibt dabei die detaillierte und vollständige anatomische Beschreibung der existierenden Gliazelltypen.

Diese Arbeit präsentiert eine detaillierte anatomische Beschreibung von Gliazellen im erwachsenen zentralen Nervensystem der Fruchtfliege. Basierend auf der Identifizierung von rund 650 synthetischen Fliegenlinien mit Glia-spezifischen Gal4 Expressionsmustern, wurden die verschiedenen Gliazelltypen in *Drosophila* charakterisiert. Besonderes Augenmerk galt dabei der Lokalisierung von verschiedenen Gliazelltypen innerhalb des Nervensystems, der Morphologie von einzelnen Zellen und den anatomischen Beziehungen verschiedener Gliasubtypen untereinander und zu Neuronen.

Zu guter Letzt nutzten wir diese neuen genetischen Werkzeuge um erste Experimente durchzuführen, mit denen wir die Funktion von Gliazellen im adulten Nervensystem testeten.

1	ACKNOWLEDGEMENT	3
2	ABSTRACT	5
3	ZUSAMMENFASSUNG	7
4	INTRODUCTION	11
4.1	THE HISTORY OF NEURONS AND GLIA	11
4.2	GLIAL CELL FUNCTION DURING DEVELOPMENT AND IN THE ADULT	13
4.3	<i>DROSOPHILA</i> AS A MODEL SYSTEM	15
4.3.1	COMPARISON OF GLIA IN VERTEBRATES AND INVERTEBRATES	15
4.3.2	SPATIALLY CONTROLLED EXPRESSION SYSTEMS IN <i>DROSOPHILA</i>	16
4.3.3	INDUCIBLE (TEMPORALLY CONTROLLED) EXPRESSION SYSTEMS	19
4.3.4	SINGLE AND MULTICOLOR FLUORESCENT REPORTERS	22
4.3.5	RNA INTERFERENCE-MEDIATED GENE KNOCKDOWN	24
4.4	DEVELOPMENT AND MORPHOGENESIS OF GLIA IN <i>DROSOPHILA</i>	26
4.4.1	MORPHOGENESIS AND PROLIFERATION OF GLIA IN THE EMBRYO AND IN THE ADULT	26
4.4.2	GLIAL POPULATIONS IN EMBRYONIC AND ADULT CNS	30
4.4.3	DEVELOPMENT, MORPHOLOGY AND FUNCTION OF GLIA IN THE VISUAL SYSTEM	34
4.4.4	GLIA IN THE OLFACTORY SYSTEM OF <i>DROSOPHILA</i>	38
4.5	RATIONALE	41
4.5.1	IDENTIFICATION AND CATEGORIZATION OF GENERIC GLIAL SUBTYPE GAL4 DRIVERS	41
4.5.2	CHARACTERIZATION OF THE GLIA IN THE ADULT FLY BRAIN	41
4.5.3	INVESTIGATION OF HOMEOSTATIC FUNCTION OF ADULT GLIAL SUBTYPES	42
5	ANNOTATION OF GLIAL DRIVERS	43
5.1	GLIAL GAL4 DRIVER LINES WITHIN THE JANELIA FARM COLLECTION	44
5.2	GENERIC GLIAL GAL4 'REFERENCE' DRIVER LINES	49
5.3	IDENTIFICATION OF REGION SPECIFIC DRIVER LINES	51
5.4	SUMMARY	54
5.5	DISCUSSION	55
6	MORPHOLOGIC CHARACTERIZATION OF GLIA IN THE ADULT FLY BRAIN	59
6.1	CHARACTERIZATION OF GENERIC GLIAL SUBTYPES	59
6.1.1	GLIAL CELL COUNTS	59
6.1.2	PERINEURIAL GLIA	62
6.1.3	SUBPERINEURIAL GLIA	64
6.1.4	CORTEX GLIA	66
6.1.5	ASTROCYTE-LIKE GLIA	69
6.1.6	ENSHEATHING GLIA	74
6.1.7	SUMMARY	79
6.2	CHARACTERIZATION OF GLIA IN THE VISUAL SYSTEM	81
6.2.1	GLIA IN THE LAMINA	81
6.2.2	GLIA IN THE MEDULLA	91
6.2.3	THE CHIASM GLIA	95
6.2.4	GLIA IN THE LOBULA COMPLEX	99
6.2.5	SUMMARY	102
6.3	CHARACTERIZATION OF GLIA IN THE OLFACTORY SYSTEM	103
6.3.1	GLIA IN THE ANTENNAL LOBE	103
6.3.2	GLIA IN THE MUSHROOM BODY	107
6.3.3	NEURON-GLIA INTERACTIONS ALONG OLFACTORY PROJECTION NEURONS	109
6.3.4	SUMMARY	113
6.4	DISCUSSION	114
7	FUNCTIONAL CHARACTERIZATION OF GENERIC GLIA IN THE ADULT CNS	123

7.1	A PRELIMINARY ADULT-SPECIFIC RNAI SCREEN	123
7.1.1	GENETIC CONSTRUCTS AND SCREENING STRATEGY	124
7.1.2	RNAI LINES	125
7.1.3	CONTROLS AND STATISTICAL ANALYSIS	126
7.1.4	THE GLIAL SUBTYPE-SPECIFIC ROLE IN CNS HOMEOSTASIS	128
7.2	SUMMARY	133
7.3	DISCUSSION	134
8	OUTLOOK	137
9	MATERIAL AND METHODS	139
9.1	FLY STRAINS AND GENETICS	139
9.2	IMMUNOHISTOCHEMISTRY	142
9.2.1	EMBRYOS	142
9.2.2	ADULT AND LARVAL CNS	143
9.3	CONFOCAL MICROSCOPY AND IMAGE ANALYSIS	145
10	SUMMARY OF FIGURES AND TABLES	151
10.1	FIGURES	151
10.2	TABLES	152
10.3	SUPPLEMENTAL FIGURES	152
11	ABBREVIATIONS	153
12	SUPPLEMENTAL MATERIAL	155
12.1	EXPRESSION PATTERN CHARACTERISTICS OF GENERIC GLIAL DRIVERS DURING DEVELOPMENT	155
12.1.1	ONSET AND GLIAL IDENTITY OF GAL4 'REFERENCE' DRIVER EXPRESSION	155
12.1.2	CHARACTERIZATION OF GENERIC DRIVER EXPRESSION IN THIRD INSTAR LARVAE	158
12.1.3	SUMMARY	160
12.2	OPTIMIZATION OF HEAT SHOCK CONDITIONS FOR ADULT SPECIFIC FLPOUTS	161
13	LITERATURE	163

4 Introduction

“What is the function of glial cells in the neural centers? The answer is still not known and the problem is even more serious because it may remain unsolved for many years to come until physiologists find direct methods to attack it. Neuronal function was clarified by the phenomena of conduction ... But how can the physiology of glial cells be clarified if they cannot be manipulated?”

Santiago Ramon y Cajal (1911)

4.1 The history of neurons and glia

More than one and a half centuries ago, Purkinje presented the first drawings of cells in the central nervous system (CNS) at a symposium in Prague (1837). Shortly after, in 1841, Rudolf Virchow described the cellular components that he found between the nerves as neuro-glia (γλοιός, greek, glue)('nerve-cement')(Virchow, 1858). A few decades later, Ramon y Cajal employed the staining technique developed by Camillo Golgi to provide the first exciting insights into the architecture and major cellular components of the brain (later summarized in (Ramon y Cajal, 1909)). From his drawings, Waldeyer (1891) postulated the term neurons – ultimately resulting in Cajals 'neuron doctrine' which describes the nervous system as being build of discrete units called neurons. In the following decades, major progress was made in understanding the fine structure of the neuron-to-neuron connection, the signaling between neurons, the molecular mechanisms of proper synapse function, reorganization and development of synaptic connections as well as complex networks (for review: (Bear et al., 2006; Kandel et al., 2000)).

The 'cement' (Virchow) was long overlooked since it was believed to simply provide the glue to keep the neurons together; the material to build the static framework for the nervous system. Nonetheless, it was observed that during evolution from lower to higher organisms, the relative fraction of glia in the brain

increased dramatically, from around 10% in the fruit fly to 90% in humans (Pfrieger and Barres, 1995). Moreover, people were excited to observe that glial cell number can reach up to 95% in certain brain regions; particularly, because those locally restricted increased glial cell numbers could be linked with an extraordinary capacity and creativity of the brain. Taking as an example Albert Einstein, when his brain was studied after his death, it was found that glial cell numbers were increased in his association cortex, more specifically in his left inferior, a region involved in the processing of information of other brain regions (Fields, 2009). Additionally, studies in rodents demonstrated that the glia-to-neuron ratio increases in animals raised in an enriched or stimulating environment (Diamond et al., 1964; Szeligo and Leblond, 1977). Together, these findings point to a role for glia in higher brain functions, which are likely to be more elaborate than the one described until then. During the last two decades, studies demonstrated that glia are involved in major functions of nervous system development, homeostasis and are important for proper signaling of the neurons with which they associate. Thus, glia gained more and more attention and today, it is a widely accepted notion that only when we understand the intriguing interaction of neurons and glia, may we finally understand the brain in its full complexity.

4.2 Glial cell function during development and in the adult

In vertebrates, glia are crucial for the migration of neurons from proliferation centers into designated areas of the brain (Hatten, 1999), they contribute to synapse formation and function (Allen and Barres, 2009; Eroglu and Barres, 2010; Pfrieger, 2010) and are essential for the maintenance of the nervous system (Fields and Stevens-Graham, 2002; Schrier and Thompson, 1974; Varon and Bunge, 1978). Recently, it could be demonstrated that improper glial function may ultimately contribute to degenerative events in the nervous system (Coleman and Freeman, 2010; Fellner et al., 2011).

In *Drosophila*, glia in the embryonic and larval nervous system have been investigated in detail anatomically (Granderath and Klambt, 1999; Ito et al., 1995; Klambt and Goodman, 1991; Klambt et al., 1996), which laid the ground for many subsequent functional studies demonstrating a role for glia in (i) axon guidance and fasciculation (Edenfeld et al., 2005), (ii) the phagocytosis of apoptotic neurons (Kurant et al., 2008), and (iii) the formation and maintenance of the blood-brain barrier (Schwabe et al., 2005; Stork et al., 2008).

For the much more complex adult nervous system, despite recent efforts (Awasaki et al., 2008; Edwards and Meinertzhagen, 2010; Edwards et al., 2012), a comprehensive description of the glia is still lacking. Nonetheless, selective studies point towards an important role of glia in the adult nervous system (reviewed in: (Edwards and Meinertzhagen, 2010)). Some of these studies have shown that glia in the adult CNS are involved in (i) neurotransmitter homeostasis (Rival et al., 2004); (ii) the blood brain barrier (Carlson et al., 2000; Edwards et al., 1993; Schwabe et al., 2005; Stork et al., 2008); (iii) Circadian rhythm (Ng et al., 2011; Suh and Jackson, 2007); (vi) in the homeostasis of neuronal metabolism (Xiong and Montell, 1995; Zhu et al., 2008) and (v) Phagocytosis (Doherty et al., 2009; MacDonald et al., 2006).

Despite those selective studies, the specific functions of glia in adult CNS homeostasis have not been systematically characterized. To investigate the distinct

functions of glial cells in general and more specifically the role of glia during development and early adulthood, the Gaul lab has conducted two screens.

In the first screen, cells in the *Drosophila* late-stage embryo were dissociated, fluorescently labeled glial cells separated from the other cell types using fluorescently-activated cell sorting (FACS) and expression profiles generated. This transcriptome profiling revealed that particular groups of genes are specifically expressed or up-regulated in glia. For example, it was demonstrated before that glial cells are important for homeostasis of neurotransmitters particularly of glutamate (Rival et al., 2004) and ions (Auld et al., 1995; Xiong and Montell, 1993). Glial transcription profiling complemented these data by showing that the glutamate transporter *excitatory amino acid transporter* (EAAT), *acetylcholinesterase* (ACE) and the potassium channel *Kir* are upregulated in glial cells. Furthermore, the expression pattern analysis revealed that many genes involved in energy metabolism and detoxification of reactive oxygen species (ROS) are upregulated (similar studies from vertebrates are available (Cahoy et al., 2008)).

In the second screen, done by Myrto Deligiannaki, ~75% of the fly genes were knocked down independently from early embryonal stages onwards throughout the life cycle using the pan-glial driver *repo-Gal4* and transgenic RNAi. Subsequently, the effect of the knockdown was evaluated by means of survival in the adult after 10 days compared to control flies. The results of this screen are unpublished. However, some of the results, together with data from the first screen, suggest a mechanism in which important homeostatic functions are outsourced to glia and consequently have dramatic effects onto the health of the organism when disrupted. This has principally been demonstrated for neurotransmitter and ionic homeostasis. For example, the glial-specific inactivation of the glutamate transporter EAAT1 by RNA-interference (RNAi) results in behavioral deficits, shortened lifespan and marked degeneration of brain neuropiles (Rival et al., 2004). Overall, these observations strongly support the idea that glia serve important functions in the adult CNS with more interactions yet to be found.

4.3 *Drosophila* as a model system

Drosophila offers a plethora of genetic tools, fast generation time, advanced imaging techniques and simple behavioral read-outs. It has even been used as a model system to mimic potential neurodegenerative defects (reviewed in (Bilen and Bonini, 2005)). Despite the previously mentioned changes in glia-to-neuron ratio (also see section: 4.1), the morphologies of glial cell subtypes in vertebrates and invertebrates remained comparably similar (Freeman and Doherty, 2006), thus making *Drosophila* an ideal model system to study glial cell functions.

4.3.1 Comparison of glia in Vertebrates and Invertebrates

In vertebrates, glia are divided into the following major subclasses: astrocytes, oligodendrocytes, microglia and Schwann cells. Astrocytes are subdivided into protoplasmic and fibrous cells, according to their association with grey matter or white matter, respectively. Oligodendrocytes myelinate axon tracts and ascertain saltatory conduction along the nerves. Microglia are found throughout the CNS and provide immune system function to the CNS. Schwann cells are the oligodendrocytes of the peripheral nervous system; they can be myelinating and non-myelinating (for review: (Kettenmann, 1999)).

In invertebrates such as *Drosophila*, glial cells are associated with all major parts of the CNS (Figure 1). In general, the *Drosophila* CNS is subdivided into brain and ventral nerve chord (VNC). The brain is subdivided into optic lobes including Lamina, Medulla and Lobula complex and central brain (CB). Neuronal cell bodies are all located in the cortex regions, whereas the neuropiles are constituted of neurites and synapses. As in vertebrates, subclasses of glia associate with neuronal tracts and processes (ensheathing glia), with synapses (astrocyte-like glia) and neuronal cell bodies (cortex glia) (Awasaki et al., 2008; Doherty et al., 2009; Edwards and Meinertzhagen, 2010; Hartenstein, 2011). In addition, so-called surface glia provide a continuous sheath around the entire *Drosophila* CNS, thus providing a blood-brain-barrier which is comparable to the vertebrate ependymal cell built counterpart (Stork et al., 2008). In *Drosophila*, a subtype such as the vertebrate microglia has not been found; microglial functions may thus be

subdivided among the existing glial subtypes (Awasaki et al., 2008; Edwards and Meinertzhagen, 2010; Freeman and Doherty, 2006), presumably between ensheathing and cortex glia (Doherty et al., 2009).

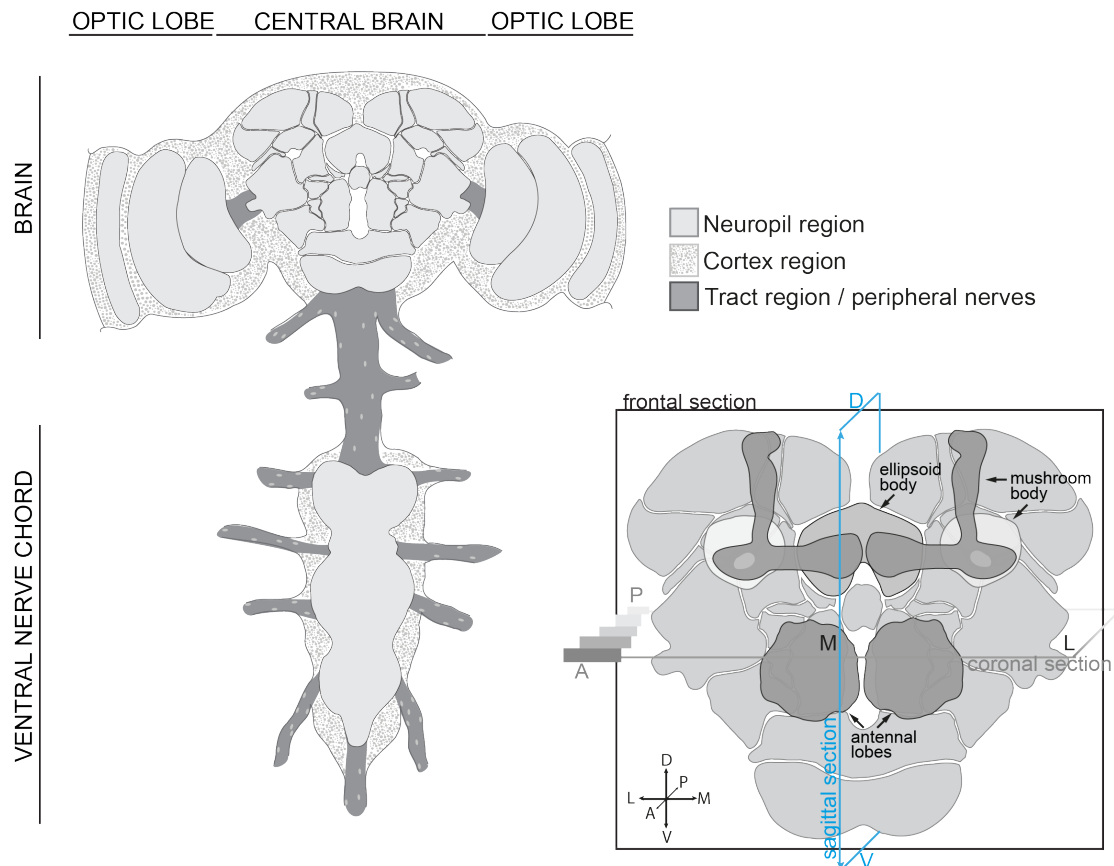


Figure 1: Anatomy of the central nervous system (CNS) of adult *Drosophila*.

The nervous system of *Drosophila* is subdivided into the ventral nerve chord (VNC) and the brain, which can be further subdivided into central brain and optic lobes, which consist of Lamina, Medulla and Lobula complex. In *Drosophila*, the cortical regions housing the neuronal cell bodies, and the neuropile regions, housing the majority of neuronal tracts and the synaptic regions, are well separated. In the left lower corner, the central brain is illustrated; brain regions, which are of major importance in this work, are highlighted as well as the most commonly used orientations of confocal sections (frontal, sagittal, coronal view). A coordinate system is shown; in all the following illustrations in this thesis it will be used to demonstrate the orientation of the pictures.

4.3.2 Spatially controlled expression systems in *Drosophila*

When studying the function of a specific gene (or endogenous transgene) it is useful to control its expression both spatially and temporally. *Drosophila* offers genetic tools for both manipulations. The very simplest way to express an

exogenous transgene is to place its expression *directly* under the control of a transcriptional enhancer/activator sequence. These are genetic sequences with the capacity to initiate transcription of the downstream-encoded genes and can express in a tissue-specific fashion. These expression systems, however, have limitations i.e. when it comes to the expression of genetic constructs that cause developmental lethality (and thus no progeny). Therefore, binary transcription systems have been developed which allow for separation of the transcription activation element and the transgene (effector). Most importantly, those heterologous expression systems do not interact with the *Drosophila* genome.

Binary transcription systems

The most commonly used binary expression system is the Gal4-system (Brand and Perrimon, 1993; Fischer et al., 1988) which has been optimized over the past years (Pfeiffer et al., 2008; Pfeiffer et al., 2010). In addition, two more binary transcription systems have been developed – the LexA/LexAop (Lai and Lee, 2006) and the QS/QUAS-system (Potter et al., 2010) – which do not interfere with the Gal4 system. They can thus be used as orthogonal systems to the Gal4 system to label two different populations of cells.

Binary transcription systems function as follows (Figure 2): An exogenous transcriptional activator (i.e. Gal4/LexA/QS) is expressed under the control of a tissue-specific enhancer (promoter). The target transgene (i.e. a RNAi, green fluorescent protein (GFP), other reporters) is encoded under the control of the exogenous upstream activating sequence (UAS, LexAop, QUAS) in all cells. Upon combination of the transcription activation element and the transgene (effector) (i.e. by crossing two fly strains each carrying one of the two elements) the expression of the transgene is initiated in those cells in which the transcriptional activator is transcribed.

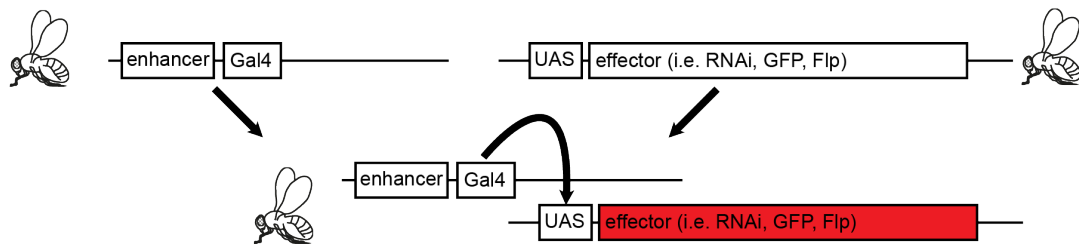


Figure 2: Binary transcription systems in *Drosophila*.

Binary transcription systems are employed in *Drosophila* to express a genetic construct of interest in a tissue-specific manner. Tissue specificity is achieved by using different enhancer sequences. In the example represented schematically here, Gal4 acts as the transcriptional activator; the effectors driven under control of the UAS could be for example an RNAi line or a GFP.

Tissue-specific drivers

In the past, tissue-specific expression was achieved by randomly placing a transcriptional activator (i.e. Gal4) under the control of regulatory elements of different genes via P-element mediated insertion into generic gene loci (O'Kane and Gehring, 1987). Those insertions were random, thus, Gal4 enhancer regions had to be mapped after the flies had been generated. Additionally, those insertions occasionally interfered with the original function of the gene. Later, this system was upgraded by inserting not only the transcriptional activator but also a specific transcriptional enhancer sequence that would define the localization of the expression of the genetic construct. However, also in this case, insertions into the genome were random and interfered with their genomic environment. Most considerably, random insertions had the disadvantage that genomic environments of different insertions were not comparable, thus making predictions about the proper functioning of inserted constructs unreliable. Nowadays, genetic constructs are inserted into the *Drosophila* genome using site-directed transgenesis via the Φ C31-integration system. In this system, specific transcriptional enhancer sequences plus transcriptional activator are inserted into a defined locus in the genome (Pfeiffer et al., 2008). In contrast to random insertions, site-directed transgenesis has multiple advantages. First, the exact location of the integration is known; for most of them, it has been evaluated, which ones are most suited for different genetic constructs (i.e. some insertion sites are better suited for

transcriptional activators). Second, side effects due to different insertion sites (and consequently different genomic environments) can be excluded when comparing the effects of different genetic constructs and third, the integration efficiency is higher compared to random insertions.

This system was employed to create a large library of enhancer lines with expression in the nervous system (Jenett et al., 2012; Pfeiffer et al., 2008), referred to as the Janelia Farm Research Center (JFRC) Gal4 collection subsequently. For this library, regulatory regions of genes that have been largely involved in nervous system function (neurotransmitters, transporters, key components of synapses) were chopped into overlapping 3kb long genetic sequence fragments. Placed upstream of a synthetic core promoter, those sequences drive the tissue-specific expression of transcriptional activator Gal4s. In order to analyze the expression pattern of each fragment, generated Gal4s were employed to drive expression of GFP-tagged membrane proteins (UAS-mCD8-GFP) and subsequently analyzed using confocal microscopy. The 'imagery' is accessible at the Janelia Farm Research Campus and online for detailed analysis. The driver lines identified with glial expression (also see 5.1-3) were characterized with respect to their expression during development (Supplemental figure 1, Supplemental figure 2) and – in detail – characterized in the adult (also see 6).

4.3.3 *Inducible (temporally controlled) expression systems*

Simple binary systems have the limitation that they cannot be temporally controlled. To overcome these disadvantages, different systems have been developed:

The *temporal and regional gene expression targeting* (TARGET) system (McGuire et al., 2003) takes advantage of the heat-dependent binding of the Gal80 repressor to Gal4. While under normal experimental conditions (temperature below 25°C), Gal80 inhibits Gal4 activity, increased temperatures (32°C) leads to the unbinding of Gal80-protein and activation of the Gal4. The major advantage of this system lies in the reversibility of the activation of Gal4. As soon as the temperature drops, Gal4 is inhibited again. However, this temperature dependence is also a major

drawback because temperature induces stress and can ultimately lead to altered behaviors or death if maintain over longer periods.

Drug inducible transcriptional activators (Gal4s/QS) are another possibility to achieve temporal control of binary transcription systems. In that case, the Gal4 is manipulated by combining the transcriptional activator with hormonal receptors (Han et al., 2000; Osterwalder et al., 2001). Only upon feeding an exogenous hormone that can bind to the hormonal receptor, Gal4 activation can be initiated. While in this system disadvantages caused by increased temperature are bypassed, the feeding of hormones and the control of Gal4 activation is imprecise and slow.

The Flp/FRT system combined with heat-shock inducible recombinases (Golic and Lindquist, 1989) offers the possibility to irreversibly activate transgene expression upon short heat shock pulses of up to 2 hours. Among the system introduced here, inducible recombinases provide the most powerful tool because they require only short induction times for the recombinase to get activated (an example experiment scheme is provided in Figure 3) (for review: (del Valle Rodriguez et al., 2012; Venken et al., 2011)). For this reason this system was employed throughout this thesis and will thus be introduced in more detail here.

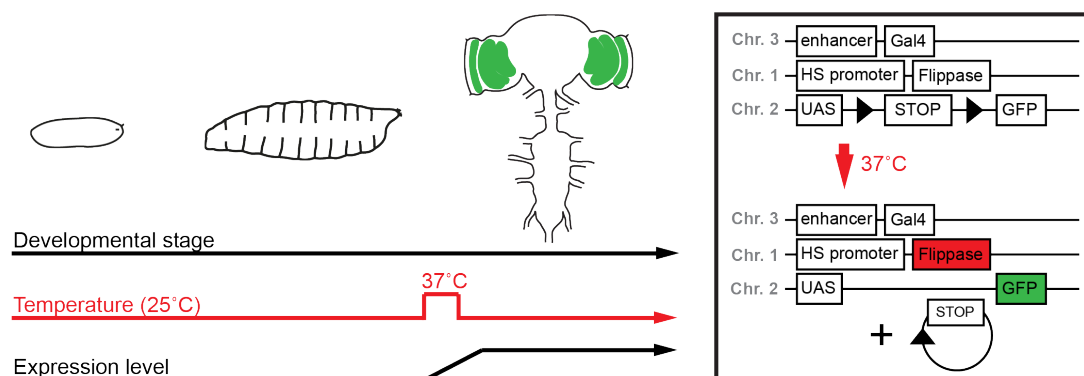


Figure 3: Schematic illustration of the heat-shock FlpOut-System.

Spatial and temporal control are added to the binary transcription system by introducing a heat-shock inducible Flp-Recombinase (Flippase). Upon temperature increase, the HS promoter gets activated, the Flippase expressed, the STOP codon, which is flanked by two FRT sites gets excised and the UAS-GFP will be expressed under the control of the tissue-specific Gal4. Note that the temperature only needs to be increased for a short period of time (approximately 1h) and that after the heat-shock; the expression of GFP is irreversibly started.

The Flp/FRT system

The Flp/FRT system principally functions as follows: A transcriptional 'STOP cassette' consisting of the transcriptional termination signals of the proteins *hsp70* and *SV40* (Nern et al., 2011; Struhl and Basler, 1993) flanked by two *flippase recognition target* (FRT) sites is inserted upstream of the genetic constructs whose expression needs to be temporally controlled. The 'STOP cassette' can be irreversibly excised (cleaved out of the sequence) by specific proteins called recombinases (Flippases). Flippases themselves can be placed under heat shock control via the heat-shock protein *Hsp70* promoter. Additionally, to avoid increased temperatures, hormone-inducible recombinases have been generated by combining hormone receptors and the recombinases (Barret Pfeiffer, Robin Harris, Jim Truman, unpublished).

In practice, the degree of activation of the transgenes, which are under Flp/FRT control, depends on the time period in which the flippase is active. Since we employed heat-shock inducible flippase in our experiments, the degree of expression depended on the length of the heat-shock induction. Without heat-shock, transcription of the glial-specific enhancers is terminated at the transcription termination signal and the reporter is not transcribed. Upon heat-shock, the *hsp70* promoter gets activated and drives the expression of the flippase. It then irreversibly excises the transcription termination signal at the two FRT sites, subsequently leading to transcription of the reporter and expression. Upon different length of heat-shock (HS), the constructs were either flipped out (and activated) in very few (short HS) or many cells (long HS), respectively.

In the experiments presented in this thesis, the Flp/FRT system in combination with heat-shock inducible Recombinases was employed to obtain flippable UAS-constructs for the purpose of stochastic cell labeling (further explained in 4.3.4) and flippable Gal4 constructs for adult specific expression of different UAS-constructs (further explained in 7.1.1) .

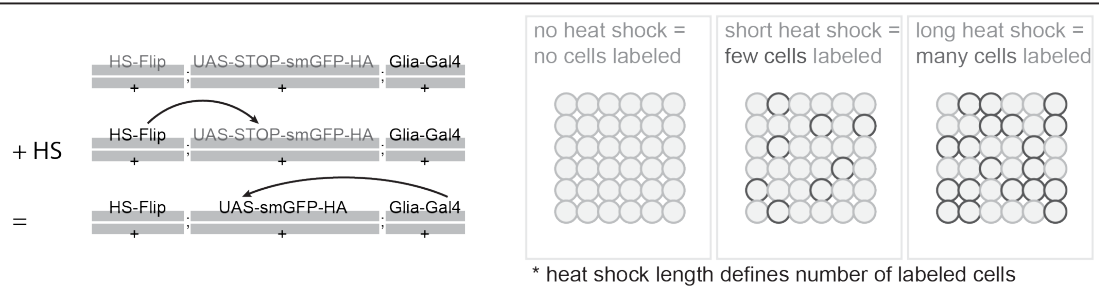
4.3.4 *Single and multicolor fluorescent reporters*

In order to analyze the morphology of cells or cellular compartments or the expression pattern of a protein, genetically encoded fluorescent probes can be employed. By placing the fluorescent protein under the control of an endogenous gene, the expression pattern of this protein can be investigated (Chalfie et al., 1994; Ormo et al., 1996; Tsien, 1998). By combining upstream activating sequences (UAS) of binary expression systems with fluorescent probes, cells are made visible particularly in tissue, which is targeted by specific drivers (also see 4.3.2). Within a targeted cell, fluorescent reporter gene expression can be directed to particular domains like the cytoplasm, the nucleus or different membrane domains (Rizzuto et al., 1996). In recent years, those constructs have been further modified. The original GFP derived from the *Aequorea victoria* was optimized in order to achieve brighter fluorescent signals; fluorescent probes to cover almost all spectra of fluorescent light were developed and targeting sequences were optimized (summarized in (Pfeiffer et al., 2010)). However, due to the weak expression of some drivers, low levels of fluorescently tagged protein and / or specificity of some stainings, it was desired to obtain fluorescent markers with even higher resolution. To this end, proteins were no longer labeled with a genetically encoded fluorescent protein itself but with an exogenous unique sequence (tag) to which specific antibodies can bind.

Different tags are available that can be targeted with differently colored fluorescent antibodies. Since the tag is characterized by a sequence, which is not found anywhere else in the fly proteome, those stainings are highly specific. In order to label the membrane of cells with these new methods, a green fluorescent protein (GFP), whose fluorescent activity was deleted via point mutations, was added 4 tags of the same kind around the circular structure of the GFP (due to its structure this construct was called 'spaghetti monster', smGFP), combined with a myristoylation (myr) sequence to target the membrane and placed under UAS control (Aljoscha Nern, Barret Pfeiffer, unpublished). The high number of tags, highly specific and sensitive fluorescent antibodies together with the optimized membrane targeting sequence enables for characterization of cellular

morphologies at unprecedented resolution. In the double labeling experiments presented here, smGFP tagged with the V5 or HA epitope tag were targeted to the membrane via the myr-targeting sequence under the control of either UAS or LexAop, respectively. For stochastic labelings, HA, Flag and V5 tags were employed (also see below)(Figure 4).

A Single-color flip outs



B Multi-color flip outs

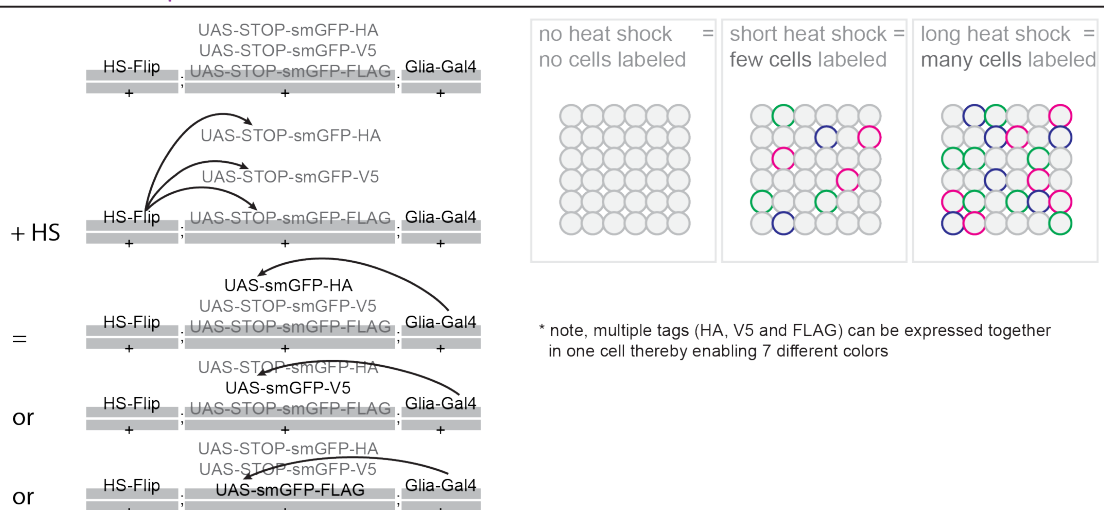


Figure 4: Single and multicolor stochastic labelings of cells within a tissue of interest.

A Single color stochastic labeling of cells of a tissue that can be targeted with a specific Gal4 driver. **B** Multicolor stochastic labeling of cells of a tissue that can be targeted with a specific Gal4 driver. Note that in both cases, the heat shock time defines the amount of cells in which the tags under UAS control are expressed. Further note that the expression is random and cannot be targeted to a specific subpopulation of cells driven by the Gal4 driver. In B, within one cell, different tags can be expressed enabling the antibody staining of different (neighboring) cells with different colors. However, occasionally, more than one tag is expressed in one cell leading to the overlap of the two colors during antibody staining. Overall, 7 colors / color combinations are possible. Illustration adopted from A. Nern and B. Pfeiffer.

Stochastic labelings of single cells can be achieved as follows: The above-mentioned reporters under UAS control are added the transcriptional ‘stop

cassette' (also see 4.3.3) between the reporter and the UAS. Upon combination with tissue specific Gal4s and the flippase, the expression of the reporter can then be controlled by temperature. The underlying general principle is that during heat shock, activation of the Flippase is not immediately achieved in all cells. The frequency with which cells of a given population are labeled depends on the length of the heat shock.

To stochastically label multiple cells with different colors, we employed the same system as described for single color labelings of single cells. However, in contrast, three flippable reporter each carrying a different tag were introduced (Figure 4B). Since under experimental conditions, reporters with different tags rarely get activated in the same cell, a stochastic multicolor labeling of cells is achieved.

During my thesis I used double labelings to investigate the morphology of single glial populations, their interaction with other glial subtypes and the interaction with neuronal cells. Multicolor-flip-outs were used to characterize single cell morphologies, the interaction of single cells with neighboring cells and overall variation in cell shape within glial subpopulations.

4.3.5 *RNA interference-mediated gene knockdown*

Tissue specific gene knockdown in *Drosophila* can be achieved by expressing RNA-interference (RNAi) constructs under the control of an upstream activating sequence (UAS). RNAi is the process in which double stranded RNAs (dsRNAs) after processing, target messenger RNAs (mRNA) with an identical sequence (Fire et al., 1998); leading to the degradation of the mRNA and gene silencing (Fire et al., 1998). Today, genome-wide screens have become possible due to the establishment of libraries of UAS-RNAi lines, in which the UAS-RNAi constructs are inserted into the genome either randomly (Dietzl et al., 2007) or via site-specific integration (Ni et al., 2009; Ni et al., 2008). Two libraries using site-specific integration that are most commonly used are the 'KK-lines' generated at the Vienna *Drosophila* Research Center (VDRC) and the 'trip-lines' generated by Harvard *Drosophila* RNAi Screening Center (DRSC) and the Perrimon lab. While the former uses long fragments of dsRNA (300-400bp) as targeting elements, the

latter library generates only very short sequence siRNAs (short interfering RNAs)(~20bp). Both libraries constitute a powerful resource for the *Drosophila* research community. Because of the broader coverage of the 'kk-lines' (for 88% of all genes in the *Drosophila* genome, RNAi constructs are available) and to compare results with results from previous screens done in the lab (also see 4.3.1), we employed the VDRC 'kk-lines' in all our experiments.

Because of this plethora of genetic tools, we believe *Drosophila* to be an ideal model system to investigate the development and function of glia, the morphology of different glial subtypes at different developmental stages and their role in the homeostasis of the adult nervous system.

4.4 Development and morphogenesis of glia in *Drosophila*

Invertebrates undergo specific phases during development, which are accompanied by stage-specific gene expression, morphologic alterations and changes in hormone levels that trigger further stage-specific developmental events (Bate and Arias, 1993). *Drosophila* are holometabolous insects, which means they undergo complete metamorphosis. At 25°C, *Drosophila* embryos develop into larvae after 24 hours, pass larval stages one to three (wandering larvae) after 5 days before they enter metamorphosis, become pupae and finally hatch from the pupal case as adult flies after approximately 10 days.

4.4.1 Morphogenesis and proliferation of glia in the embryo and in the adult

In the developing *Drosophila* embryo, neurons and glia are generated from precursors that produce only neurons (Neuroblasts), neurons and glia (Neuroglioblasts) or only glia (Glioblasts). They predominantly derive from the neuroectoderm. In the developing embryonic nerve chord, most neurons and glia cells in the CNS originate from 29 neuroblasts and one glioblast (per hemisegment), which are arranged at the perimeter of each neuromere. In the developing embryonic and larval brain, glial progenitors are also found in designated clusters in the early stages of development of these areas (for review: Hartenstein 2011) from where they migrate during further development.

In the embryo, glial fate is determined by *glia cell missing* (*GCM*) and its homolog *GCM2*. *GCM/GCM2* are transcription factors, whose loss-of-function prevents the generation of glia of neuroglioblasts, and promotes differentiation of early neurons into glial cells when overexpressed (Hosoya et al., 1995; Jones et al., 1995; Kammerer and Giangrande, 2001). Notably, *GCM2* expression is slightly delayed and moderately weaker than the expression of *GCM*; a mutation of *GCM2* alone does not induce lethality (Alfonso and Jones, 2002; Kammerer and Giangrande, 2001). *GCM/GCM2* target glial-specific transcription factors such as *reverse polarity* (*REPO*) that underlies glial cell differentiation (Halter et al., 1995), and other transcription factors preventing neuronal differentiation such as *tramtrack*

(*TTK*) (Xiong and Montell, 1993). *GCM* and *REPO* are the most commonly used markers to label glia; *GCM* is expressed only in differentiating glial precursors while *REPO* labels all glial cells throughout development, but whose expression starts slightly later than *GCM* (Campbell et al., 1994; Halter et al., 1995; Hosoya et al., 1995; Vincent et al., 1996). Interestingly, it was found that the generation of midline glia is not accompanied by *GCM* or *REPO* in any developmental stage (Jacobs, 2000). In the adult, glial cell fate determination is more complicated and has not been entirely resolved. While *GCM*, but not *GCM2*, has been shown to be required for the generation of glia in restricted clusters of the developing medulla and ventral nerve chord (Soustelle and Giangrande, 2007) and presumably also in the central complex (Izergina et al., 2009), both *GCM* and *GCM2* are required for proper differentiation of glia AND neurons in the developing lamina (Chotard et al., 2005). Thus, the generation of glial does not solely depend on *GCM/GCM2*-induced mechanisms but likely underlies more complicated molecular mechanisms yet to be discovered.

During development, glial cell numbers increases dramatically from a few hundred cells in the late stage embryos to approximately 15.000 cells in the adult (our counts, also see 6.1.1). This massive proliferation is achieved by two principal mechanisms: First, differentiated glial cells divide themselves (Colonques et al., 2007; Pereanu et al., 2005); second, throughout metamorphosis, neuroglioblasts produce glial progeny (Izergina et al., 2009). Noteworthy, different types of neuroblasts (neuroglioblasts) exists that can either directly produce ganglion mother cells (GMCs) (classical Type I neuroblast) (Udolph et al., 2001) or undergo a series of symmetric cell divisions before generating GMCs (Type II neuroblast, transient amplifying neuroblast (TAN)) (Bello et al., 2008; Boone and Doe, 2008). In comparison to Type I neuroblasts, TANs have the potential to produce much larger lineages, thus contributing to the massive generation of glia that accompanies larval and pupal development (reviewed in: (Hartenstein, 2011)).

The fates of different glial subtypes have been mapped in much detail (Schmid et al., 1999; Schmidt et al., 1997) and are reviewed elsewhere (Hartenstein, 2011).

They are not majorly important for the understanding of the scientific questions asked in this thesis. In contrast, the proliferation pattern of the different generic glial subtypes are noteworthy because they explain the different glial subtype counts we obtained for the adult *Drosophila* CNS (also see 6.1.1). To determine when precursors of different glial subtypes are proliferating, Awasaki and colleagues used the MARCM technique. They found that precursors of perineurial glia begin to proliferate during early larval stages, and form the outermost glial sheath, on top of subperineurial glia (Awasaki et al., 2008). Subperineurial glia proliferate to form a contiguous, insulating sheath in the late embryonic nerve chord (Awasaki et al., 2008) (Figure 5). Interestingly, while perineurial glia continue proliferation throughout larval stages, subperineurial glia do not proliferate significantly anymore. They predominantly accompany the growth of the organism by massive growth of the single cells (Unhavaithaya and Orr-Weaver, 2012). With respect to cortex glia, Awasaki et al. suggested that the majority of cells are generated before larval hatching. Most neuropile glia derive from different precursors in specific proliferation centers from which they begin to migrate at the onset of metamorphosis (Awasaki et al., 2008). They divide symmetrically, but with irregular timing, presumably upon locally restricted cues (Awasaki et al., 2008). Additionally, some cells, predominantly in the central complex of the adult brain, also arise from neuro-glioblasts, which become activated larvally (Izergina et al., 2009). Final mitosis to derive postmitotic astrocyte-like glia and ensheathing glia, respectively, remains synchronized around puparium formation thus suggesting a stage-specific initiation mechanism (Awasaki et al., 2008). The different glial subtypes thus show very distinct and different proliferation pattern, which are further expressed in the glial counts.

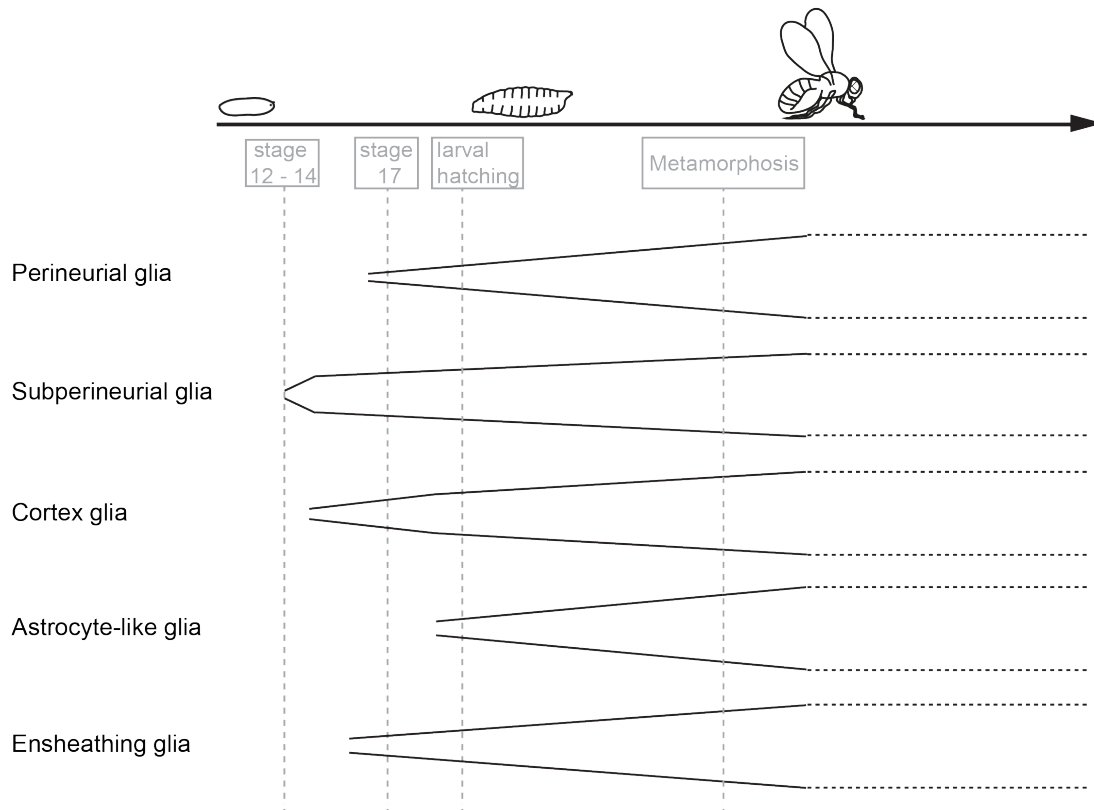


Figure 5: Development and proliferation of the different generic glial subtypes.

Subperineurial glia are generated first around stage 12, followed by cortex glia and ensheathing glia. Perineurial glia as well as astrocyte-like glia begin to proliferate in late embryonic stages. While subperineurial glia and cortex glia massively proliferate in embryonic stages and accompany organismal growth by growth of the single cells, perineurial, ensheathing and astrocyte-like glia undergo cycles of mitotic cell division also during larval stages and pupariation.

4.4.2 Glial populations in embryonic and adult CNS

In the *Drosophila* embryo, glial cells can be subdivided broadly into surface-associated, cell body, neuropile (Ito et al., 1995) and midline glia (Jacobs, 2000) (also see Figure 6).

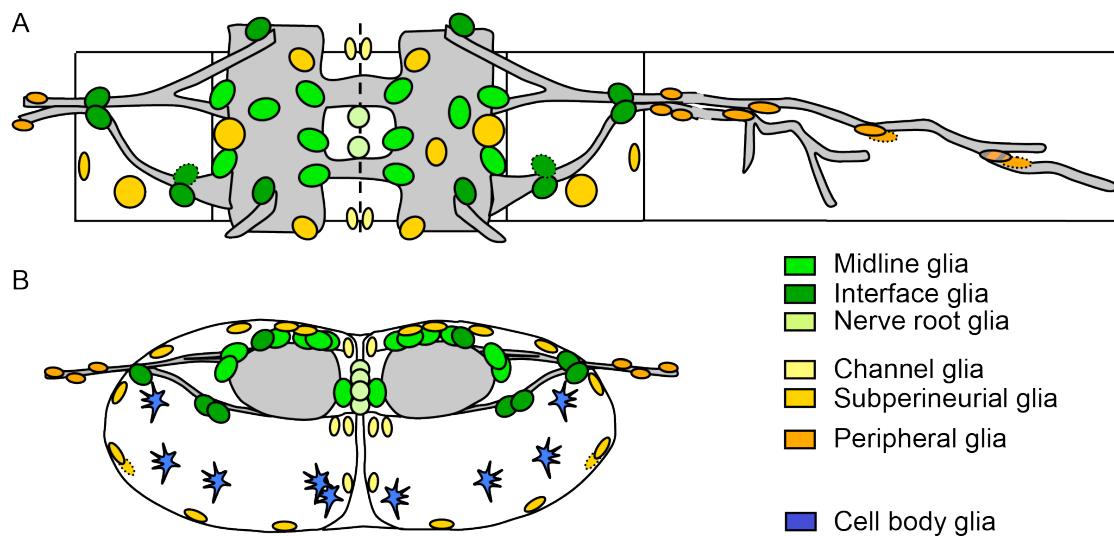


Figure 6: Glial populations found in the embryonic ventral nerve chord.

Schematic of the localization of different glial subtypes in the embryo. A Dorsal view. B Crosssection. Neuropile glia (shades of green) contain Midline glia, Interface glia and Nerve root glia. Surface glia (shades of yellow) contain subperineurial glia and its subtype channel glia. Cell body glia (cbg) populate the ventral cortical region. Schematic prepared by Tina Schwabe and Ulrich Unnerstall, AG Gaul, based on data presented in (Ito et al., 1995; Schmid et al., 1999; Schmidt et al., 1997).

In studies performed by Ito, Klaemdt and others (summarized in: (Ito et al., 1995)), position, numbers and morphology of these glial subtypes have been characterized. In these studies, cell-type specific Gal4 drivers were identified using the enhancer trap technique (also see 4.3.2) and employed to label glial populations at defined stages of development. In addition, glial fates were determined predominantly using Dil labelings to trace the precise origin of each cell type (Schmid et al., 1999; Schmidt et al., 1997). In his study, Ito and colleagues demonstrated that at stage 16, the glial population within a hemisegment is constituted of 24-28 subperineurial glia, 6-8 cell body glia and 25-30 neuropile glia (Ito et al., 1995) (also see Figure 6). At this stage, subperineurial glial cells (including 6-8 channel glia per hemisegment) already

form a contiguous sheath around the entire embryonic CNS (Schwabe et al., 2005; Stork et al., 2008). Cell body glia populate the lateral and ventral embryonic VNC cortex region (Ito et al., 1995). Neuropile glia can be further subdivided into nerve root glia (intersegmental and segmental) (8-10 cells per hemisegment), interface glia (14-16 per hemisegment) (a subset of them is called longitudinal glia) and midline glia (3-4 cells per hemisegment).

In the adult *Drosophila* CNS, the three major embryonic subclasses suggested by Ito and colleagues (surface-associated, cortex-associated and neuropile-associated) are maintained. They are further subdivided into perineurial glia and subperineurial glia (surface-associated), cortex glia (cortex-associated) and astrocyte-like glia and ensheathing glia (neuropile-associated). Thus, the glial subtypes assigned to these categories vary slightly compared to the embryo.

In the embryo, the segregation of neuronal cell bodies into cortical regions and synapses into neuropile regions is not fully completed; there has only been one glial subtype characterized in this overlapping region, which is called cell body glia (cbg). In contrast, in the adult, different glial populations are found within the cortex (cortex glia) and in proximity to synapses within the neuropiles (astrocyte-like glia). We have indication to believe that the embryonic cell body glia correspond with the larval and adult cortex glia and that larval and adult astrocyte-like glia are only beginning to be generated in late embryonic and early larval stages (also see 12.1). Consequently, in the embryo, also the term neuropile-associated glia does not fully correspond with the adult counterpart. In the embryo, most if not all neuropile-associated glia associate with neuronal processes while cell body glia (cortex-associated) maintain proximity to the synaptic regions. In the adult, neuropile-associated glia also contain synapse-associated astrocyte-like glia. Ensheathing glia in the adult, which have been implicated with associating with neuronal tracts and processes, have not been further subcategorized yet.

With the exception of the glia in the visual system, which are generated later in development, glial subtypes found in the larvae largely correspond with the subtypes characterized in the adult.

Multiple studies have begun to characterize the glia in the adult *Drosophila* CNS. The shape of the two surface glial subtypes has been shown to differ in that perineurial glia form small elongated cells that are oriented dorso-ventrally whereas subperineurial glia have a sheet (or square)-like shape with no particular orientation (Awasaki et al., 2008); the shape of the perineurial cell bodies was described as small and elongated, whereas the subperineurial glial cell bodies are rather large and roundish (Awasaki et al., 2008; Hartenstein, 2011). It was demonstrated that cortex glia encapsulate neuronal cell bodies (Awasaki et al., 2008; Hoyle, 1986; Pereanu et al., 2005) and enwrap newly formed secondary neuron processes which need to cross the cortex region in order to enter the neuropiles (Pereanu et al., 2005; Spindler and Hartenstein, 2010). Except for the satellite glia in the optic lobes, for which two distinct subtypes have been described (Edwards et al., 2012; Tix et al., 1997) (Figure 20), region-specific morphologies have not been found. It was thus suggested, that there is only a single type of central brain cortex glia cells that together constitute the cortex glia mesh (Awasaki et al., 2008). Neuropile-associated glia in the adult populate the neuropile regions and the tract regions between the neuropile regions. Astrocyte-like glia predominantly are found in the neuropile regions themselves and thus likely associate with synapses, whereas ensheathing glia form a dense lamellar sheet around each neuropile region (Awasaki et al., 2008). However, due to the position of some glia between the neuropiles / around tracts or brain compartments such as the neck connective and the position of their nuclei, it was suggested, there may be a third glial subgroup called tract glia which enclose bundles of neurons within the main tracts of the brain (Edwards and Meinertzhagen, 2010). Astrocyte-like glia morphologies were described as dendritic with tiny spines (Awasaki et al., 2008), branched and filliform (Hartenstein, 2011) and elaborate with extensive processes in the neuropile (Edwards and Meinertzhagen, 2010). In contrast, ensheathing glia morphologies

were characterized as fibrous, lamellar ensheathing the neuropile and subcompartments (Awasaki et al., 2008), flattened cells that do not penetrate deep into the neuropile (Hartenstein, 2011) and lamellar with processes which extend along the outer neuropile surface to isolate neurons (Edwards and Meinertzhagen, 2010).

4.4.3 Development, morphology and function of glia in the visual system

The Optic lobes (OL) are constituted of the optic lobe ganglia Lamina, Medulla and Lobula complex, which is further subdivided into Lobula and Lobula plate. The neuropiles of the optic lobes make up a large portion of the fly brain; they have been studied in great detail functionally and anatomically (for review: (Borst, 2009; Borst et al., 2010; Fischbach and Hiesinger, 2008; Meinertzhagen, 1993; Morante and Desplan, 2008)) (Figure 7).

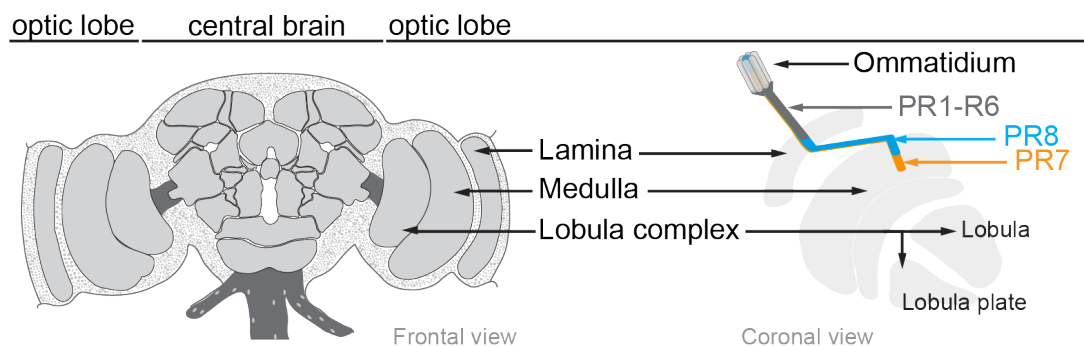


Figure 7: Schematic illustration of the anatomy of the optic lobes of adult *Drosophila*.

In the left schematic, a frontal view of the central brain is presented. The major optic lobe neuropile regions are highlighted. The right schematic represents shows a coronal view of the same neuropile regions. The incoming photoreceptor axons R1-R8 are illustrated in grey (R1-R6) and light blue (R8) / orange (R7).

The Lamina

The Lamina, the first optic ganglion, is the first relay station where the R1-R6 photoreceptors terminate in a retinotopic fashion (Photoreceptors R7 and R8 terminate in the Medulla). Here they convey sensory information important for motion and spatial vision. Incoming photoreceptor axon bundles enter the Lamina and connect to interneuronal units called cartridges, where complex synaptic contacts are made between photoreceptors and Lamina monopolar neurons L1-L5. Laminar monopolar cell axons project through the outer chiasm into defined layers of the distal Medulla (for review: (Clandinin and Zipursky, 2002; Sanes and Zipursky, 2010; Ting and Lee, 2007)).

Glial cells play an important role for proper visual system development (for review: (Chotard and Salecker, 2007)). Six types of glial cells were identified and

characterized in the Lamina that are organized in distinct layers: fenestrated, pseudocartridge, distal and proximal satellite, epithelial and marginal glia ((Edwards et al., 2012; Tix et al., 1997), for review: (Edwards and Meinertzhagen, 2010)). Pseudo-cartridge and distal satellite glia and, presumably, also fenestrated glia, derive from precursors in the optic stalk (Edwards et al., 2012). The optic stalk is a peripheral region from which newly generated cells migrate towards higher brain centers like the Lamina. In contrast, proximal satellite, epithelial and marginal glia derive from glial precursor cells (GPC) inside the larval brain (Dearborn and Kunes, 2004; Winberg et al., 1992).

The functions of the Lamina glial cells have been studied in some detail. Fenestrated and pseudo-cartridge glia provide glial insulation at the optic lobe-retina interface and thus are believed to be specialized types of perineurial and subperineurial glia, respectively (Edwards et al., 2012; Shaw and Varney, 1999). Satellite glia – the Lamina counterpart of cortex glia – enclose neuronal cell bodies and presumably provide homeostatic function (Freeman and Doherty, 2006). Epithelial glia are important for neurotransmitter recycling (Borycz et al., 2002; Richardt et al., 2003; Richardt et al., 2002; Ziegler et al., 2012). Marginal glia may be involved in photoreceptor targeting in the larvae (Poeck et al., 2001) (reviewed in: (Chotard and Salecker, 2007)). Furthermore it was suggested based on driver line expression, anatomy and morphologic specialization, that epithelial glia may be a specialized form of astrocyte-like glia whereas marginal glia correspond to ensheathing glia (Edwards and Meinertzhagen, 2010).

The Medulla

The Medulla, the second optic ganglion, is the second major relay station for processing visual information. In contrast to the Lamina, the Medulla receives its visual input predominantly from photoreceptors R7 and R8; R7 and R8 are responsible for color vision. In addition, L1-L5 Lamina interneurons project in a retinotopic fashion onto the Medulla, which comprises ten distinct layers of synaptic connections that are organized into retinotopic columns (Fischbach, 1989). R8 terminates in layer M3, R7 terminates in layer M6 (Fischbach, 1989).

Visual information is predominantly relayed to the Lobula via transMedulla cells (Tm) and Lobula complex via transMedulla Y cells (TmY) ((Fischbach, 1989), for review: (Fischbach and Hiesinger, 2008; Meinertzhagen, 1993)). Developmentally, the Medulla is formed by two distinct primordia; the distal Medulla together with the Lamina derives from the outer optic anlage, whereas the proximal Medulla as well as the Lobula complex derives from the inner optic anlage (Hofbauer, 1990; Meinertzhagen, 1993). During late third instar and pupariation, the Medulla rotates 90° in the horizontal plane until it reaches a position, perpendicular (or lateral) to the Lobula complex neuropiles (Meinertzhagen, 1993). As a consequence, formerly subdivided proximal and distal Medulla fuse at the serpentine layer. To which extent glial cells developmentally mediate these processes has not been resolved. Nonetheless, it was shown (1) that glia provide boundaries between developing neuropile areas in the larval brain (Younossi-Hartenstein et al., 2003) and (2) that glial boundaries likely are crucial for the precise migration of neurons and thus, proper neuropile development, as shown in the optic lobes (Tayler et al., 2004). The major generic glial populations – surface, cortex and neuropile glia - were also found in the optic lobe regions Medulla and Lobula complex (Edwards et al., 2012; Tix et al., 1997). However, in contrast to the Lamina, cortex glia were not further subdivided in the central brain, Medulla and Lobula complex (Awasaki et al., 2008).

Neuropile glia in the Medulla have only recently been described in more detail: astrocyte-like glia were found to enter the Medulla (1) from the distal Medulla surface (“distal Medulla astrocyte-like glia”) (Edwards et al., 2012), (2) from the serpentine layer (“serpentine glia”) (Edwards et al., 2012) and (3) from the proximal surface (“chandelier glia”) ((Edwards et al., 2012), in honeybee: (Cantera and Trujillo-Cenoz, 1996; Sánchez, 1935)). The existence of an ensheathing glia subtype and its morphology has been proposed (Chotard and Salecker, 2007; Edwards et al., 2012; Gao et al., 2008; Hadjieconomou et al., 2011). A potential role for Medulla astrocyte-like glia in neurotransmitter recycling was suggested based on its expression of *ebony*, a β -alanyl biogenic amine (Richardt et al., 2002;

Wagner et al., 2007), but Medulla ensheathing glia function has not been further investigated.

The chiasms

The optic lobes comprise two major neuropile-connecting axon tracts, the outer chiasm, which connects Lamina and Medulla, and the inner chiasm, which connects Medulla and Lobula complex (Fig. 11A.1- 2). The neuronal tracts that cross these regions in the adult fly are well described (Fischbach, 1989), so is the development of these neurons (Clandinin and Zipursky, 2002; Fischbach and Hiesinger, 2008; Meinertzhagen, 1993; Ting and Lee, 2007). Two types of chiasm glia have been characterized: giant outer chiasm glia and inner chiasm glia (Edwards et al., 2012; Tix et al., 1997). Developmentally, chiasm glia arise from dorsal and ventral glial precursor cell areas (Chotard et al., 2005); in BrdU labeling experiments, it was shown that at least some of the outer chiasm glia are born in second instar larvae (Tix et al., 1997). The time point of their generation coincides with the period in which photoreceptor neurons R8 and R7 begin to project into the Medulla region. This process is accompanied by some glia, which enwrap R8, R7 and target neurons. If those glia were outer chiasm glia was discussed as well as their (and the inner chiasm glia) role in axon guidance (Chotard and Salecker, 2007)). However, due to a lack of specific glial Gal4 drivers, the general glial involvement could never be specifically attributed to single glial subtypes. During pupal formation, the Lamina rotates by 180° with respect to the Medulla neuropile (Braitenberg, 1970; Meinertzhagen, 1993). Most likely, the outer chiasmata glia are also rotated giving them a characteristic crossover morphology. The inner chiasm (xgⁱ) forms during the growth of neurites between the developing optic lobe neuropiles Medulla, Lobula and Lobula plate (Bate and Arias, 1993; Tix et al., 1997) around late mid-larval stage (Tix et al., 1997).

The Lobula complex

The Lobula complex neuropiles Lobula and Lobula plate have not been studied in detail. While the neuronal cell types have been comprehensively investigated with

respect to morphology (Fischbach, 1989; Otsuna and Ito, 2006) and wiring (reviewed in: (Clandinin and Zipursky, 2002), knowledge about the function of the two neuropiles in visual processing is only emerging (Borst, 2009; Borst et al., 2010; Joesch et al., 2010; Yamaguchi et al., 2008). It was shown that the Lobula plate is predominantly involved in motion processing (Borst et al., 2010), whereas the Lobula serves as a relay station where visual cues about color are further processed (Morante and Desplan, 2008). So-called visual projection neurons (VPNs) connect the secondary neuropiles within the optic lobes with the central brain (Hausen et al., 1980; Otsuna and Ito, 2006; Scott et al., 2002), where they converge onto regions in the ventrolateral protocerebrum, posterior lateral protocerebrum and optic tubercle (Otsuna and Ito, 2006). The glia of the Lobula complex have not been described in further detail.

4.4.4 *Glia in the olfactory system of Drosophila*

The *Drosophila* olfactory system consists of four main regions called primary, secondary, and higher olfactory centers. Primary olfactory organs include antennae and maxillary palp, secondary olfactory organs are the antennal lobes and higher olfactory centers can be subdivided into mushroom bodies and the lateral horn. Odors are detected by olfactory receptors (OR) in olfactory receptor neuron (ORN) dendrites in the antennae and maxillary palps (Hallem and Carlson, 2004a). Around 1300 ORNs converge towards 43 distinct glomeruli in the antennal lobe (Laissue et al., 1999; Stocker, 1994). Odorant receptors of one subtype project to one, very rarely onto two distinct glomeruli (Gao et al., 2000). Odor coding in the antennal lobe (AL) appears to include a spatial map of odorant receptor activation (Hallem and Carlson, 2004b), which is achieved by a network of three different classes of neurons, which are olfactory receptor neurons (ORNs,) projection neurons (PNs) and local interneurons (LNs). Antennal lobe and higher brain centers are connected by around 150-200 projection neurons (PNs), which project their dendrites into specific glomeruli of the antennal lobe and send their axons towards mushroom body (MB) and lateral horn (LH) (Ito et al., 1998; Stocker, 1994). Axonal fibers of PNs to both MB and lateral horn go through the antenno-cerebral tract (ACT). Mushroom bodies receive olfactory input from PNs

within a substructure called the calyx. The MB calyx houses the connections between PNs and Kenyon cells (KC) which are the predominant type of neurons in the mushroom bodies. Evidence suggests stereotyped axonal projections of projection neuron boutons in the mushroom body calyx (Jefferis et al., 2007; Tanaka et al., 2004). In total about 1115 projection neuron boutons (Turner et al., 2008) connect with intrinsic mushroom body Kenyon cells in large synaptic complexes called microglomeruli, of which around 1000 can be found in the calyx (Leiss et al., 2009). Kenyon cells can be further subdivided into at least three subsets which are referred to as α/β , α'/β' and γ according to their axonal projection (Crittenden et al., 1998; Strausfeld et al., 2003). Different subsets have been suggested to house different functions during the formation of memories (Dubnau et al., 2001; Krashes et al., 2007; McGuire et al., 2001; Pascual and Preat, 2001; Schwaerzel et al., 2002; Tanaka et al., 2008; Yu et al., 2006; Zars et al., 2000).

The glia in different parts of the olfactory network have been studied in *Drosophila* (antennae (Sen et al., 2005), antennal lobe (Oland et al., 2008), mushroom body (Ito et al., 1997; Ito et al., 1998)) and other insects (honeybee: (Hahnlein and Bicker, 1996), moth: (Oland and Tolbert, 1989)). In the antennae, three population of glial cells – perineural glia, cell body glia and ensheathing glia were characterized using GH146-GFP and Mz317:GFP marker (Sen et al., 2005). While the perineural (presumably an equivalent to perineurial or subperineurial glia) and cell body glia (an equivalent to cortex glia) derive from the sensory lineages in the antennae, the ensheathing glia (which are called GH146-glia in the paper from Sen et al., 2005) appear to derive from the brain (Sen et al., 2005). In the antennal lobe, the secondary olfactory information processing center, cortex glia and ensheathing glia were characterized with respect to their general expression pattern and location inside the neuropile (Doherty et al., 2009; Oland et al., 2008). Cortex glia are found all around the antennal lobe and encapsulate neuronal cell bodies (Oland et al., 2008). The morphologic characteristics of ensheathing ('neuropile') glia were described as (1) forming a sparse mesh like network of processes around the neuropiles; (2) ensheath large dendrites and axon

tracts in the different regions of the AL and (3) to enter the glomeruli neuropiles (Oland et al., 2008). Astrocyte-like glia project a major branch into the neuropile from which small projections ramify and loosely associate with the synapse-rich neuropile regions inside the glomeruli (Doherty et al., 2009).

In the mushroom body, neuropile glia enwrap the entire neuropile; they have processes inside the MB calyx, even though with no obvious spatial relation to the neuronal features of the MB calyx (Leiss et al., 2009), inside the pedunculus and within the lobes (Doherty et al., 2009; Leiss et al., 2009; Sinakevitch et al., 2010). A detailed description of the contribution of astrocyte-like and ensheathing glia, is still lacking.

4.5 Rationale

The nervous system is of major importance for the development and viability of most organisms. It deals with a constant influx of stimuli from the environment and translates them into appropriate responses. Within the central nervous system, different cell-types act together in a well-orchestrated manner to fulfill these tasks. Cell-specific requirements for this balance and what functions these cell types serve has been investigated in some detail for neurons, but much less so for glia.

This project aimed to establish and employ novel tools for glial subtype-specific characterization and manipulations *Drosophila*. In particular, the glial cells of the adult central nervous system were characterized in detail and novel tools to investigate their adult-specific function were introduced and employed in a preliminary functional RNAi screen.

According to the main scientific goals of this project, this thesis was broken down into the following subprojects with their specific objections:

4.5.1 Identification and categorization of generic glial subtype Gal4 drivers

Glial cells in the adult *Drosophila* CNS had been identified previously, however, due to a lack of glial-specific driver lines, this analysis had not been comprehensive. Tissue-specific enhancers and site-directed transgenesis in combination with different, exchangeable yet inducible transcription systems like Gal4/UAS, LexA/LexAop, QS/QUAS, TARGET and HsFlp (also see section: 4.3) are powerful tools that can be used to investigate the specific functions of different cell types throughout development, or only at defined periods. The JFRC Gal4 collection combines all these advantages. Thus, in order to make this system available for the *Drosophila* glia community, specific enhancers, also called drivers, with glial-specific expression patterns should be identified from their collection of Gal4 lines (also see 5).

4.5.2 Characterization of the glia in the adult fly brain

Glial cell morphologies in the adult fly had been investigated previously. However, there is good evidence that those studies have not completely resolved

all the different existing glial subtypes. For this reason, we thoroughly characterized the driver lines we identified within the JFRC collection in adults. To do so, we employed new fluorescent probes developed at Janelia Farm to gain high-fluorescent intensity labeling of cell populations or single-cell labeling with different colors. We characterized all generic glial subtypes with respect to their cell number, single cell anatomy and relation to neighboring cells including other glial subpopulations and neurons. Additionally, we characterized the region-specific morphologies of all generic glial subtypes in the visual system including Lamina, Medulla and Lobula complex and in the olfactory system including antennal lobe and mushroom body. To prove equivalency between region-specific glial subtypes and generic glial subtypes as well as to study the interaction of different glial populations and between glia and neurons, LexAs were generated for around 50 driver lines. The combination of newly generated Gal4s/LexAs with optimized reporter constructs thus allowed for a systematic cell-type specific analysis of glial morphology at a resolution previously unreached (also see 6).

4.5.3 Investigation of homeostatic function of adult glial subtypes

Glia in the developing nervous system had been extensively studied anatomically and functionally. In contrast, the glia in the mature nervous system are far less understood. This is because of a lack of suitable tools to target the different glial subtypes and to restrict the genetic manipulations to the adult organism. In collaboration with Sara Batelli, AG Gaul, we developed tools to investigate the functions of different glial subtypes specifically in adult flies. Based on observations made previously in the Gaul lab, we assumed glia would be involved in the homeostasis of the mature CNS. To elucidate this hypothesis, and to test those newly developed tools, we performed a preliminary adult-specific RNAi screen. We specifically compared the functions of different glial subtypes with respect to their involvement in ion and neurotransmitter homeostasis, nutrient supply, circadian rhythm and detoxification (also see 7).

5 Annotation of glial drivers

We screened the entire Janelia Farm Gal4 collection for drivers with glial expression in the adult brain. Our goal was two-fold – to identify and annotate all lines with significant glial expression and to find, within this subset, lines that are well suited for both descriptive and functional analysis. We examined the existing image collection consisting of maximum density projections and confocal stacks of brains from 6,650 Gal4 lines driving the membrane-tagged reporter UAS-mCD8-GFP.

The strategy for the annotation was the following: Based on previously described glial morphologies (Awasaki et al., 2008), conspicuous location and non-neuronal pattern, we identified lines with (potential) glial expression (Figure 8). Subsequently, driver lines were categorized into three different ‘quality’ lists A, B and C (Figure 10). The parameters that defined the quality of a given driver line were (1) specificity, (2) mosaicism and (3) background expression. Specificity is a measure for the ability of a given driver to label all or a defined subpopulation of cells of a glial subtype. Mosaicism describes the situation in which not all cells of a particular glial subtype are labeled but only a random, stochastic portion of them (mosaic pattern). Background expression means that non-glial tissue like neurons and trachea are also labeled by the glial driver.

A-drivers contain driver lines with predominant and complete, non-mosaic glial expression. They have little or no neuronal background. Also included on this list are drivers with unique glial pattern. In addition, we added to the A-list driver lines that label clean subsets of generic glial subtypes in particular brain regions or entirely label multiple glial populations. B-drivers contain driver lines with predominant glial expression but high neuronal background or glial pattern, which are already represented by another driver line with less background. C-drivers contain driver lines with partial glial expression but high neuronal background. B and C-driver lines may display useful glial patterns but are either severely mosaic or have strong neuronal expression and thus cannot be used for

functional studies without applying elaborate intersectional strategies (del Valle Rodriguez et al., 2012; Venken et al., 2011).

Drivers with unknown pattern were tested for nuclearly expressed GFP in glia using double-labelings with glial-specific *REPO* antibodies.

5.1 Glial Gal4 driver lines within the Janelia Farm Collection

Among the ~6.650 imaged Gal4 driver lines within the Janelia Farm Collection, we identified 669 with expression in glia (Figure 8A). All glial driver lines were categorized into the 5 major generic glial subtypes – perineurial glia, subperineurial glia, cortex glia, ensheathing glia and astrocyte-like glia (Figure 8). Driver lines with expression in multiple subtypes as well as driver lines with expression in trachea were categorized separately.

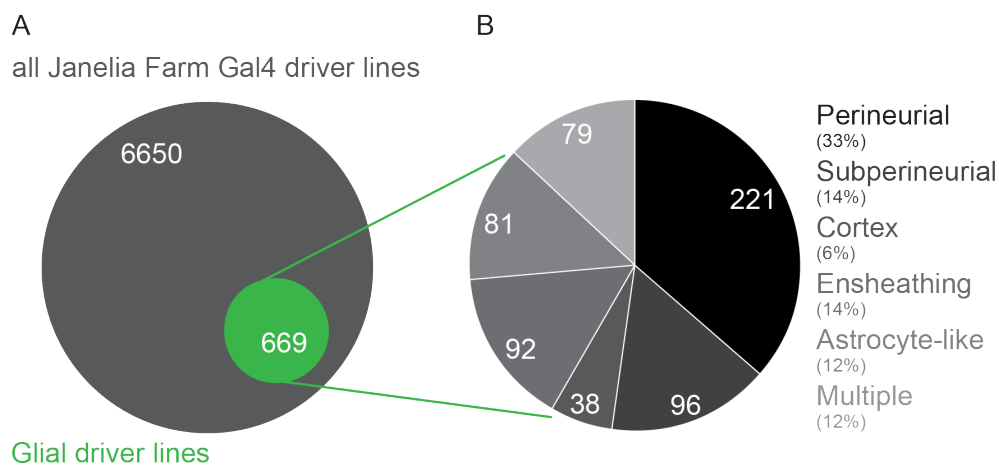


Figure 8: Glia in the Janelia Farm Gal4 collection.

A Ten percent of all the driver lines within the JFRC Gal4 Collection contain glial expression. **B** They can be subdivided into perineurial, subperineurial, cortex, astrocyte-like and ensheathing glia. The number of driver lines specifically expressed in either of these lines is indicated with numbers in the pie chart. Additionally, driver lines, which express in more than one subtype, are registered as *Multiple*.

Among all generic glial subtypes, perineurial glia drivers are found most frequently (33%), followed by subperineurial glia (14%), ensheathing glia (14%)

and astrocyte-like glia (12%). Cortex glial drivers are most rare (6%). Expression in more than one generic subtype is observed in 12 percent of all drivers (Figure 8B).

Further subdivision placed them into categories according to lines, which express in all glia of one or more generic glial subtypes, *All*, or only in a region-restricted manner, *region-specific*. Additionally, we annotated if the driver lines shows *mosaic* or *non-mosaic* expression (Figure 9).

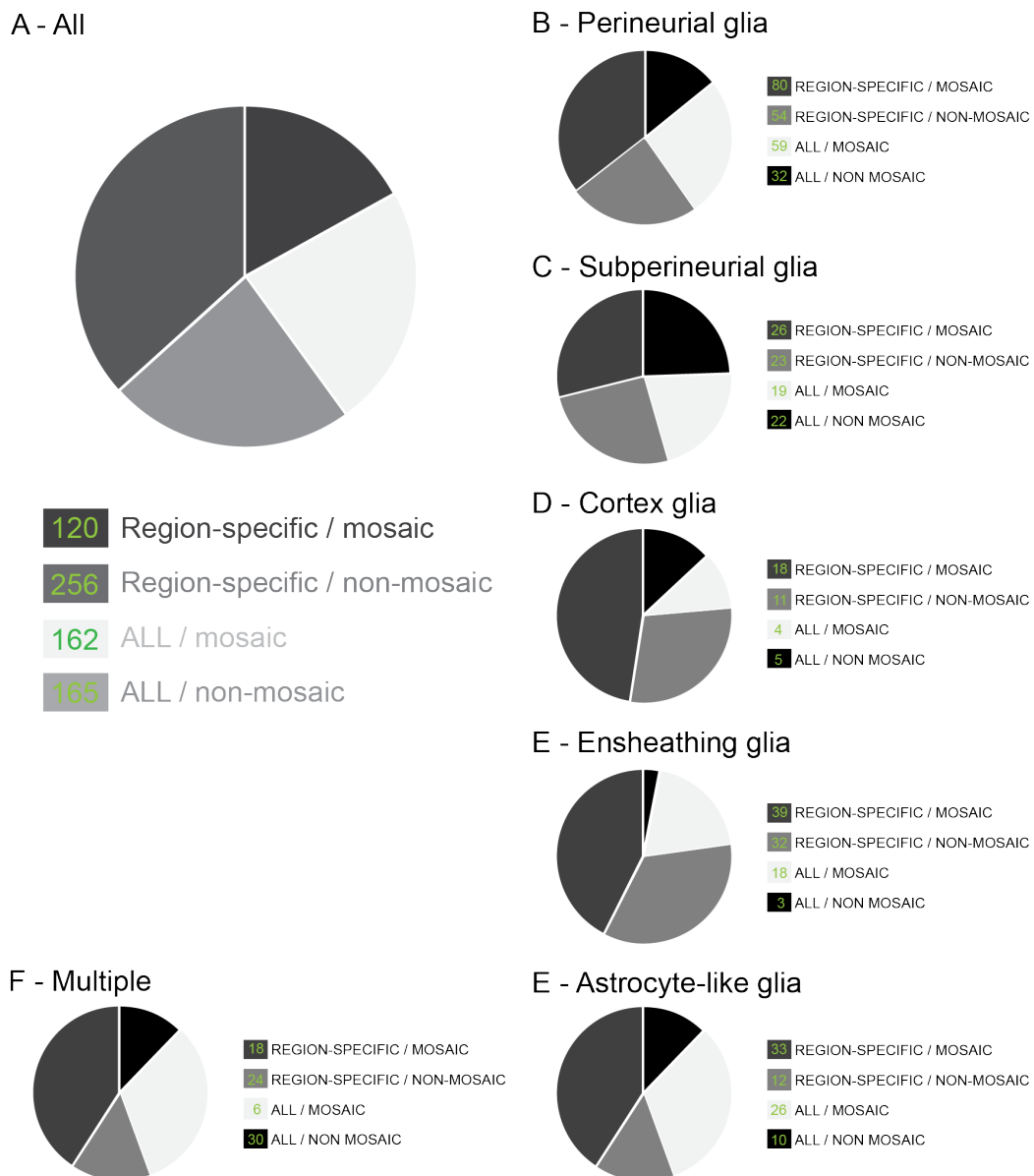


Figure 9: Classification of glial Gal4 drivers into generic subtypes.

Driver lines found within the Janelia Farm Gal4 Collection were categorized according to their global expression characteristics. **A** Among the glial driver lines, 16 percent express in all glia of one or multiple generic glial subtypes in a non-mosaic fashion (All / non-mosaic); 22 percent express in all glia of one or

multiple generic glial subtypes in a mosaic fashion (All / mosaic); 23 percent express in a region specific subset of one or multiple generic glial subtypes in a non-mosaic fashion (Region-specific / non-mosaic); 35 percent express in a region-specific subset of one or multiple generic glial subtypes in a mosaic fashion (Region-specific / mosaic). For further details please refer to the annotation details in the attached excel-spreadsheet. **B-F** As introduced in Figure 8, subtypes (in this case, all the drivers of one generic subclass) can be subdivided according to expression in the entire subtype or only a particular region, as well as by the degree of mosaicism. The numbers (green) in the figure legend box of each single generic glial subgroup (B-F) depict the number of actual driver lines with corresponding expression pattern. We found 44 driver lines with expression in Trachea. Those drivers are not considered in the present annotation analysis.

Within the glia-containing drivers of the Janelia Farm Gal4 collection, 61 percent show region specific expression pattern; among those, the majority (65 percent) of drivers induce mosaic expression. The minority of drivers promotes expression in all glia of one or multiple generic glial subtypes; among those, the majority (58 percent) induces mosaic expression (Figure 9A).

More specifically, we observe the following subtype characteristics: In the perineurial glial subtype (Figure 9B), the distribution between the different subcategories (All or region-specific / mosaic or non-mosaic) is relatively even, with a drift towards mosaic expression pattern (63%). In the subperineurial glial subtype (Figure 9C), the distribution between the different subcategories is relatively even; among all subgroups, subperineurial glia show the least percentage of region-specific mosaic driver lines. In the cortex glia subtype (Figure 9D), the distribution between the different subcategories is uneven; region-specificity is observed in 75percent of all driver lines with the majority (~2/3) showing mosaic expression patterns. In the astrocyte-like glia subtype (Figure 9E), the distribution between the different subcategories is uneven; mosaicism is observed in 75 percent of all driver lines, half of them show region-specific expression patterns. In the ensheathing glia subtype (Figure 9F), the distribution between the different subcategories is uneven; region-specificity is observed in 75 percent of all driver lines, half of them show mosaic expression patterns. Notably, a driver line that expresses in all ensheathing glia could not be identified; the 3 drivers counted here show high neuronal background or very weak glial expression.

For the reasons described in the beginning of this section, all glial drivers, after the initial characterization described above, were classified into A, B and C-drivers according to their quality and usability for further analysis (Figure 10A). The results as well as the proportion of generic glial subtypes in the group of A-drivers are presented in (Figure 10B).

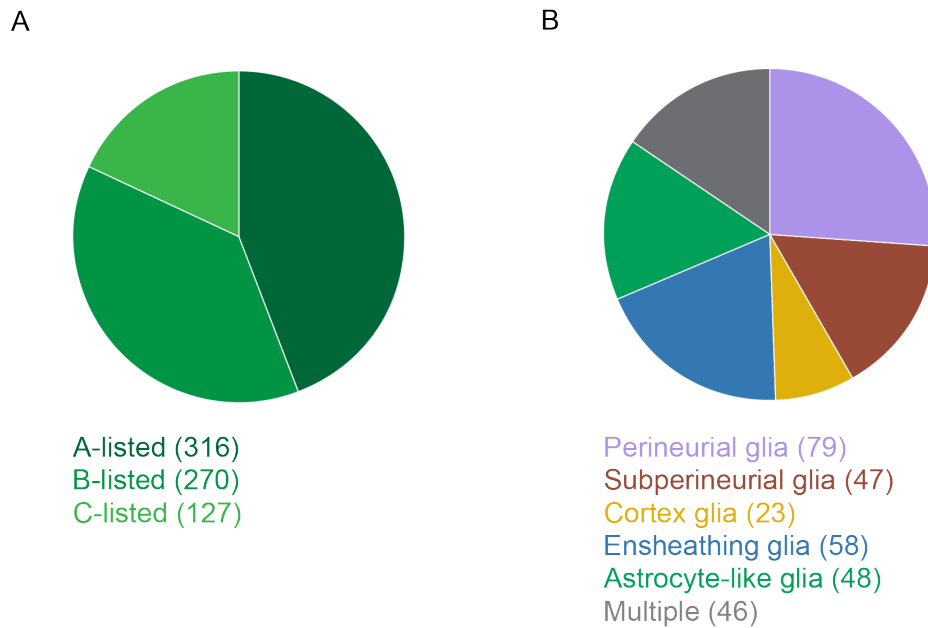


Figure 10: Triage of glial driver lines and classification of A-listed drivers into generic subtypes.

A Glial driver found in the Janelia Farm Collection were categorized as introduced previously into A, B and C-lines. **B** A-listed driver lines were further subdivided into the 5 major generic subclasses and those that label multiple generic subclasses. Since A-listed lines were selected subjectively according to uniqueness of pattern, strength of the driver and usability for functional analysis of glial cell function, global expression characteristics as in Figure 9B-F will not be explicitly plotted here. However, this data is contained Excel-spreadsheet attached to this thesis.

316 lines were A-, 270 lines B- and 127 lines C-‘listed’. Among the A-drivers, we identified 79 with perineurial and 47 with subperineurial glial expression, 23 with cortex glial expression, 48 with astrocyte-like and 58 with ensheathing glial expression. In 46 lines, expression was found in more than one glial subtype (Figure 10B).

Altogether, the driver lines contained in the A-list provide us with the necessary bandwidth of drivers to characterize both generic (also see 5.2) and region-specific glial populations (also see 5.3).

5.2 Generic glial Gal4 ‘reference’ driver lines

From our A-drivers, we established a set of ‘reference lines’ that label the generic glial subtypes (Figure 11, Table 1).

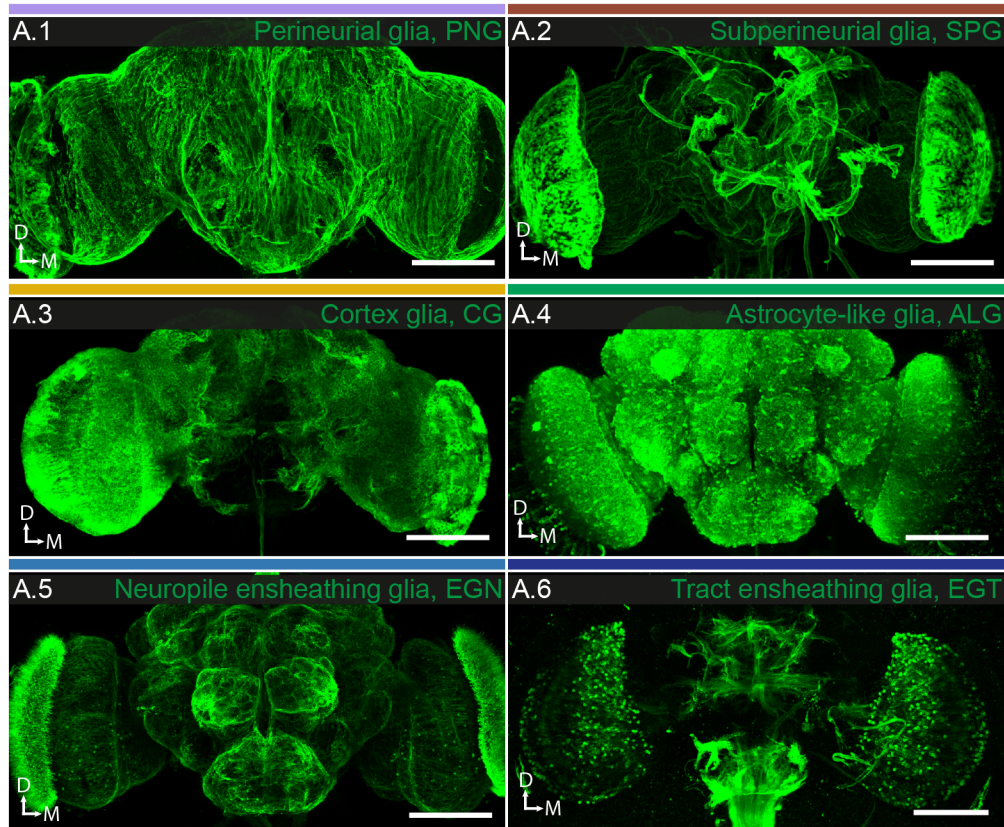


Figure 11: Anatomy of the *Drosophila* central nervous system and generic glial cell types

The different generic glial cell types as visualized by subtype-specific Gal4 driving a UAS-mcCD8GFP reporter; frontal view of maximum density projections (130-160x1 μ m optical sections). **A.1** Perineurial glia (85G01) (lavender), **A.2** Subperineurial glia (54C07) (dark red), **A.3** Cortex glia (77A03) (mustard), **A.4** Astrocyte-like glia (86E01) (green), **A.5** Neuropile-ensheathing glia (56F03) (light blue), and **A.6** Tract-ensheathing glia (75H03) (dark blue). Note that the different colors indicated in the bars above each image will be used throughout the thesis to distinguish the different glial subtypes. Scale bar = 100 μ m in all images.

Based on its stable and strong expression in *all* perineurial glia, we picked 85G01 as our perineurial glia reference line (Figure 11A.1, Table 1, further characterized in: 6.1.2, Figure 13). 54C07 was used as subperineurial glia reference line (Figure 11A.2, Table 1, further characterized in: 6.1.3, Figure 14). We used 54H02 and 77A03 as a reference line for cortex glia. Unfortunately, 54H02 is not expressed in the Lamina cortex glia; 77A03 expression in the VNC is mosaic (Figure 11A.3,

Table 1, further characterized in: 6.1.4, Figure 15). In future experiments, this needs to be considered. We employed *86E01* as a reference line for astrocyte-like glia even though it shows mosaic expression in the Lamina astrocyte-like glia; for this specific subpopulation, we used *55B03* as a replacement line (Figure 11A.4, Table 1, further characterized in: 6.1.5, Figure 16). None of the ensheathing glia drivers are expressed in *all* ensheathing glia. 24 are only expressed in neuropile associated glia, 16 are only expressed in tract associated glia; the remaining 12 lines are expressed in both neuropile- and tract-associated glia in varying proportions. To account for this problem, we picked three reference lines: *56F03*, which drives expression in all neuropile and only very few tract associated glia (Figure 11A.5, Table 1); *75H03*, which drives expression in all tract but no neuropile associated glia (Figure 11A.6, Table 1); *28A04*, which drives expression in all tract and most neuropile associated glia (data not shown, Figure 17 for a detailed characterization of ensheathing glia subtypes).

Generic glial subtype	Details / Characteristics	Gal4	Alternative
PNG	<i>All</i>	<i>85G01</i>	<i>31F02 / 86E02 / 30A03</i>
SPG	<i>All</i>	<i>54C07</i>	<i>79H09</i>
CG	77A03 not in VNC, 54H02 not in Lamina	<i>54H02</i>	<i>77A03</i>
EG	Neuropile-associated, moderate neuronal background in optic lobe	<i>56F03</i>	<i>84B06 / 83E12</i>
	Tract-associated, moderate neuronal background in optic lobe	<i>75H03</i>	<i>93H03 / 51B05</i>
ALG	Mosaic in epithelial glia	<i>86E01</i>	<i>75H11</i>

Table 1: Summary of generic reference lines and potential alternative drivers.

Aside from the selected reference lines, in almost all cases (with the exception of ensheathing glia), driver lines with comparable expression pattern are available (also see Table 1, Alternative). They were used if problems with the initial reference lines occurred and / or if the original expression pattern could not be reproduced with a different reporter. Altogether, this set of generic glia reference lines provides the basis for the detailed study of glial anatomy in the adult fly brain presented in section 6 and in functional experiments (also see 7).

5.3 Identification of region specific driver lines

Driver lines that label unique region-specific subpopulations of generic subtypes were also considered under ‘A-lines’. An overview about the predominant pattern found per generic subtype is given in Figure 12 and Table 2.

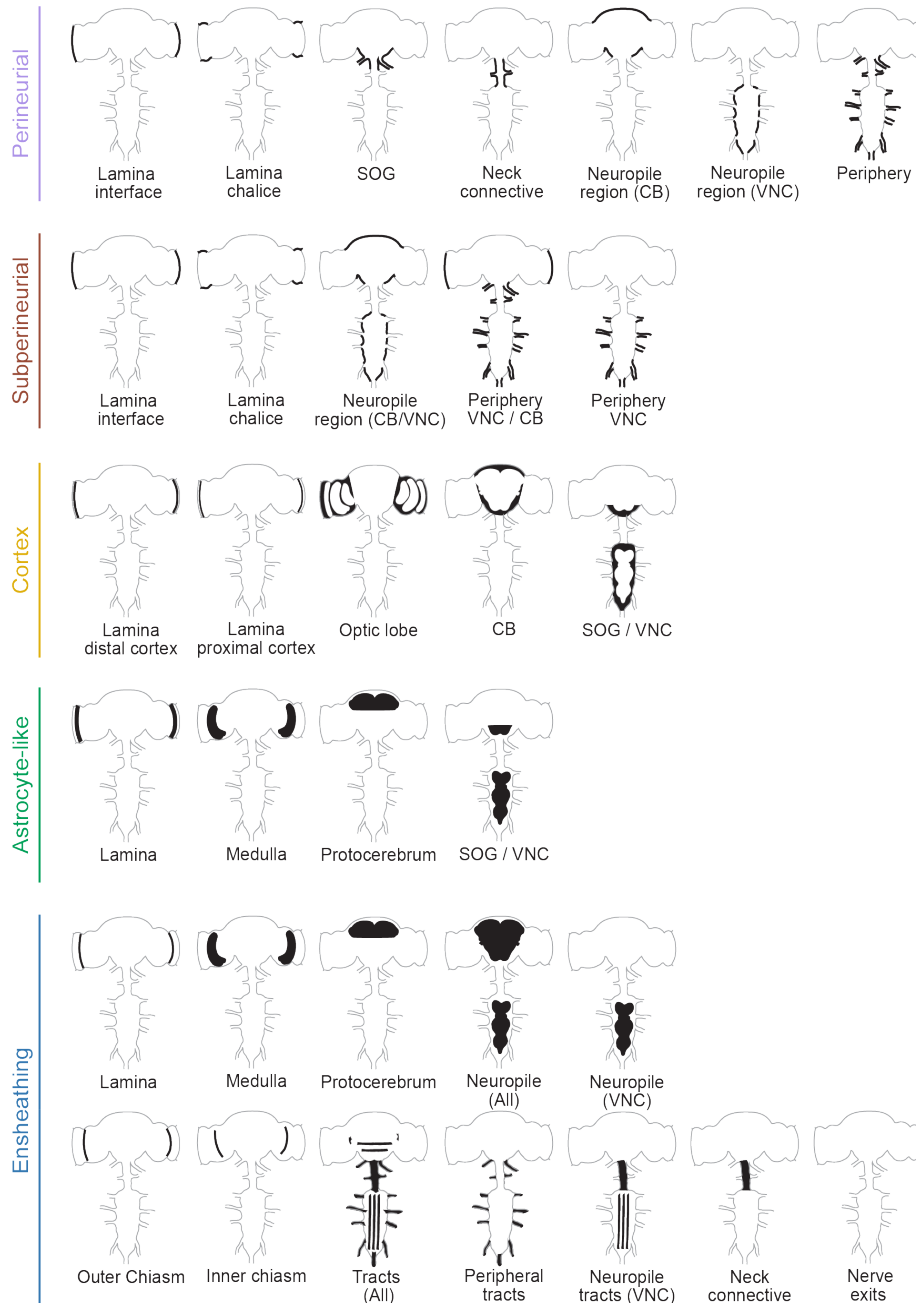


Figure 12: Illustration of the different region-specific expression pattern within each generic subclass.

For the different generic subtypes of glial cells, different region specific driver lines were found and schematically illustrated here. The corresponding driver lines are listed in Table 2.

Generic glial subtype	Region	Subtype	Details / Characteristics	Driver	Alternative
PNG	L	L-iPNG	(Fenestrated)	47G01	19D10
PNG	L	L-PNG	(Chalice-like perineurial)	10C12	27H11
PNG	CB		only SOG	40A03	
PNG	VNC		Only neuropile region	38E12	
PNG	Neck		Only neck connective	60B10	
PNG	B/VNC		neuropile region, no periphery	94A04	85C04
PNG	CB	Ventral part		86C05	
PNG	All	Only periphery		79H10	
SPG	L	L-iSPG	(Pseudo-cartridge)	50A12	
SPG	L	L-SPG	(Chalice-like subperineurial)	(24A11)	
SPG	B/VNC		Periphery, also pseudo-cartridge	37G04	31H12
SPG	B/VNC		Neuropile region, no periphery	94B06	59F06
SPG	VNC		Neuropile region, no periphery	88A04	
CG	L	L-dCG	(Distal satellite)	53B07	
CG	L	L-pCG	(Proximal satellite)	44B12	
CG	OL	ME / LoC cortex	ME / LoC cortex, no Lamina	65B12	
CG	CB	All CB	Mosaic co-expression in other glia	9F07	
CG	CB / VNC	CB only SOG	Co-expression in ALGs	54D10	
EGN	L	L-EGN	(Marginal)	35E04	19C02
EGN	OL	ME-EGN		73B10	41G04
EGN	CB	Protocerebrum	Co-expression in marginal glia	54E05	
EGN	B/VNC		Neuropile-associated	56F03	15B05
EGT	B/VNC		Tract-associated	75H03	93H03
EGN	B/VNC		No protocerebrum	83E12	(28A04)
EGT	B/VNC		Peripheral tracts	43H01	
EGT	CB / VNC	Neck	Only neck connective	74E08	
EGT	B/VNC	Nerve exits	Interface peripheral nerves / neuropile-region / optic lobe neurons	95B11	
EGN	VNC		Mosaic neuropile-associated	69G05	
ALG	L	L-ALG	(Epithelial)	55B03	
ALG	OL	ME-ALG	Medulla astrocyte-like	31E10	84B11
ALG	CB	Protocerebrum	Mosaic expression in protocerebrum	81A12	
ALG	B/VNC		All mosaic	77B12	
ALG	CB / VNC	CB only SOG	Co-expression in cortex	54D10	
ALG	B/VNC		Mosaic in Lamina	86E01	75B11 25H07
ALG	CB	AMMC	Co-expression in exit ensheathing glia	86F01	
ALG	VNC		Mosaic expression	29A12	70G03
ALG	CB / VNC	CB only SOG		78D09	

Table 2: Summary of drivers with region-specific expression pattern per generic subtype.

The driver lines for the most characteristic region-specific expression pattern (including driver lines which label all glia of one subtype) are shown. Additionally, alternative drivers are listed.

These region-specific drivers contain driver lines expressed in subsets of glia with either specialized morphologies in particular regions of the brain or spatially restricted expression in particular brain regions but without obvious morphologic adaptations. For example, in the optic lobes - particularly at the Lamina-retina interface -, we identified subperineurial glia that enclose (and presumably seal) incoming photoreceptor axons, whereas subperineurial glia in the rest of the brain form a tight layer which is not foraminated by any other tissue (Figure 14, Figure 20). In interesting opposition, we found driver lines, which label subperineurial glia only around the VNC neuropiles and not in the central brain or periphery. In all the given examples, the drivers consistently label the designated glial populations; however, in most drivers, neuronal expression is very high.

5.4 Summary

In this first set of experiments, we have annotated the entire *Janelia Gal4* collection for glial expression in the (central) nervous system (a complete list will be available on the Gaul lab homepage). For each driver line with glial expression, we annotated all the glial populations found and subdivided them into classes according to the 'quality' of the driver line. We have identified *Gal4* driver lines, which are specific for a given generic subtype and for a particular region. Notably, the generic subtype drivers are also glia subtype-specific throughout development (Supplemental figure 2) and onset of expression broadly coincides with previously published observations (Supplemental figure 1) (Awasaki et al., 2008; Ito et al., 1995). For each generic subtype, we identified driver lines with different region-specific expression pattern. Furthermore, we found subtype-specific drivers, which express stochastically only in a variable subset of cells. Altogether, we characterized ~100 lines with subtype- or region-specific expression in glia in greater detail, and generated LexA versions for ~50 of them to facilitate further investigations.

5.5 Discussion

The annotation of the glial drivers within the Janelia Farm Gal4 collection revealed driver lines that can be used to characterize the multitude of glial subtypes in their full complexity. Based on data presented in the second part of this thesis (also see 6), the described driver lines represent all different existing subtypes of glia. Even though generic glial drivers had been established previously (Awasaki et al., 2008; Doherty et al., 2009; Edwards and Meinertzhagen, 2010; Oland et al., 2008; Sen et al., 2005; Yao et al., 2007), none of them combined a reproducible generic glial pattern with the advantages of the design of the Janelia Farm driver line collection (Jenett et al., 2012). The design allows for easy replacement of Gal4s with other genetic modules (i.e. LexA-system, QS-system, Gal80 and recombinases, also see 4.3.2), consistent expression pattern, reliable estimation of the strength of the driver and possibilities to enhance or weaken the expression of the drivers genetically. Altogether, the combination of characterized drivers and optimized genetic constructs (Pfeiffer et al., 2008; Pfeiffer et al., 2010) (also see 4.3.4) and intersection strategies for anatomical and functional analysis opens up an entire new toolbox for the *Drosophila* community to look at the function of single genes in small subpopulations of cells up to a single cell.

Within the collection, about ten percent of the driver lines contain glial expression pattern. In section 6.1.1, we show that the glial population accounts for about ten percent of the cells in the CNS. However, we do not see a causal link between these two ratios. This is because the driver lines were generated with 3kb long fragments of regulatory regions of genes, which have been selected by their (presumed) expression or function in the CNS. They do not necessarily represent an unbiased selection of genes in neurons *and* glia. As a matter of fact, neuronal background and mosaicism is a problem in the majority of the glial driver lines, which could potentially be minimized with a biased selection of 'glial' genes.

In general, a higher variance of expression pattern is observed in subtypes with higher cell number (perineurial) and/or more elaborate morphologies (ensheathing). We find two expression characteristics that occurred frequently:

Region-specificity of driver lines and mosaicism within a given expression pattern. The majority of driver lines show region-specific glial pattern. We believe region-specificity is the result of either specialized glial subtypes / morphology within particular brain regions or local cues which would enhance or restrict the expression of otherwise generic drivers to confined regions. The occurrence of mosaicism in the Gal4 lines had previously been noted in the context of neuronal expression (Arnim Jenett, personal communication). With regard to the glial lines, we find that mosaicism correlates with the size of the population in which the driver is expressed. For example, the perineurial and astrocyte-like glial cell populations are large (15 and 30% of the total glial population) and most lines are mosaic, while subperineurial glial cell population is smaller (3% of the total glial population) and fewer lines are mosaic.

The major goal of the annotation was to find reference line for all generic glial subtypes, which have strong consistent expression throughout development, in all cells of a subtype. We found reference lines for generic glial subtypes that meet these criteria. Those included perineurial and subperineurial glia drivers. In the case of cortex, ensheathing and astrocyte-like glial drivers, we were not able to meet all desired criteria. In these cases, expression did not cover *all* the cells of a given subtype. Specifically, in cortex glia, two drivers had to be employed because none of the generic drivers labeled all cortex glia cells in optic lobe, central brain and ventral nerve chord at the same time. In astrocyte-like glia, the expression is mosaic in the subpopulation of cells in the Lamina (epithelial glia) (Figure 19, Figure 20) making us replace this subpopulation with a specific driver (55B03). Ensheathing glia presented the biggest difficulty since no driver line was found which labels all cells of all the ensheathing glia subpopulations (neuropile- and tract-ensheathing glia). Therefore, one driver line was selected that labels each individual subpopulation (Figure 17). In the case of the neuropile-ensheathing glial driver *56F03*, which was the best neuropile ensheathing driver identified the expression was still moderately mosaic. Additionally, we found neuronal 'background' expression in the optic lobes of this driver line as well as in the tract-associated reference driver *75H03*. Based on these findings, one may

suggest selecting different reference drivers. In both cases, this was not possible due to incomplete or weak expression in alternative drivers as well as even higher neuronal 'background' expression. In future experiments, those observations will have to be considered when analyzing phenotypes for these subpopulations. In the case of functional experiments, we would also recommend to suppress neuronal expression with a neuronal Gal80, a specific Gal4 inhibitor, or to use combinatorial / intersectional expression systems to constrain the expression to the population of glial cells of interest.

The second major goal of the annotations was to find region-specific glial drivers, which are strong, show a stable and consistent expression and express in all cells of one subtype in a region-restricted manner. We believed that region-specific expression pattern would represent glia with either specialized morphologies or other region-restricted functional adaptations. They would thus help us to define and characterize the different subtypes of glia in the adult *Drosophila* CNS. We found region-specific expression patterns in all glial subtypes (also see Figure 12, Table 2). However, only in the case of Lamina glia (fenestrated and pseudo-cartridge, distal and proximal satellite, epithelial and marginal glia, Figure 20) as well as the ensheathing and astrocyte-like in the Medulla, region-specific expression pattern were accompanied by obvious region-specific morphologies not having been observed in any other part of the brain. To which extent the other region-specific drivers represent glial subpopulations with specialized functions will have to be further investigated. Unfortunately, with the exceptions of the Lamina glia, most other region-specific drivers show neuronal 'background' expression; in case they would be required for functional analysis, neuronal expression would have to be removed from their expression pattern as described above.

6 Morphologic characterization of glia in the adult fly brain

6.1 Characterization of generic glial subtypes

The major goal of the glial driver characterization was to generate a comprehensive catalog and description of glia in the adult (central) nervous system. Specifically, we sought to assess the number, location and morphology of different glial subtypes, the variation in cell size and shape within a given cell type and the physical relationship between cells of the same type, with other glial subtypes and with neurons. For every generic subgroup, we employed the following strategy: (1) We confirmed the glial identity and its cell numbers by expressing a nucleary-expressed GFP under the control of subtype specific drivers and co-labeled all glial and all neuronal cell bodies additionally with specific antibodies. (2) Using membrane targeted GFP expression in the generic glial subpopulations, we investigated the overall glial pattern; additional co-labeling with specific antibodies such as nc82, which specifically labels synaptic regions, allowed us to determine the spatial relation of glial populations and major brain regions. (3) The variation in cell size and shape within a given cell type in different brain regions and the physical relationship between cells of the same type were characterized with a novel multi-color mosaic technique (described in 4.3.4). Finally, we investigated region-specific morphologic differences within the same glial subtype, the morphologic interaction between different glial subtypes, and the interaction between glial and neuronal entities, by employing two orthogonal expression systems (Gal4-UAS, *lexA-lexAop*) and highly sensitive reporters.

6.1.1 *Glial cell counts*

In the adult *Drosophila* CNS, the five major generic glial subtypes – perineurial, subperineurial, cortex, astrocyte-like and ensheathing glia – are found. In order to determine the overall number of glia, we counted *all* glial cells using the glial-specific repo-antibody (all glia). Labeled glial cell bodies were counted with a Definiens script developed together with Christophe Jung, AG Gaul (for detailed

methodological explanation refer to 9.3). Overall, the total number of glial cells was counted to be around 15 000 (Table 3).

Driver	Generic subtype	Expression	Compensatory drivers	Cell Count (generic)	Cell count (compensation)	Subtype counts	+/- (SEM)
85G01	Perineurial	entire CNS	---	2246	---	2246	41 (n=5)
54C07	Subperineurial	entire CNS	---	300	---	300	15 (n=12)
54H02	Cortex	not in Lamina	53B07 46H12	1409	1226	2635	46 (n=9)
86E01	Astrocyte-like	mosaic in Lamina	55B03	3668	950	4618	176 (n=7)
56F03	Neuropile-associated	no tracts	(75H03)	3106	next row	3106	116 (n=8)
75H03	Tract-associated	not in Lamina	---	616	---	616	56 (n=7)
ALL						13523	
REPO-positive						15703	1717

Table 3: Generic glial counts.

The best driver for each generic glial subtype is listed and described with regard to its expression pattern and the number of cells in which it is expressed. The Driver-Number is a unique identifier for each driver, by which the line can be ordered from the Bloomington Stock Center. Expression may not include specific brain regions or show mosaicism. In these cases, compensatory drivers, which are expressed exclusively in the missing/suboptimal region, were used to complete the cell count. In particular, a pan-ensheathing glial driver was not recovered, and therefore complementary neuropile- and tract-ensheathing glial drivers were used. Subtype count is thus the sum of generic+compensatory cell count; the number of brains counted is indicated, as well as the standard error of the mean. The total number of glia within the adult brain was additionally estimated by counting REPO-positive nuclei.

The surface of the entire nervous system, including CNS and PNS, is covered by two thin glial layers, the perineurial and subperineurial glia (Figure 11A.1- 2, characterized in Figure 13, Figure 14). Our cell count places the total number of perineurial glia covering brain and ventral nerve cord at ~2250, around 15% of the total glial cell population and subperineurial glia at ~300, around 3% of the total glial cell population (Table 3). The cortical regions of the CNS are populated by a single glial subtype, the cortex glia (Figure 11A.3), which encapsulate neuronal cell bodies and wrap neuronal processes as they cross the cortex region before entering the neuropile (Awasaki et al., 2008; Hoyle, 1986; Peraanu et al., 2005; Spindler and Hartenstein, 2010) (Figure 15). The total number of cortex glia was ~2600, around 17% of the total glial population (Table 3). Astrocyte-like glia

are found in neuropile regions (Figure 11A.4, Figure 16), together with ensheathing glia (Figure 11A.5-6, Figure 17). We determine the total number of astrocyte-like glia to be 4,600 cells, around 30% of the total glial cell population (Table 3). Ensheathing glia are found associated with both neuropiles and axon tracts and thus show a broader range of morphologies than other glial subtypes (Figure 17)(Hartenstein, 2011). Combining the cell counts of the two 'cleanest reference' lines (*56F03* and *75H03*), we estimate the number of ensheathing glia at ~3,100 in neuropiles and ~600 in tracts, ~3,700 altogether, which represents around 25% of the total glial population (Table 3).

Considering the CNS to consist of roughly 150.000 neurons (Jenett et al., 2012), the population of glial cells thus accounts for about 10% of the cells in the CNS.

6.1.2 *Perineurial glia*

Perineurial glia provide the outermost glial sheath to the nervous system (Figure 13A.1-2). Multi-color mosaic experiments reveal perineurial glia as narrow, elongated cells (Figure 13A.3-5) with only moderate variations in shape and orientation. In the central brain and optic lobes, the cells are elongated along the dorso-ventral and antero-posterior axis (8-12 μ m wide, 100-120 μ m long) (Figure 13A.3-5 and Figure 13A.8-9). In the ventral nerve cord, the cells are wider and shorter and often oriented along the medio-lateral axis (Figure 13A.10-11). In the PNS, the cells are oriented along the long axis of the nerves (Figure 13A.12-15). Altogether, the perineurial glia cover the entire nervous system in a densely tiled fashion. They send out long thin extensions that bracket/clamp their anterior neighbors and form ledge-like overlaps with their lateral neighbors. Amongst the perineurial glia lines we identified, some show region-specific expression in the optic lobes, the central brain and the ventral nerve cord (Figure 12, Table 2). However, only in the Lamina, region-specific expression is accompanied by pronounced morphological specialization (Figure 20).

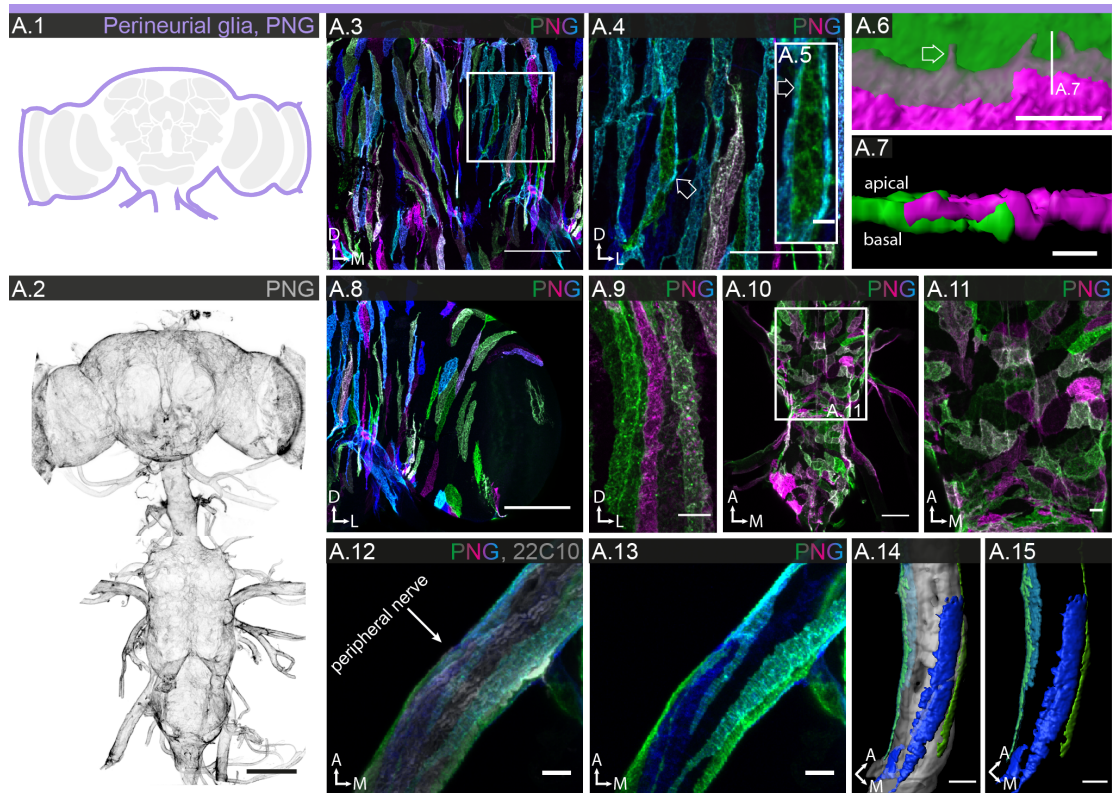


Figure 13: Morphology of perineurial glia.

A.1 Schematic showing the location of perineurial glia, PNG (lavender) in the brain. **A.2** Perineurial glia enclose the entire CNS and PNS (85G01-lexA; lexAOp-myr-smGFP-HA)(frontal view; maximum density projection, 85x1 μ m sections). **A.3- 5, 8- 15** Individual cell morphologies of perineurial glia in different regions of the CNS (85G01-Gal4; McFlip; hs= 2.5min in **A.3-5, A.8-9** and 15min in **A.10-15**). **A.3** In the central brain, perineurial glia appear as long thin strips oriented along the dorso-ventral axis (frontal view; maximum density projection; 61x1 μ m sections). **A.4** Higher magnification of the boxed region in **A.3**. Perineurial glia have long thin extensions that interdigitate with neighboring cells (open white arrow). These interdigitations can reach far along the neighboring cells, as seen in **A.5**. **A.6-7** 3D reconstruction of the cell boundary between two perineurial glia. The region of contact between two cells show small protrusions of one cell over the other cell's surface (open white arrow in **A.6**). Cross section (**A.7**) reveals that the cells retain their relative proximo-distal position along the entire length of contact. **A.8** In the optic lobe, perineurial glia also appear as long thin strips along the dorso-ventral axis (frontal view; maximum density projection; 20x1 μ m sections). **A.9** High magnification of single cells (frontal view; maximum density projection; 22x1 μ m). **A.10** In the ventral nerve cord, perineurial glia show a more varied morphology, ranging from elongated to square shaped, with orientation mostly along the medio-lateral axis (frontal view; maximum density projection, 43x1 μ m sections). **A.11** High magnification of the boxed region in **A.10**. **A.12-13** In the peripheral nervous system, perineurial glia enclose the peripheral nerves (labeled with 22C10 in **A.12**) (frontal view; maximum density projection; 75x0.5 μ m sections). **A.14-15** 3D reconstructions of **A.12** and **A.13**, respectively. The cells form narrow strips along the long axis of the nerve, without covering its entire circumference. Scale bar = 100 μ m in **A.2**; 50 μ m in **A.3, A.8, A.10**; 10 μ m in **A.4, A.9, A.11-15**; 5 μ m in **A.5**; 2 μ m in **A.7**; 1 μ m in **A.6**.

6.1.3 Subperineurial glia

Subperineurial glia form the second glial layer around the CNS, directly underneath the perineurial layer (Figure 14A.1-2, Figure 18A.2-4). Multi-color mosaic experiments show subperineurial glia as large, almost square-shaped cells (40-100 μ m x 40-100 μ m) (Figure 14A.3-4), with moderate variation in size and little variation in shape between different brain regions (central brain (Figure 14A.3); optic lobe (Figure 14A.4) and VNC (data not shown). In the PNS, subperineurial glia can form elongated tubes around small peripheral nerves (Figure 14A.10, white open arrow), but enclose larger nerves jointly with other cells (Figure 14A.8-10, open red arrow in A.10). Altogether, the subperineurial glia form a densely tiled and tight epithelium (Figure 14A.2) with modest overlap between neighboring cells (Figure 14A.7). From their basal surface, subperineurial glia send deep protrusions into the underlying cortex region that individually cap neuronal cell bodies (Figure 14A.6). Among the subperineurial glial drivers we identified, some show region-specific expression in the optic lobe, central brain, ventral nerve cord and peripheral nerves (Figure 12, Table 2). As has been observed for perineurial glia, region-specific expression characterized by distinct morphological specialization is only found in the Lamina (Figure 20).

The perineurial and subperineurial glia form a contiguous layer around the entire brain (Figure 18A.2), approximately 2-3 μ m thick (Figure 18A.3), which in turn is covered by extracellular matrix. The continuity of these glial sheaths is not interrupted at the boundary between CNS and PNS (Figure 18A.4). However, at the retina-Lamina interface of the optic lobe, both perineurial and subperineurial glia show morphological specializations not found elsewhere in the brain, presumably due to the need of maintaining insulation of the CNS while accommodating the massive incoming parallel photoreceptor projections from the retina (Figure 7, Figure 20).

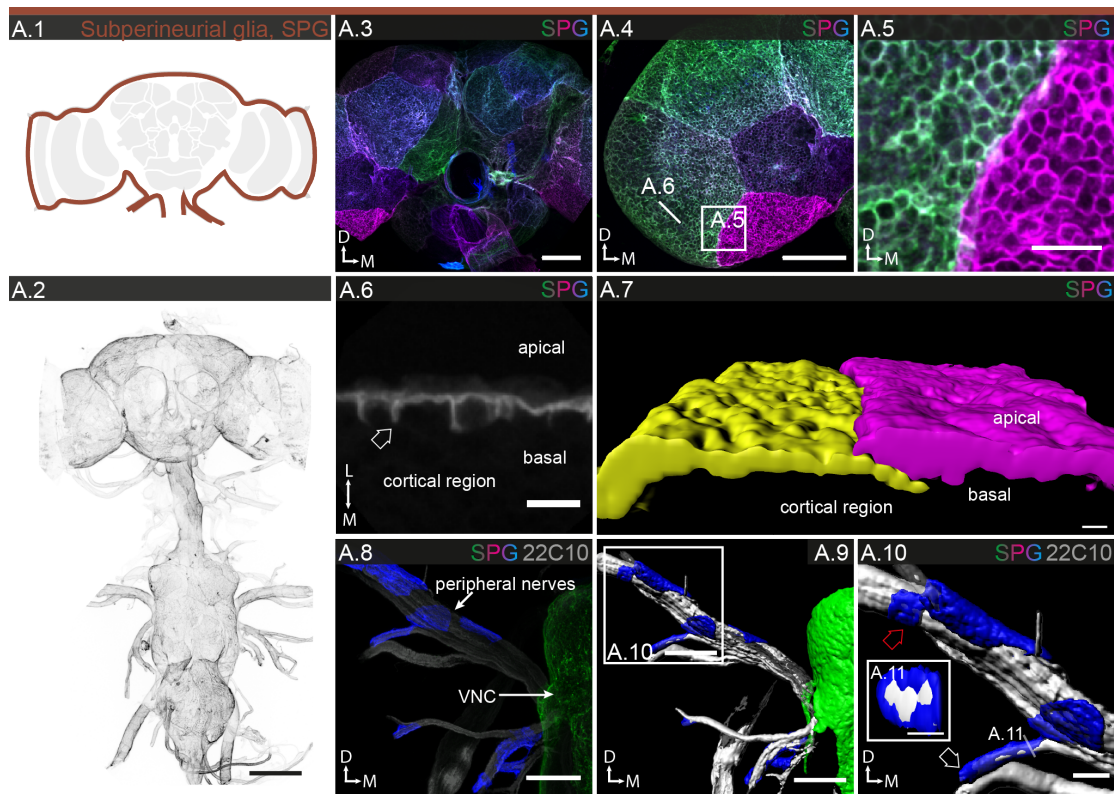


Figure 14: Morphology of subperineurial glia.

A.1 Schematic showing the localization of subperineurial glia, SPG (dark red) in the brain. **A.2** Subperineurial glia enclose the entire CNS and PNS (54C07-Gal4; UASmyr-smGFP-V5) (frontal view; maximum density projection; 85x1 μ m sections). **A.3-11** Individual cell morphologies of subperineurial glia in different regions of the CNS and PNS (54C07-Gal4; McFlip; hs= 7 min). In the central brain (**A.3**) and optic lobe (**A.4**), subperineurial glia are thin, very large square-shaped cells (frontal views; maximum density projections; 76x0.5 μ m sections). **A.5** Magnification of the boxed region in **A.4**. Many ring-like membranous structures within the subperineurial glia are visualized. In cross section (**A.6**), they reveal themselves as cap-like basal protrusions (open white arrow) that cover individual neuronal cell bodies within the cortex. **A.7** 3D reconstruction of the overlap of two neighboring subperineurial glia cells. Subperineurial cell-cell contacts appear smoother than those of perineurial glia (Figure 13A.6). **A.8-11** Single subperineurial glia cells around a peripheral nerve (22C10, grey) of the ventral nerve chord (frontal view; maximum density projection; 102x1 μ m sections). Cells have a square to oblong shape that extends along the nerve (open red arrow); thinner nerves can be completely enveloped by a single cell forming a tube (open white arrow), as revealed by a cross section in **A.11**. **A.9-11** 3D reconstructions of **A.8** at two magnifications. Scale bar = 100 μ m in **A.2**; 50 μ m in **A.3-4**, **A.8-9**; 10 μ m in **A.5**; 5 μ m in **A.6**, **A.10-11**; 1 μ m in **A.7**.

6.1.4 *Cortex glia*

Cortex glia are found exclusively in the cortex region of the brain (Figure 15A.1-2). Their cell bodies are found irregularly placed in the cortical region (Figure 15A.3). Cortex glia are large mesh-like structured ('honey-combed') cells, in which neuronal cell bodies are enveloped individually as revealed by multi-color mosaic experiments (Figure 15B.1). The number of enveloped cell bodies varies from a few (Lamina; Figure 20) up to one hundred (central brain; Figure 15B.1). Neighboring cortex glia show little if any overlap; at their boundary, two cells often jointly create the enclosure for one neuronal cell body (Figure 15B.2-3). 3D reconstruction of cortex glia reveal an overall round, lobular shape with finer protrusions reaching into neighboring areas (Figure 15B.4, open white arrow). In addition to enveloping neuronal cell bodies, cortex glia wrap neuronal processes as they travel across the cortex (Figure 15C.1-2). Amongst the cortex glial lines we identified, a few show region-specific expression in the optic lobe, central brain and ventral nerve cord (Figure 12, Table 2). Among all cortex glia, only those in the Lamina show specialized morphologies (Figure 19, Figure 20).

Cortex glia show minimal interaction with their neighboring glial subtypes: On the outer surface of the cortex, cortex glia encounter subperineurial glia. Occasionally/not infrequently, cortex glia fail to envelop the distal-most segment of neuronal cell bodies. In these cases, subperineurial glia complete the enclosure (Figure 18B.1-3). On the inner surface of the cortex, cortex glia encounter both ensheathing and astrocyte-like glia. Cortex and ensheathing glia abut forming very smooth boundaries with little if any overlap between the two cell types (Figure 18C.1-2). On the other hand, astrocyte-like glia do send thin processes into the cortical region but nevertheless show little direct contact with cortex glial surfaces (Figure 18E.1-5).

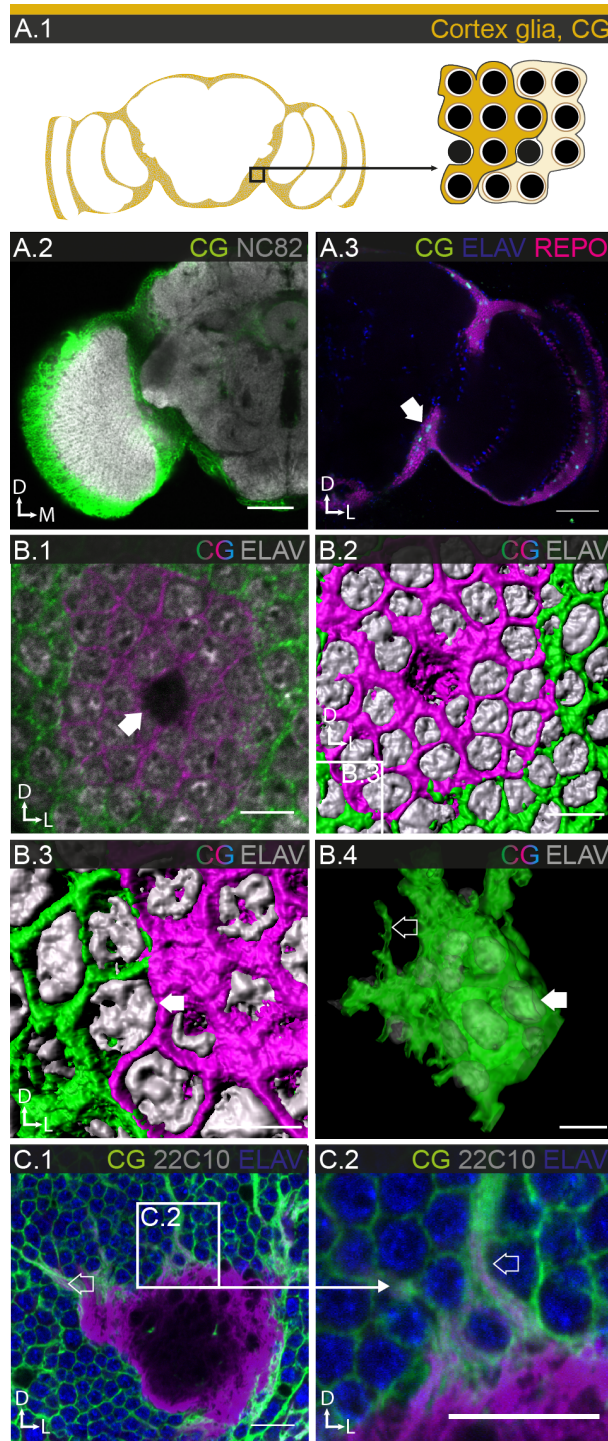


Figure 15: Morphology of cortex glia.

A.1 Schematic showing the localization of cortex glia, CG (mustard) in the brain (left) and the relationship between individual cortex glial cells and neuronal cell bodies (right). **A.2** Cortex glia fill the cortical regions of the brain without entering the neuropile regions (77A03-Gal4; UASmCD8GFP; nc82, grey) (single frontal section). **A.3** Cortex glial cell bodies in the central brain are found exclusively in the cortical regions of the brain (filled white arrow) (77A03-Gal4; UAS-nls-GFP; green; REPO, blue; ELAV, magenta) (single frontal section). **B.1-4** Individual cell morphologies of cortex glia in the central brain (54H02-Gal4; McFlip; hs= 4-12min; ELAV; grey) (**B.1**; single frontal section) **B.2-3** 3D reconstruction of **B.1**. A single cortex glial cell

envelopes 20-100 neuronal cell bodies (85 in this example). Each neuronal cell body is wrapped individually, however, two neighboring cortex glia can contribute to wrapping one cell body (filled white arrow in **B.3**). **B.4** 3D reconstruction of an entire cell with translucent membrane to reveal neuronal cell bodies within (filled white arrow). Note the fine membrane protrusions extending in all directions (open white arrow) (frontal view; maximum density projection; 32x1 μ m sections). **C.1-2** Interaction of cortex glia with neuronal cell bodies and fiber tracts (77A03-Gal4; UASmCD8GFP; green; ELAV; blue; 22C10; magenta). Cortex glia support (enwrap) neuronal fibers (open white arrow) until they leave the cortical region. Scale = 50 μ m in **A.2-3**; 10 μ m in **B.1-2, C.1-2**; 10 μ m in **B.3-4**.

6.1.5 *Astrocyte-like glia*

Astrocyte-like glia populate the neuropile regions of the CNS (illustrated in Figure 16A.1). The cell bodies of astrocyte-like glia are found at the interface between cortical regions and neuropiles (boundaries/margins of all neuropiles), but also between neuropile regions deep inside the brain (Figure 16A.2, filled white arrow). Amongst the astrocyte-like glial lines we identified, a few show region-specific expression in the optic lobe, central brain and ventral nerve cord (Figure 12, Table 2). Astrocyte-like glia vary in size and shape and have a spongy and/or fine-meshed structure as demonstrated by multi-color mosaic experiments (Figure 16A.3). The cells maintain their own territories and thus show the neat tiling observed in the other glial subtypes; at the boundaries between two cells, their protrusions may intermingle, if they physically contact each other cannot be determined on the level of light microscopy (Figure 16A.4).

High magnification of the generic expression pattern of astrocyte-like glia reveals two important features of this cell type: First, astrocyte-like glia processes density varies between different neuropile regions (Figure 16A.5) (in this example, between mushroom body and crepine). Second, astrocyte-like glia send fine protrusions into the regions outside the neuropile (Figure 16A.6) (for explanation, also see Figure 18D.1, E.1-5, Figure 21B.7- 8).

Mosaics of astrocyte-like glia reveal that astrocyte-like glia processes vary strongly in their structural density, from filigrane arborization (Figure 16B.1) to a dense spongy mesh (Figure 16B.5). This morphologic feature seems to be a function of the specific neuropile the glia invade. Of two glia, whose cell bodies lie next to each other, one may form a spongy mesh, the other filigrane arborization as each invades a different neuropile (Figure 16B.2). Even more, astrocyte-like glia do not respect neuropile boundaries and often project two independent branches into two different neuropile regions (Figure 16A.6 (compare regions highlighted by the two arrows), B.2- 4). In those situations, as two branches of the same glial cell invade different neuropiles one may show low, the other high process density (Figure 16B.3-4).

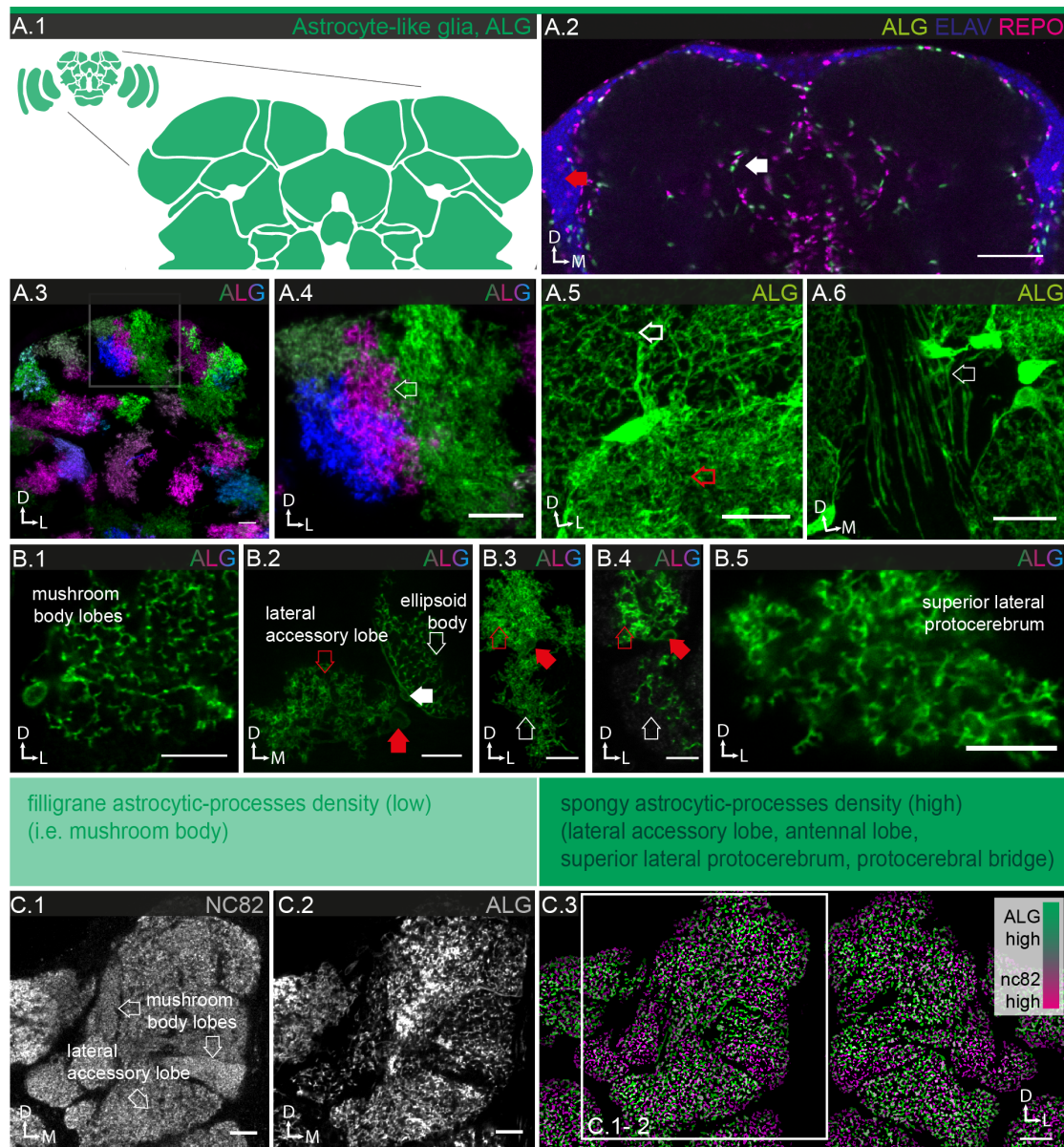


Figure 16: Morphology of astrocyte-like glia.

A.1 Schematic showing the localization of astrocyte-like glia in the brain. **A.2** Relative location of astrocyte-like and neuronal cell bodies in the central brain (86E01-Gal4; UAS-nls-GFP; green, REPO; magenta; ELAV; blue) (single coronal section). While neuronal cell bodies are always located in the cortical regions (filled red arrow), astrocyte-like cell bodies are frequently found in between neuropile regions (filled white arrow). Note that, unlike other glial subtypes, ALG nuclei are only weakly REPO-positive. **A.3-4** Individual cell morphologies of astrocyte-like glia in the central brain (86E01-Gal4; McFlip; hs= 6 min) (single frontal sections). Astrocyte-like glia show variable size and morphologies but cover non-overlapping areas (open white arrow highlight the boundaries). They do however form a continuous mesh in which single cells cannot be visually separated when all cells are labeled (**A.5**). **A.5-6** Magnified view of the morphology of astrocyte-like glia in the central brain (86E01-Gal4; UAS-DM21-GFP; green) (frontal view; maximum density projection; 9x0.3 μ m sections). **A.5** The glial meshwork can be dense (open red arrow) or sparse (open white arrow) within the neuropiles. **A.6** Astrocyte-like glia project fine thready processes outside the neuropiles, presumably into tract regions (open white arrow) (also see Figure 18E.1- 2). **B.1-5** Individual cell

morphologies of astrocyte-like glia in the central brain (86E01-Gal4; McFlip; hs= 4 min). **B.1** A single cell with low density of processes projecting into two neuropile (sub)-regions, specifically the α and α' lobes of the mushroom body (single section). **B.2** Two neighboring cells, one projecting into the ellipsoid body (eb, filled white arrow pointing to cell body, open white arrow to filligrane processes), the other into the lateral accessory lobe (lal, filled red arrow pointing to cell body, open red arrow to spongy processes) showing markedly different density of processes (frontal view; maximum density projection; $4 \times 0.5 \mu\text{m}$). **B.3-4** A single cell projecting into two different neighboring neuropiles but with different structural density, low in the peduncle of the mushroom body (ped), high in the superior intermediate protocerebrum (sip) (filled red arrow points to cell body, open arrows to low (white) and high density (red) regions) (**B.3**; frontal view, maximum density projection, $81 \times 0.5 \mu\text{m}$ sections; **B.4**; single section). **B.5** A cell with high density processes in the lateral medial protocerebrum (single section). **C.1-2** Astrocyte-like glia (**C.1**; 86E01-Gal4; UAS-DM21-GFP-BP) and neuropile regions (**C.2**; nc82) of one hemisphere of the dorso-medial protocerebrum including mushroom body a and b lobes, crepine and medial protocerebrum (single frontal section). **C.3** The stainings shown in **C.1-2**, are converted into structural density maps based on the distance between objects within a brain region. Superimposition of the two maps, showing the anti-correlation of glial and synaptic densities. Regions with high density of astrocyte-like glia appear green; areas with high density of synapses appear magenta (for description of algorithm see Figure 31). Brain regions are characterized by their densities of astrocyte-like glia processes and synapses. Scale bar = $50 \mu\text{m}$ in **A.2**; $10 \mu\text{m}$ in **A.3-6**, **B.1**, **2,5**, **C.1-3**; $5 \mu\text{m}$ in **B.3-4**.

Lower magnification views of the central brain further support this notion that the density of astrocyte-like glia processes is indeed a neuropile-specific feature and that it is in fact anti-correlated with the synaptic density of the respective neuropile region (defined by the Insect Brain Name Working Group, unpublished data). For instance, the mushroom body, which has a high density of synapses, shows a low density of astrocyte-like glia processes. In contrast, the antennal and lateral accessory lobe as well as the optic tubercle, which have lower densities of synapses, show moderate to high densities of astrocyte-like glia processes. To investigate this phenomenon further, we quantified both densities in confocal sections (Figure 16B.1-2) using a home-written Definiens algorithm (also see Figure 31, Figure 32). Superimposition of the density maps of astrocyte-like glia processes (green is high) and of synaptic areas (magenta is high) reveals systemic anti-correlation (Figure 16C.3). Additionally, we manually determined the densities of astrocyte-like glia processes in the major brain neuropiles (Table 4) as classified by the Insect Brain Name Working Group (Insect Brain Name Working Group, unpublished data) (for detail about the analysis, also see Figure 32).

Region		ALG density			Comment
Abbrev.	Full name	low	medium	high	
AL	antennal lobe		+		
AME	accessory Medulla		++		
AMMC	antennal mechanosensory and motor center			+	Many spongy processes
ATL	antler		++		
AVLP	anterior ventrolateral protocerebrum		++		
BU	bulb (or LTR: lateral triangle)				
CAN	cantle (fka wedge)		+		
CRE	crepine		+	+	Many spongy processes
EB	ellipsoid body				
EPA	epaulette		+	++	Many filligrane processes
FB	fan shaped body				
FLA	flange		+		
GA	gall		+		
GOR	grochette		+		
IB	inferior bridge		+		
ICL	inferior clamp		++		
IPS	inferior posterior slope		++		
LAL	lateral accessory lobe			+	
LH	lateral horn			+	
LO	Lobula			+	
LOP	Lobula plate				
MB	mushroom body	--			very low density in calyx, low and filligrane in lobes
ME	Medulla			+	Many spongy processes
NO	noduli			+	
OTU	optic tubercle			+++	Many spongy processes
PB	protocerebral bridge			+++	Many spongy processes
PLP	posterior lateral protocerebrum		+		
PRW	provw		+		
PVLP	posterior ventrolateral protocerebrum		+		
SAD	saddle		+		
SCL	superior clamp			+	
SIP	superior intermediate protocerebrum				
SLP	superior lateral protocerebrum		+		
SMP	superior medial protocerebrum		+		
SOG	suboesophageal ganglion		++		
SPS	superior posterior slope				
VES	vesta		++		
WED	wedge (fka inferior ventrolateral protocerebrum)				

Table 4: Summary of astrocyte-like glia densities in the brain.

Densities of astrocyte-like glia processes were determined as explained in supplemental figure 4. Major brain regions were determined according to the suggestions for classification by the Insect Brain Name Working Group (Insect Brain Name Working Group, unpublished data). Classification has been performed by brain region; the average density was determined as being either low, medium or high. If it was medium, a further

degree of subdivision was introduced (+ = less; +++ = many). For cases in which we observed notable morphologic exceptions, they were described in the comments column.

6.1.6 *Ensheathing glia*

Ensheathing glia are found at the interface between cortical and neuropile regions (dark blue, illustrated in Figure 17A.1) and entering the neuropile regions (light blue, illustrated in Figure 17A.1). They can be broadly subdivided into neuropile and tract associated ensheathing glia (Figure 17A.2-3). The cell bodies of neuropile associated ensheathing glia are found at the boundaries of all neuropiles, not only at the distal boundaries adjacent to the cortex regions but also at the proximal boundaries deeper in the brain which are abutting other neuropiles (Figure 17B.2). Multi-color mosaic experiments show that the ensheathing glia form a dense layer around the neuropile regions (Figure 17B.1, 3). In addition, they frequently branch into the neuropiles first perpendicular and then parallel to their surface, presumably to accompany neuronal projections, but possibly also tracheal branches (see Figure 21D.6-8) (Pereanu et al., 2007).

The cell bodies of tract associated ensheathing glia are found in non-cortical regions deep inside the brain (Figure 17C.2) and along the neuronal tracts with which they associate (data not shown). Tract-associated ensheathing glia envelop neuronal projections that connect different neuropiles and brain regions, such as the giant fiber tract (Figure 17C.3), the neck connective (Figure 17C.4) and peripheral nerves (Figure 17A.3). The tract ensheathing glia form flat, long parallel strands that are frayed at the margins. Neighboring cells can interweave without much direct cell-cell contact (Figure 17C.3). Cross-section reveals that the glia enmesh multiple fiber tracts. Ensheathing glia interact in various ways with other glial subtypes: At the cortex-neuropile interface, cortex and ensheathing glia form a fairly smooth layer of contact (Figure 18C.1- 2). In the cortex region, cortex glia wrap neuronal projections; this task is taken over by the ensheathing glia, once the neuronal projections reach the cortex-neuropile border. Ensheathing glia generally enclose the cell bodies of astrocyte-like glia at the boundaries of the neuropiles (Figure 18D.1-2). Fine astrocyte-like glia processes project into the neuropile sheath (Figure 17E.1-2) and even beyond, into the cortical region (Figure 18E.1- 5). Within many neuropiles, ensheathing glia define the boundaries

of subcompartments, while astrocyte-like glia ignore such boundaries. More generally, astrocyte-like and ensheathing glia jointly populate the neuropiles but – except for Lamina and Medulla (also see Figure 20, Figure 21) - without any obvious spatial organization. The following sections, in which we describe the visual and olfactory systems, will provide ample examples for these general observations.

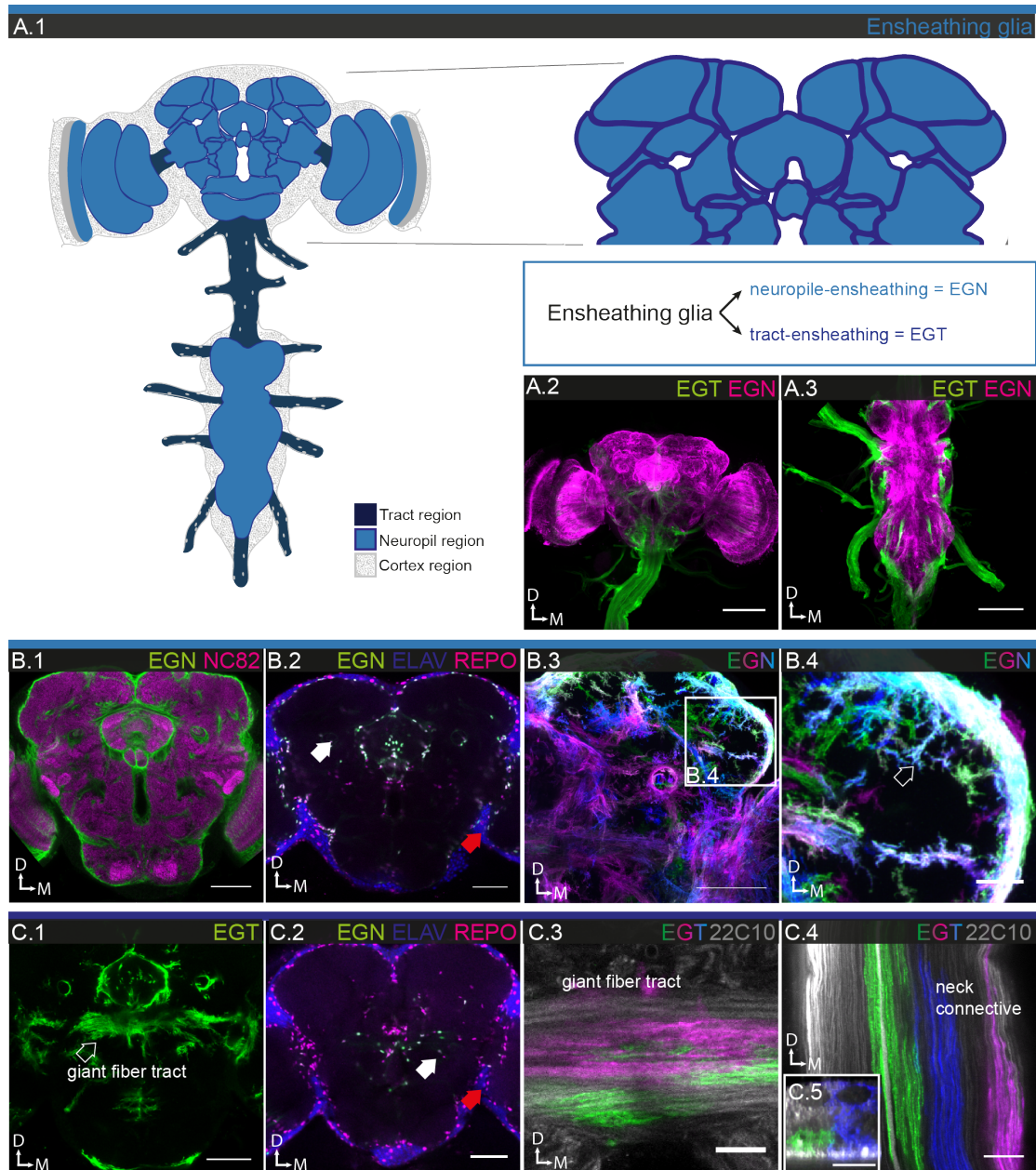


Figure 17: Morphology of ensheathing glia.

A.1 Schematic showing the localization of ensheathing glia in the nervous system. One set of ensheathing glia are closely associated with the neuropiles (neuropile-ensheathing glia; EGN), where they are predominantly found at the boundaries (dark blue) and from whence they branch into the neuropile region (light blue). A

second set of ensheathing glia are associated with large axon tracts (tract-ensheathing glia; EGT) in both CNS and PNS. **A.2-3** Double labeling of tract-ensheathing and neuropile ensheathing glia reveals the entire population of ensheathing glia in the CNS (EGN; 56F03-LexA;lexAOp-myr-smGFP-V5; magenta; EGT; 75H03-Gal4; UAS-myr-smGFP-HA, green) (frontal view, maximum density projection, 122x1 μ m sections). **A.2** Brain and neck connective, **A.3** Ventral nerve cord and PNS. **B.1-4** Neuropile ensheathing glia (EGN) **B.1** General expression pattern in the central brain (56F03-Gal4; UASmyr:smGFP-V5; green; nc82; magenta) (single frontal section). **B.2** Location of neuropile-ensheathing glia cell bodies in the central brain (56F03-Gal4; UAS-nls-GFP; green; REPO; magenta; ELAV; blue) (single coronal section). While neuronal cell bodies are always located in the cortical regions (blue, filled red arrow), neuropile ensheathing glial cell bodies are mostly found in between neuropile regions (filled white arrow). **B.3-4** Individual cell morphologies of neuropile-associated ensheathing glia in the protocerebrum (56F03-Gal4; McFlip; hs= 10 min) (frontal view; maximum density projection, 25x1 μ m sections). The glia take on many different shapes and sizes, as they ensheath and enter the neuropile regions. Note the complex and fine protrusions (arrow) projecting into the neuropile regions. **C.1-4** Tract-ensheathing glia (EGT) **C.1** General expression pattern in the central brain (75H03-Gal4; UASmyr:smGFP-V5; green) (single frontal section). **B.2** Location of neuropile-ensheathing glia cell bodies in the central brain (75H03-Gal4; UAS-nls-GFP; green; REPO; magenta; ELAV; blue) (single coronal section). While neuronal cell bodies are always located in the cortical regions (filled red arrow), tract-ensheathing glia cell bodies are mostly found in between neuropile regions (filled white arrow). **C.3-4** Individual cell morphologies of neuropile-associated ensheathing glia in the protocerebrum (75H03-Gal4; McFlip; hs= 5 min; 22C10; grey) (single frontal sections). **C.3**. Giant fiber tract and **C.4** Neck connective. Tract glia are extended along the long axis of the nerves; their ends are ragged but with their lateral neighbors they form a neatly contiguous sheath (see **C.5**). Scale bar = 100 μ m in **A.2-3**; 50 μ m in **B.1-3**, **C.1**; 10 μ m in **B.4**, **C.3-5**.

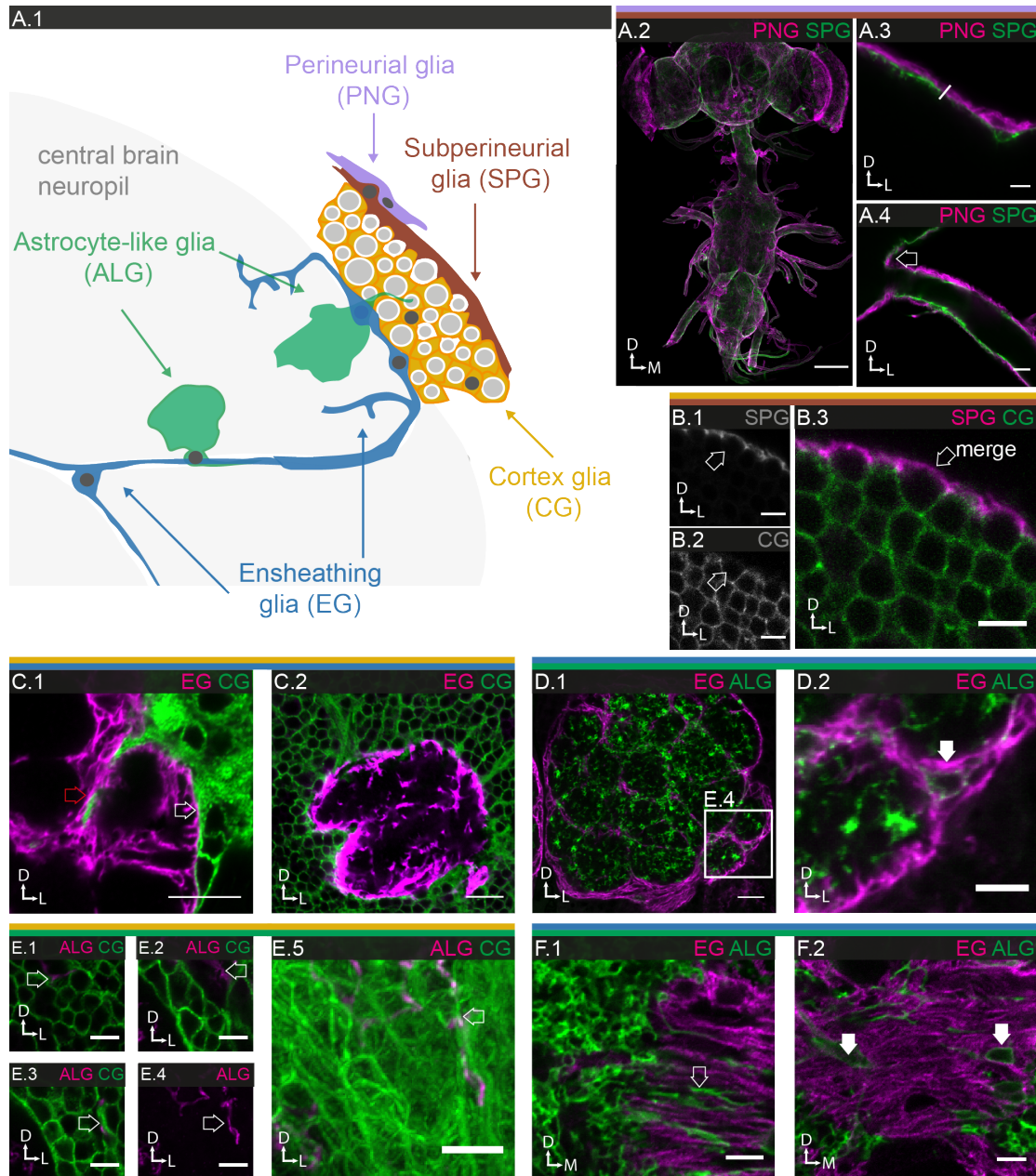


Figure 18: Characterization of glia-glia interactions.

A.1 Schematic illustrating the interactions of the different generic glial subtypes in a central brain neuropile.

A.2-4 Relationship between perineurial and subperineurial glia on the surface of CNS and PNS (PNG; 85G01-LexA; lexAop-myr-smGFP-V5; magenta; SPG; 54C07-Gal4; UAS-myr-smGFP-HA; green) (frontal view, maximum density projection, 85x1 μ m sections). **A.3** High magnification view showing that perineurial glia (magenta) lie directly on top of the subperineurial glial layer. The overall thickness of the surface glial sheath is ~2-3 μ m, but varies from region to region. **A.4** Continuation of the surface glial sheath at the boundary of CNS and PNS, as seen at the exit of a peripheral nerve. **B.1-3** Relationship between subperineurial (**B.1**) and cortex (**B.2**) glia, merge in (**B.3**), in the central brain (SPG; 54C07-LexA; lexAop-myr-sm-GFP-V5; magenta; CG; 77A03-Gal4; UAS-myr-smGFP-HA; green) (single frontal section). Subperineurial glia (**B.1**) form a contiguous cover over the entire cortical region. Occasionally, cortex glia do not fully envelope neuronal cell bodies, in which cases the subperineurial glia provide the necessary closure (open white arrow in **B.3**). **C.1-2**

Relationship between cortex and neuropile-ensheathing glia (EGN) in antennal lobe (**C.1**) and mushroom body calyx (**C.2**) (CG; 77A03-Gal4; UAS-myr-smGFP-HA; green; EGN; 56F03-LexA; lexAop-myr-smGFP-V5; magenta) (single frontal section). The two subtypes abut in a very smooth fashion with little or no intermingling at the interface between the two cell types (open white arrow). However, occasionally, cortex glial protrusions reach into the neuropile regions, as seen here at sub-compartmental boundaries within the antennal lobe (open red arrow **C.1**). **D.1-2** In the antennal lobe, cell bodies of astrocyte-like glia are embedded within the ensheathing glial layer (ALG; 86E01-Gal4; UAS-myr-smGFP-HA; green; EGN; 56F03-LexA; lexAop-myr-smGFP-V5; magenta)(filled white arrow)(single frontal sections). **E.1-5** Relationship between cortex and astrocyte-like glia in the cortical regions (CG; 77A03-Gal4; UAS-myr-smGFP-HA, green; ALG; 86E01-LexA; lexAop-myr-smGFP-V5; magenta) (**E.1-3**; single sections; **E.4-5**; frontal view, maximum density projection, 14x1 μ m sections; dorsal posterior protocerebrum). Astrocyte-like glia sends fine processes into the cortex glia region (open white arrows). **F.1-2** In the protocerebrum, astrocyte-like glial processes are seen projecting into the ensheathing glia layer that forms the boundary of this neuropile region (open white arrow) (ALG; 86E01-LexA; lexAop-myr-smGFP-V5; EGN; 56F03-Gal4; UAS-myr-smGFP-HA; magenta)(arrows)(single frontal sections). **F.2** As has been observed in the antennal lobe, ALG cell bodies in this region are also embedded into the ensheathing glial sheath (filled white arrow). Scale bar = 100 μ m in **A.1**; 10 μ m in **C.2**; 5 μ m in **A.2-3**, **B.1-3**, **C.1**, **D.1-5**, **E.1-4**.

6.1.7 *Summary*

In addition to having access to the largest Gal4 collection with expression in the adult fly brain, the current study benefited from several technical developments. A novel multi-color mosaic technique with highly sensitive immuno-histochemical reporters permitted visualization of finest morphological details in individual cells. Moreover, the use of two sensitive yet completely orthogonal expression systems facilitated the analysis of glia-glia and glia-neuron interaction. Finally, excellent commercial as well home-scripted image analysis tools made possible the 3D rendering of the often complex glial cell morphologies as well as a quantitative analysis of key morphological features. Using these tools, we characterized the generic glial features of the five major glial populations at unprecedented resolution. We not only looked at the generic expression pattern and overall subtype-specific cell counts, but also investigated the morphology of single cells, the interaction of cells of one subtype with one another, the interaction of one subtype with the neighboring subtypes and not at last, the interactions of glial cells and neuronal entities.

6.2 Characterization of glia in the visual system

The visual system makes up a large portion of the fly brain and has been studied in great detail anatomically and functionally (for review: (Borst, 2009; Borst et al., 2010; Fischbach and Hiesinger, 2008; Meinertzhagen, 1993; Morante and Desplan, 2008)). The glia of the visual system have been investigated in previous work, in particular in the Lamina (Edwards et al., 2012). Especially in the Lamina the glia show very strong regional specializations, earning them a dedicated nomenclature, yet at the same time raising the question whether the different types of glia found in the Lamina are in fact equivalent to the generic subtypes we described before (also see 6.1.1-6.1.6). In the following sections, we will describe the glia in the different portions of the visual system, from Lamina, Medulla, inner and outer chiasm to Lobula complex, and address the issue of equivalency between region-specific and generic subtypes. To this end, we employ the previously introduced tools – Gal4 driven generic expression pattern co-labeled with specific antibodies, double labelings of Gal4/LexAs and multicolor-flpouts. Whenever available, we make use of region-specific Gal4 drivers; otherwise, region-specific morphologies are characterized using the previously identified generic Gal4 driver lines.

6.2.1 *Glia in the Lamina*

The Lamina is the distal-most optic neuropile and the first relay station in which photoreceptor axons terminate in a retinotopic fashion. Incoming photoreceptor axon bundles connect to Lamina cartridges, in which complex synaptic connections are made between photoreceptors R1-R6 and Lamina monopolar neurons L1-L5. Six types of glial cells have been identified, which are organized in distinct layers: fenestrated, pseudo-cartridge, distal and proximal satellite, epithelial and marginal glia ((Edwards et al., 2012; Tix et al., 1997), for review: (Edwards and Meinertzhagen, 2010)). Based on anatomy and, for some cases, marker gene expression, fenestrated and pseudo-cartridge glia are believed to be specialized types of perineurial and subperineurial glia, distal and proximal satellite glia specialized cortex glia, epithelial glia specialized astrocyte-like glia,

and marginal glia specialized ensheathing glia (Edwards and Meinertzhagen, 2010; Edwards et al., 2012; Shaw and Varney, 1999).

In the *Janelia Gal4* collection, we identified driver lines specifically expressed in each of these Lamina glial subtypes (see also Table 5). To establish equivalency with the generic glial subtypes, we combined Lamina glial drivers with generic glial drivers and appropriate reporters using the orthogonal expression systems *Gal4:UAS* and *LexA:LexAop* and checked for co-expression of the two drivers in the same cell populations.

Driver	Region-specific subtype	Generic subtype	Description	Cell count	+/- (SEM)
47G01	Fenestrated	Perineurial	Thin sheet of cells forming distal-most layer of Lamina		
50A12	Pseudo-Cartridge	Subperineurial	Thin sheet of cells–enwrap entering photoreceptor axons, handcounts	~100 (n= 2)	
27H11	Perineurial chalice	Perineurial	Chalice-forming thin layer of perineurial glia surrounding the Lamina		
no specific	Subperineurial chalice	Subperineurial	Chalice-forming thin layer of subperineurial glia surrounding the Lamina		
53B07	Distal satellite (distal Lamina cortex)	Cortex	Honey comb-like morphology, surrounding neuronal cell bodies in the distal Lamina cortex	127 (n=9)	22
46H12	Proximal satellite (proximal Lamina cortex)	Cortex	Flat dense cells capping neuronal cell bodies in the proximal Lamina cortex	255 (n=8)	12.46
55B03	Epithelial	Astrocyte-like	Long thin mesh-like cells intercalating between the synaptic portion of several neighboring Lamina cartridges	475 (n=14)	14.3
35E04	Marginal	Ensheathing	ensheath the proximal third of Lamina cartridges	109 (n=12)	4.9

Table 5: Summary of Lamina-specific driver lines, cell counts per subtype and description of drivers.

The fenestrated glia of the Lamina make up the distal-most layer, which is thin and tightly enwraps the entrance points of the photoreceptor axon bundles. Double labeling with the perineurial-specific reference driver (*85G01*) shows that fenestrated glia are a specialized form of perineurial glia (Figure 19B.1-3), adapted to accommodate the ingrowth of the 800 photoreceptor axon bundles into the optic lobe.

The next proximate layer is also thin and formed by the pseudocartridge glia (*50A12*), which also enwrap the entrance points of the photoreceptor axon

bundles (Figure 20, Panel B). Double-labeling with the generic subperineurial reference driver (*54C07*) shows that pseudocartridge glia are a specialized form of subperineurial glia (Figure 19C.1- 3). Our cell count places the total number of pseudocartridge glia at ~100 (handcounts) (Table 5), suggesting that, on average, a single glial cell enwraps ~7 incoming photoreceptor axon bundles. Multi-color mosaic experiments show pseudocartridge glia as large irregularly shaped cells that extend along the antero-posterior axis of the Lamina (Figure 20B.1- 2); co-labeling of axons reveals that indeed multiple ommatidial axon bundles are enveloped by a single glia cell (Figure 20B.3- 6). Higher magnification views show that pseudocartridge glia ensheath individual fibers (Figure 20B.3-4) but, interestingly, individual glia do not follow the axon tracts along their entire route along the distal-proximal axis (Figure 20B.5-6).

Directly underneath lies the Lamina cortex, which harbors the cell bodies of the L1-L5 interneurons and two layers of glial cells, the distal (*53B07*) and proximal (*44B12*) satellite glia (Figure 20, Panels C, D). Double labeling with the generic cortex glia reference driver (*77A03*) shows that both types of satellite glia are indeed specialized forms of cortex glia (distal satellite glia: Figure 19D.1- 3, proximal satellite glia: Figure 19D.4- 6). Our cell count places the total number of distal satellite glia at ~125 and that of proximal satellite glia at ~250 (Table 5), suggesting that individual distal satellite glia enwrap ~10, proximal satellite glia ~3 Lamina cartridges. Multi-color mosaic experiments reveal distal satellite glia as uniformly large and oblong in shape extending along the anterior-posterior axis of the Lamina and enveloping ~10 cartridges (Figure 20C.1- 2). Higher magnification shows that distal satellite glia form a thin honeycomb-like mesh that houses the Lamina neuron cell bodies. As observed for other glial subtypes, neighboring distal satellite glia frequently collaborate in enclosing a single neuronal entity, here, along all three axes: Within the plane of the cortical layer, two glial cells may contribute to forming the honeycomb that encloses a single Lamina cartridge (Figure 20C.4). Along the proximal-distal axis, neighboring distal satellite glial cells overlap and secure the enclosure of the cartridge along its long axis (Figure

20C.2). Unlike cortex glia elsewhere in the CNS, more than one neuronal cell body can be found within one glial pocket (Figure 20C.3).

By comparison, the proximal satellite glia have very distinct morphological characteristics. The cells are smaller and show more variable orientation along the anterior-posterior axis as compared to their distal counterparts (compare Panels C and D of Figure 20). Higher magnification shows that the cells are compact and form a dense layer at the interface of Lamina cortex and neuropile (Figure 20D.1-3). On their distal surface, they form pocket-like structures that enclose neuronal cell bodies, presumably of L5 Lamina interneurons (Figure 20D.4), on their proximal surface, they send protrusions into the synaptic region (Figure 20D.3, open white arrow).

The next proximate layer is deep and comprises the neuropile portion of the Lamina, together with the epithelial glia (*55B03*) (Figure 20, Panel E). Double labeling with the generic astrocyte-like glia reference driver (*86E01*) shows that epithelial glia are a specialized form of astrocyte-like glia (Figure 19E.1-3). Our cell count places the total number of epithelial glia at ~470 (Table 5), suggesting that, on average, one glial cell associates with two Lamina cartridges (Edwards and Meinertzhagen, 2012). Multi-color mosaic experiments show epithelial glia forming a well-ordered honeycomb lattice in which the synaptic portions of the cartridges are ensconced (Figure 20E.1). Interestingly, individual cartridges are not wrapped by one glial cell (Figure 20E.3); instead, epithelial glia are located at the corners of cartridges and contribute to the wrapping of up to three units (Figure 20E.3). The main branching/segmentation pattern of an individual epithelial glia is maintained along the distal-proximal axis (Figure 20E.4-6); however, the glia also form smaller protrusions into the cartridge, which appear to be more localized. Incoming photoreceptor axons are found in close association with the epithelial glial lattice (Figure 20E.1-2).

Finally, the marginal glia (*60F04*) form a contiguous layer at the proximal margin of the Lamina (Figure 20, Panel F). Double-labeling with the generic ensheathing glial reference driver (*56F03*) shows that marginal glia are a specialized form of

ensheathing glia (Figure 19F.1- 3). Our cell count places the total number of marginal glia at ~100 (Table 5), suggesting that, on average, one glial cell associates with 8 cartridges. Multi-color mosaic experiments reveal marginal glia as long, narrow cells oriented along the dorso-ventral axis of the Lamina (Figure 20F.1- 2), associating with up to ten cartridges. Co-labeling with synaptic marker shows that marginal glia ensheath the proximal portion of the cartridges and extend processes into the bottom third of the neuropile layer (Figure 20F.2). The length of these processes projecting into the Lamina neuropile is variable (Figure 20F.5). Marginal glia also send protrusions proximally into the outer chiasm (Figure 20F.2).

In addition to these known Lamina glia subtypes, we found two new glial expression patterns. Both types form a thin chalice-like ensheathment of the outer perimeter of the Lamina. Double labeling of *27H11* with the perineurial reference driver (*85G01*) show that these glia are a specialized version of perineurial glia (Figure 19A.4- 6); in multi-color mosaic experiments with the subperineurial reference driver (*54C07*), we found single cells in the Lamina chalice, suggesting that the chalice also comprises a subperineurial layer (Figure 19B.4), like every other surface of the *Drosophila* peripheral and central nervous system.

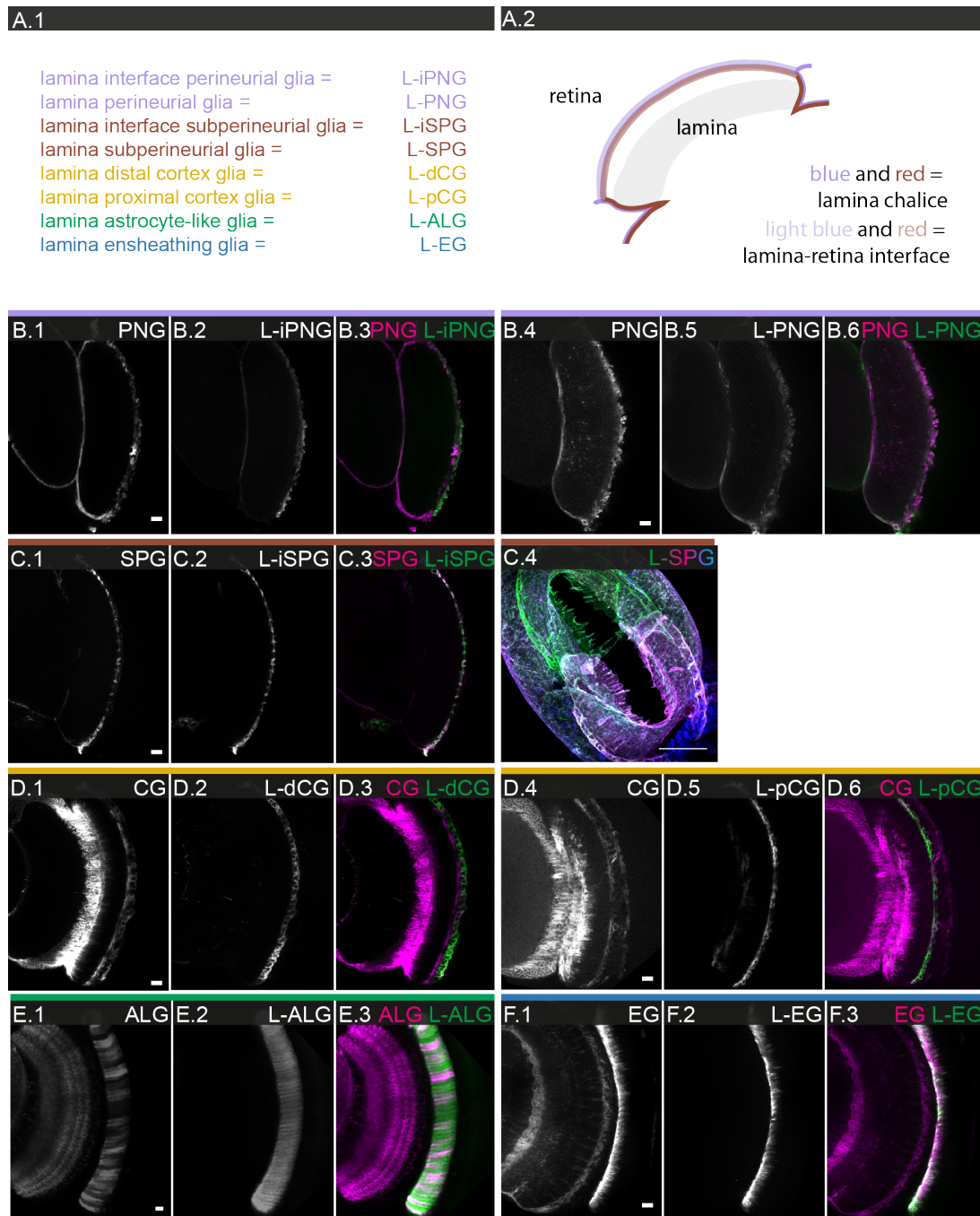


Figure 19: Equivalency of Lamina-specific glial subtypes with generic glial subtypes.

Prior studies had classified the glia of the Lamina into different subtypes, based on position and morphology. The current study identifies specific drivers for known and novel Lamina-specific glial subtypes and demonstrates equivalency between these region-specific cell types and generic cell types. The reporters are *lexAop-myr-smGFP-V5* and *UAS-myr-smGFP-HA*. Based on the equivalency evidenced for all the Lamina glia and generic glial subtypes, we suggest the nomenclature drawn in **A.1**. **A.2** illustrates the relative location of newly identified chalice-like surface glia. **B.1-3** Double labeling of generic perineurial glia (85G01-LexA; A1) and Lamina fenestrated glia (19D10-G4; A2); a single frontal section (1µm) is shown. **B.4-6** Double labeling of generic perineurial glia (85G01-LexA; A4) and perineurial chalice-like glia (27H11-Gal4; A5); merge (A.6); single frontal section (1µm). **C.1-3** Double labeling of generic subperineurial glia (54C07-Gal4; B.1) and

Lamina pseudo-cartridge glia (50A12-LexA; B.2), merge (B.3); single frontal section (1 μ m) shown. **C.4** Structure of chalice-like subperineurial glia (maximum density projection, tilted sagittal section, 84x1 μ m projection.) **D.1-3** Double labeling of generic cortex glia (77A03-LexA; D.1) with Lamina distal satellite glia (53B07-Gal4; D.2), merge (D.3); single frontal section (1 μ m) shown. **D.4-6** Double labeling of generic cortex glia (77A03-LexA ;C.4) with Lamina proximal satellite glia (44B12-Gal4; C.5), merge (C.6); single frontal section (1 μ m) shown. **E.1-3** Double labeling of generic astrocyte-like glia (86E01-LexA; F.1) with Lamina epithelia glia (55B03-Gal4; F.2), merge (F.3); single frontal section (1 μ m) shown. **F.1-3** Double labeling of generic ensheathing glia (56F03-LexA; G.1) with Lamina marginal glia (60F04-Gal4; G.2), merge (G.3); single frontal section (1 μ m) shown. Scale bar = 10 μ m in all images.

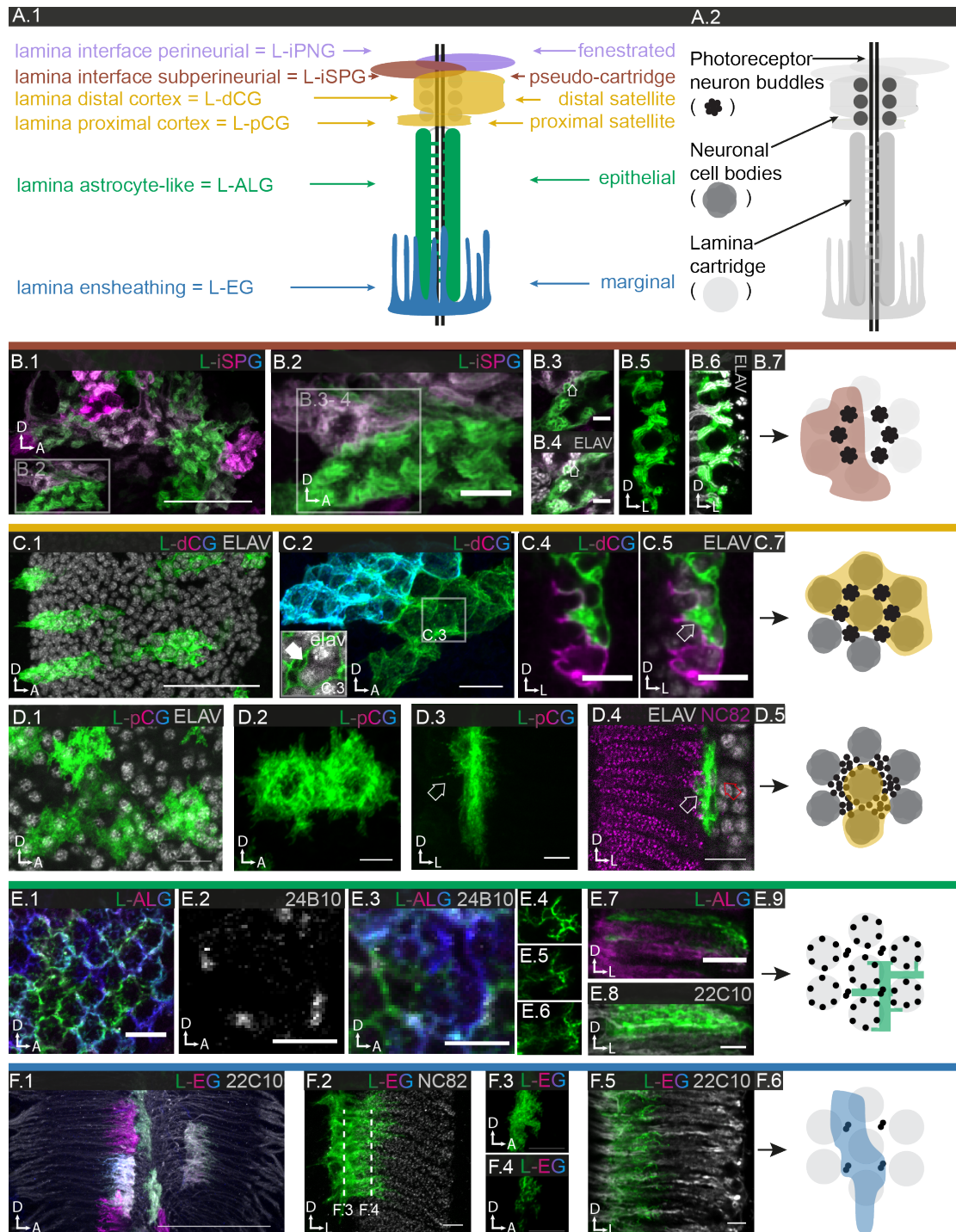


Figure 20: Glial cell morphologies in the Lamina and interactions with neurons.

A.1 Illustration of the general Lamina anatomy. The Lamina is the first neuropile in the visual pathway where photoreceptor axons project retinotopically onto Lamina interneurons. Shown on the left is a Lamina cartridge, the physical entity formed by photoreceptor-interneuron contact. All generic glial subtypes are present but show Lamina-specific morphologies, inspiring the distinct nomenclature for Lamina glia. In the schematic on the right, the planes of the most frequently used confocal sections are depicted. In the panels below, sagittal and frontal views of the different glial cell types in combination with different neuronal entities are presented and illustrated schematically (last column). **B.1-6** Individual cell morphologies of Lamina subperineurial (pseudo-cartridge) glia, as visualized by a subperineurial (54C07)-Gal4 driving multicolor-

flpout reporters (4 min hs), neuronal tracts are co-labeled (22C10; grey; **B.4, B6**). **B.1-2** Sagittal views, maximum density projections, 9x0.5µm sections, different magnifications. Subperineurial (pseudo-cartridge) glia are large oblong cells (extended along a-p axis), with each cell enveloping several/multiple incoming retinula fibers. **B.3-4** Sagittal section (1µm) of a single subperineurial (pseudo-cartridge) glia. Glia (green, **B.3**), axon tracts (grey, **B.4**). **B.5-6** Single cell, frontal view, maximum density projection, 6x0.5µm sections. Glia (green, **B.5**), axon tracts (grey, **B.6**). **B.3-6** Retinula fibers are ensheathed by fine protrusions of the distal surface of the subperineurial (pseudo-cartridge) glia (open white arrows). **B.7** Scheme illustrating the position of a single cell relative to neuronal tracts (black dots). Note that a single dot may represent tracts constituted of multiple neurons. **C.1-5** Individual cell morphologies of distal cortex (satellite) glia, as visualized by a distal satellite (53B07)-Gal4 driving multicolor-flpout reporters (3-4 min hs); neuronal cell bodies are co-labeled (ELAV; grey; **C.1, C.3**). **C.1** Sagittal view, maximum density projection, 84x0.5µm sections. Distal cortex (satellite) glia are uniformly large and oblong in shape (along a-p axis) and envelop several/multiple cartridges. **C.2** Sagittal view, maximum density projection, 12x0.5 µm sections. Distal satellite glia form honey comb-like structures that house Lamina neuron cell bodies. Note that at their borders, two satellite glia may jointly form one honeycomb. **C.3** Distal satellite glia ensheath neuronal cell bodies as well as neuronal tracts running through the distal part of the cortex (filled white arrow). Unlike elsewhere in the CNS, more than one neuronal cell body can be found within one distal cortex glial pocket. **C.4-5** Single frontal section (1µm) of two adjacent distal cortex (satellite) glia (green, magenta), showing that the cells partially grow on top of each other (open white arrow). **C.6** Scheme illustrating the position of a single distal satellite glia cell relative to neuronal tracts (black dots) and neuronal cell bodies (grey filled circles). **D.1-5** Individual cell morphologies of proximal cortex (satellite) glia, as visualized by a proximal satellite (44B12)-Gal4 driving multicolor-flpout reporters (3-4 min hs); neuronal cell bodies are co-labeled (ELAV; grey, **D.1, D.5**). **D.1** Sagittal view, maximum density projection, 8x0.5µm sections. Proximal cortex (satellite) glia are smaller and show more variable orientation along the antero-posterior axis, as compared to their distal counterparts. **D.2-3** Magnification of a single cell. **D.2** Sagittal view, maximum density projection, 12x0.5µm sections. **D.3** Frontal view, maximum density projection, 25x0.5µm sections. Proximal cortex (satellite) glia are thin and compact/dense cells. **D.4** Frontal view, single 0.5µm section. Proximal satellite glia lie at the interface between Lamina cortex and neuropile. On their distal surface, they form pockets (open white arrow) for neuronal cell bodies (ELAV, grey), on their proximal surface, they send protrusions into the neuropile (nc82, magenta). **D.5** Scheme illustrating the position of a single proximal satellite glia cell relative to neuronal tracts (black dots) and neuronal cell bodies (grey filled circles). **E.1-7** Individual cell morphologies of astrocyte-like (epithelial) glia, as visualized by an epithelial glial (55B03)-Gal4 driving multicolor-flpout reporters (9 min hs); sagittal views. **E.1** Single sagittal section showing honeycomb lattice of epithelial glia. **E.2-3** Single sagittal section (1µm) through one cartridge. **E.2** Photoreceptor projections (24B10, grey), **E.3** Merge with epithelial glia (blue, green). Photoreceptor projections are in close contact with epithelial glial lattice. **E.4- 6** Different sagittal sections (0.5 µm) through a single epithelial glia cell. **E.4** Distal, **E.5** Medial, **E.6** Proximal section, showing that the main branches of the epithelial glia are maintained but smaller processes appear and disappear. **E.7** Single frontal section (0.5µm) of mosaic epithelial glia (magenta, green) revealing a mesh-like structure extending throughout the Lamina neuropile region. **E.8** Frontal view, maximum density projection, 8x0.5µm sections, showing co-labeling of single epithelial glia cell (green, mosaic driver 86E01-LexA) with neural tracts (22C10, grey). **E.9** Scheme illustrating the position of a single epithelial glia cell relative to Lamina columns (grey surrounded circles). **F.1-2** Individual cell morphologies of ensheathing (marginal) glia,

as visualized by a marginal glial (35E04)-Gal4 driving multicolor-flpout reporters (6 min hs). **F.1** Sagittal view, maximum density projection, 59x0.5 μ m sections. Marginal glia are narrow cells oriented along the dorso-ventral axis. **F.2** Co-labeling of single marginal glia (green) with synaptic marker (nc82, grey). Marginal glia send many fine protrusions deep into the Lamina neuropile (30% of Lamina thickness) as well as fine processes medially into the outer chiasm. A single marginal glial cell may ensheath as many as 8 Lamina cartridges. **F.3-4** Sagittal views of single marginal glial cell. **F.3** Maximum density projection, 34x0.5 μ m, **F.4** single 0.5 μ m section, showing that protrusions are uneven in length. **F.5** Single frontal (1 μ m) section showing double labeling of marginal glia (56F03-Gal4, green) and axons (22C10, grey). Marginal glia send many fine protrusions deep into the Lamina neuropile (30% of Lamina thickness). **F.6** Scheme to illustrate the position of a single cell relative to neuronal tracts (black dots) and Lamina columns (grey circles). Scale bar = 10 μ m in **B.1-2, C.1-2, D.1-2, F.1**; 5 μ m in **B.3-5, D.3-5, E.4-8, F.2-5**.

6.2.2 *Glia in the Medulla*

The Medulla is the second optic relay station onto which photoreceptor neurons R7-R8 and Lamina interneurons L1-L5 project in a retinotopic fashion. The Medulla neuropile comprises ten distinct layers of synaptic connections (M1-M10) that are organized into retinotopic columns. R8 terminates in layer M3, R7 in layer M6 (Fischbach, 1989). Notably, the Medulla derives from two distinct primordia; only during pupariation, distal (M1-M6) and proximal (M7-M10) Medulla fuse at the serpentine layer (M7) (Hofbauer, 1990; Meinertzhagen, 1993). The Medulla cortex contains cortex glia that are morphologically similar to those found in the central brain and have been described under generic glial subtypes. The Medulla neuropile is populated by two types of glia – astrocyte-like and ensheathing glia.

Driver	Region-specific subtype	Generic subtype	Description	Cell count	+/- (SEM)
31E10	Medulla ALG	ALG	Wide columnar or square shape cells of variable length/size	371 (n=18)	32.8
73B10	Medulla EGN	EGN	Long, thin columnar cells with collateral branches in specific distal Medulla layers (M3, M6, M7)	345 (n=)	7.9

Table 6: Summary of Medulla-specific driver lines, their cell counts and description of the drivers.

In the *Janelia Gal4* collection, we identified lines with Medulla-specific expression (Table 6), but in all cases the expression is somewhat mosaic. The cell bodies of both types of glia are found surrounding the Medulla neuropile, but also in the serpentine layer, which forms the boundary between distal and proximal Medulla. Using these Medulla-specific drivers (*31E10*, *73B10*), we count ~370 and ~350 cells (Table 6), respectively, which is an underestimate but nevertheless suggests a 1:1 ratio between astrocyte-like and ensheathing glia. For astrocyte-like glia, multi-color mosaic experiments reveal three different situations (Figure 21, Panel B). Astrocyte-like glia with cell bodies located in the distal Medulla cortex occupy the distal Medulla, forming irregular columnar structures and sending fine long processes into the outer chiasm (Figure 21B.1-2, 7). These processes run alongside neuronal tracts and are ensheath by outer chiasm glia (Figure 21B.7, 8) (also see 6.2.3, Figure 22). Astrocyte-like glia with cell bodies located in the proximal

Medulla cortex occupy the proximal Medulla and form irregular square-shaped structures (Figure 21B.1- 2, open red arrow). Astrocyte-like glia with cell bodies located in the cortical circumference of the serpentine layer branch out into both distal and proximal Medulla (Figure 21B.1- 2, white filled arrow). All astrocyte-like glia in the Medulla look spongy / show a high structural density that is typically associated with lower synaptic density (Figure 21B.3- 6). Like elsewhere in the brain, they show neat tiling and do not overlap with neighboring astrocyte-like glia (Figure 21B.1- 2). For ensheathing glia, multi-color experiments also reveal three different scenarios (Figure 21, Panels C, D). Ensheathing glia with cell bodies located in the distal Medulla cortex invade the distal Medulla as highly columnar structures (Figure 21C.2- 3). These glia show a characteristic branching pattern around layers M3 and M6 (Figure 21C.3), where photoreceptors R8 and R7 terminate, and in M7, the serpentine layer. Both at the distal margin and in the serpentine layer, these ensheathing glia form a rather dense sheath (Figure 21C.4). Ensheathing glia with cell bodies located in the cortical circumference of the serpentine layer send columnar branches into both distal and proximal Medulla (Figure 21C.4). However, we find no cell bodies of ensheathing glia at the proximal margin of the Medulla. Instead, we find many fine processes invading the proximal Medulla from the inner chiasm; these processes are formed by the inner chiasm glia (Figure 21C.5) (also see 6.2.3). To have a closer look at the distal ensheathing glia, we co-labeled the incoming photoreceptor axons. In all layers, the photoreceptor axons are closely associated with the ensheathing glia, however, in the layers in which photoreceptor axons terminate the glial processes are enlarged (M3) or even form a broad meshwork (M6) (Figure 21D.1- 5). Finally, we examined the relationship between ensheathing glia and the tracheal network, which pervades the Medulla mostly in a columnar fashion. We observe close association of glia with tracheal branches and 3D reconstruction suggests that tracheal branches are largely if not completely covered by the ensheathing glia (Figure 21D.6 -7).

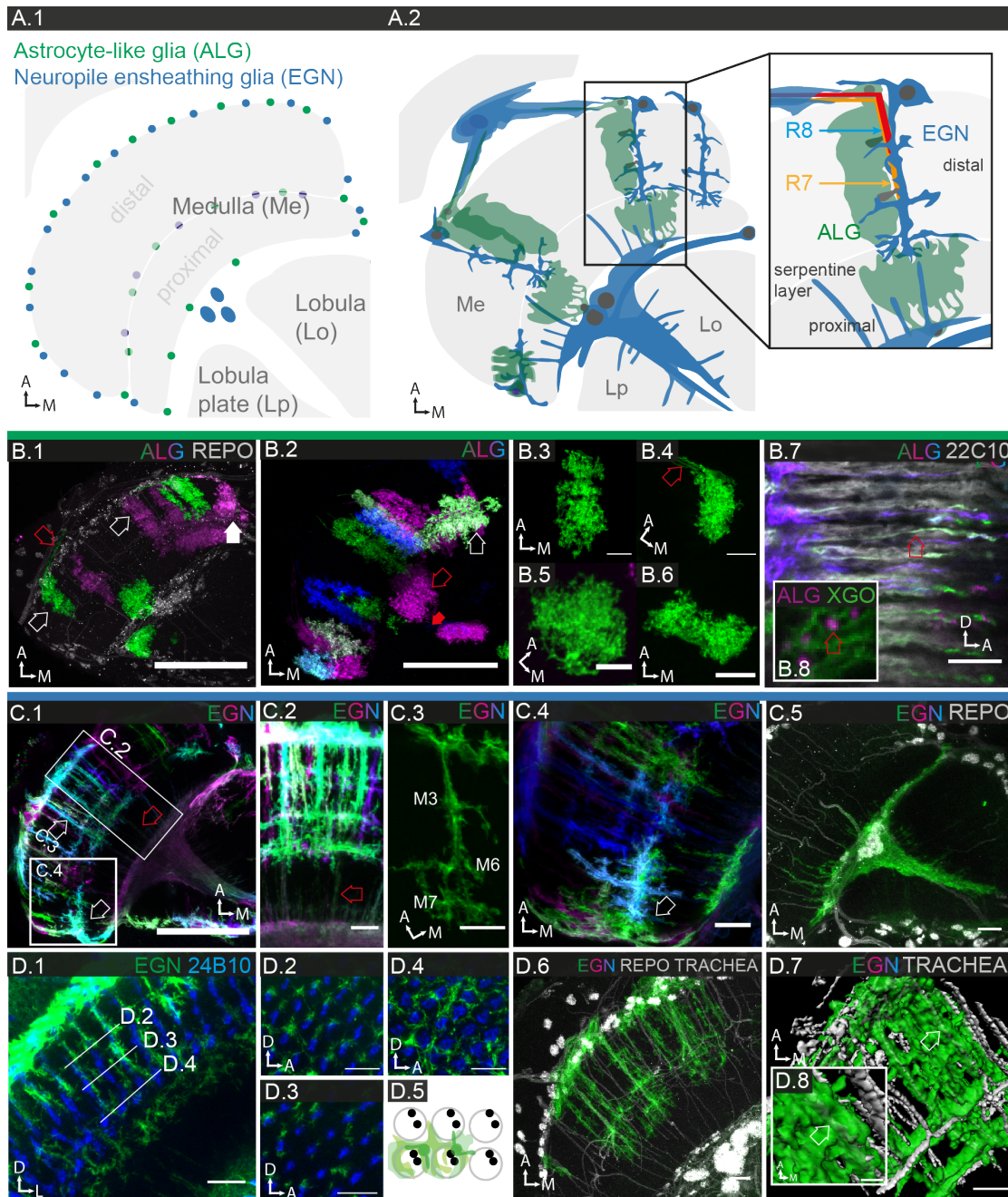


Figure 21: Glial cell morphologies in the Medulla and interactions with neurons.

A.1 Schematic depicting the main features of the two major glial subtypes that populate the Medulla, astrocyte-like glia (ALG, green) and ensheathing glia (EG, blue). A Medulla column is magnified and illustrates the relationship between different glial subtypes and photoreceptor projections. **A.2** Schematic depicting the location of astrocyte-like (green) and ensheathing (blue) glial cell bodies. Cell bodies are located at the distal and proximal border of the Medulla, as well as the serpentine layer, which forms the border between distal and proximal Medulla. **B.1-7** Individual cell morphologies of astrocyte-like glia, as visualized by the astrocyte-like glial (86E01-) Gal4 driving multicolor-flpout reporters (3-8 min hs). Coronal view; maximum density projections; **B.1** 6x0.5 μ m sections, co-labeling of glial nuclei (REPO, grey); **B.2** 60x0.5 μ m sections. Three different situations are observed. Astrocyte-like glia with cell bodies located in the distal Medulla cortex occupy the distal Medulla, forming irregular columnar structures (open white arrows) and sending fine

processes toward the outer chiasm (open red arrow, **B.1-2**). Astrocyte-like glia with cell bodies located in the proximal Medulla cortex occupy the proximal Medulla, similarly forming irregular square-like structures ('chandelier glia')(open red arrow, **B.2**). Astrocyte-like glia with cell bodies around the serpentine layer branch out into both distal and proximal Medulla (white filled arrows, **B.1**). **B.3-6** Individual astrocyte-like glial cells; coronal views, maximum density projections, 19-36x 0.5µm sections. **B.3-4** distal Medulla, **B.5** proximal Medulla, **B.6** serpentine layer. **B.7-8** Astrocyte-like glia of the Medulla send long processes into the outer chiasm (red open arrow in **B.7**). **B.7** Single sagittal section (0.5µm) (22C10, grey) **B.8**. Double-labeling of astrocyte-like glial (86E01-) Gal4 (magenta) and chiasm glial (53H12-) LexA (green) shows that the astrocyte-like glia processes lie within the sheath of chiasm glia next to neuronal tracts. **C.1-5** Individual cell morphologies of ensheathing glia in the Medulla, as visualized by the ensheathing glial (56F03-) Gal4 driving multicolor flp-out reporters (3-5 min hs), coronal views, maximum density projections, 6-11x0.5µm sections. **C.1-2** The ensheathing glia in the distal Medulla are organized in highly columnar structures (white open arrow, **C.1**). **C.3** The ensheathing glia show a characteristic branching pattern around layers M3 and M6, where photoreceptors R8 and R7 terminate, and in M7, the serpentine layer. The fine processes in the proximal Medulla (open red arrow) belong to the inner chiasm glia. **C.4** Magnification of the serpentine layer of the Medulla; coronal view, maximum density projection, 16x0.5µm. Ensheathing glia growing within the serpentine layer send columnar branches into both distal and proximal Medulla. **C.5** Coronal view, maximum density projection, 22x1µm sections. Ensheathing glia of the inner chiasm send fine protrusions into the proximal Medulla. **D.1-5** Ensheathing glia accompany photoreceptor projections (24B12, blue), which terminate in Medulla layers M3 and M6. **D.1** frontal view, maximum density projection, 6x0.5µm sections. **D.2-4** Cross sections (3x1µm) through M3 (**D.2**), in between (**D.3**) and M6 (**D.4**) show differences in the density of enmeshing (loose in between, tight around M3/M6). **D.5** Schematic illustration to demonstrate how a single Medulla ensheathing glia associates with Medulla columns. **D.6-8** Relationship between Medulla ensheathing glia and the tracheal system. Co-labeling of ensheathing glia (green, magenta), glial nuclei (REPO, grey) and auto fluorescence of trachea (grey). **D.7** 3D reconstruction of a substack of **D.6**. **D.8** Magnification of the boxed region in **D.7**. Ensheathing glia envelop the many tracheal branches that invade the Medulla (open white arrow, **D.7-8**). Scale bar = 10µm in **B.1,5-6, C.1-4, D.1-6**; 5µm in **B.2-4, 6**.

6.2.3 The chiasm glia

The optic lobes contain two major tracts that connect the different neuropiles. The outer chiasm connects Lamina and Medulla. During larval and early pupal stages, retinotopic projections are made by the R7-R8 axons and Lamina interneurons (L1-L5) from the Lamina into the Medulla; the crossover of fibers ('chiasm') occurs in the pupa, after the Lamina-Medulla connections are established, due to a 180° rotation of the Lamina against the Medulla neuropile (Braitenberg, 1970; Meinertzhagen, 1993). The inner chiasm connects the Medulla with the Lobula complex; fibers connecting Medulla with Lobula and Lobula plate, as well as Lobula with Lobula plate, are running through this chiasm.

Driver	Region-specific subtype	Generic subtype	Description	alternative drivers	Cell count	+/- (SEM)
53H12	Outer chiasm	Ensheathing	enwrap and accompany bundles of 10-20 Lamina-to-Medulla projections	9G07-Gal4 (specific)	48 (n=13)	2.39
53H12	Inner Chiasm (counted within generic chiasm driver)	Ensheathing	Long sheet-like cells with different orientation that ensheath neuronal projections between Medulla, Lobula and Lobula plate and send fine processes into these neuropiles	---	43 (n=4)	2

Table 7: Summary of chiasm-specific drivers, their cell counts and driver description.

In the *Janelia Gal4* collection, we identified only very few drivers that are specifically expressed in chiasm glia. In most cases, expression in chiasm glia is mixed with expression in ensheathing glia. Only one of the drivers (*53H12*) is expressed in both outer and inner chiasm. Our cell count places the number of outer chiasm glia at ~50, suggesting that, on average, one glial cell enwraps 15 Lamina-Medulla fiber tracts; the number of inner chiasm glia is ~40 (Table 7). The nuclei of the outer and inner chiasm are large and located in the middle of the chiasm regions (Tix et al., 1997). The outer chiasm glia are clearly distinct from the glia ensheathing the proximal Lamina and the distal Medulla; unlike inner chiasm glia, outer chiasm glia does not invade the neuropiles it connects (Figure 22B.1- 2, C.1- 5). Multi-color mosaic experiments together with co-labeling of axon tracts reveals that Lamina-Medulla connections are bundled into larger strands (Figure 22C.1- 3). More than one glial cell participates in wrapping fibers

within one such strand; in cross section, multiple enclosures are visible in which small sets of neuronal tracts run (Figure 22C.3). Conversely, 3D reconstructions show that individual chiasm glia participate in the ensheathing of several of the larger strands (Figure 22C.4- 5). In contrast, inner chiasm glia form large sheet-like structures (Figure 22D.1- 2) that are stacked on top of each other (Figure 22D.3). The inner chiasm glia envelop neuronal tracts (Figure 22D.3) and send fine protrusions into all three neighboring neuropiles (Figure 22D.2, white none filled arrows).

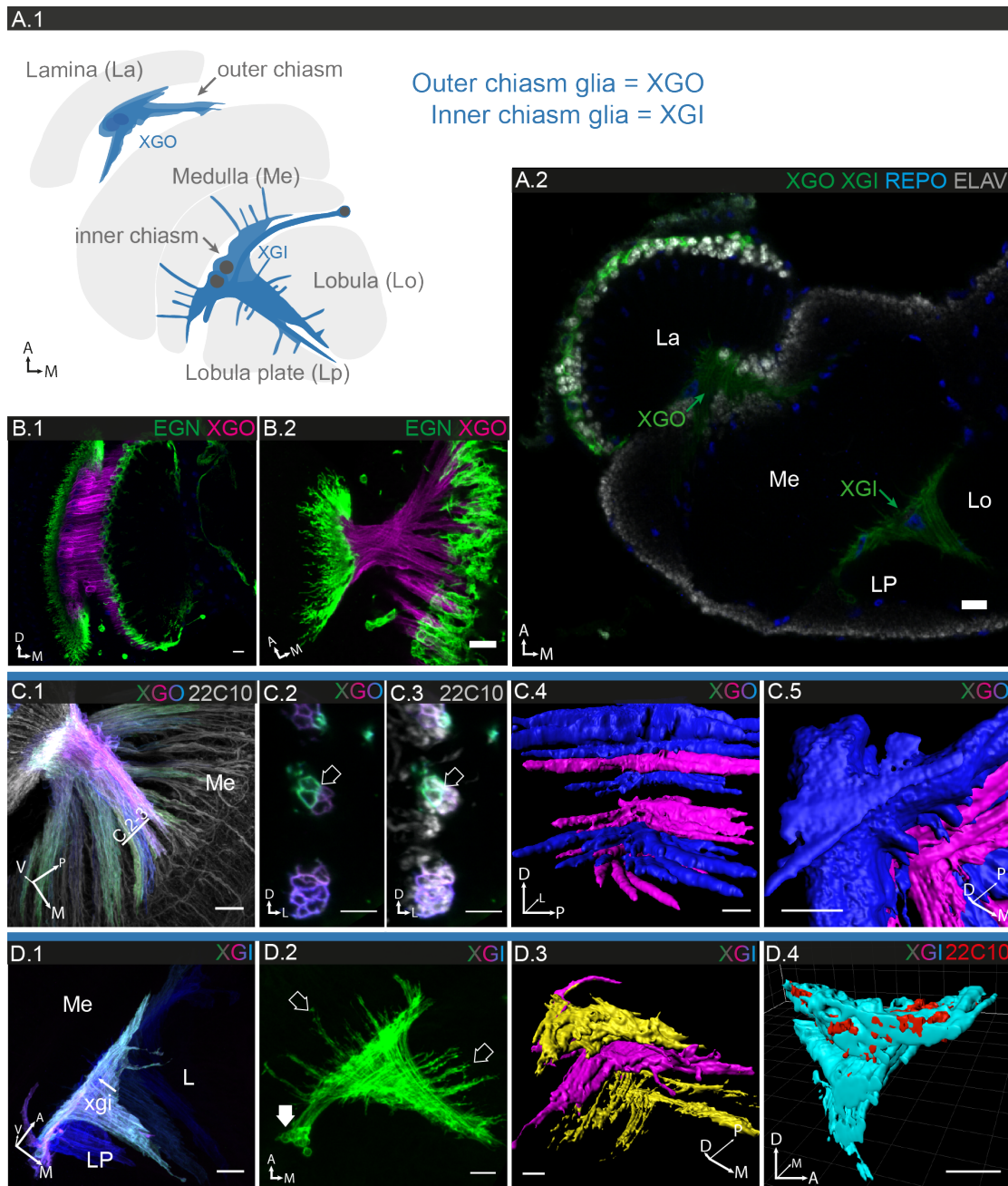


Figure 22: The glia of the outer and inner chiasm.

A.1 Schematic of the neuropiles of the optic lobe and the chiasms that connect them. The outer chiasm connects Lamina and distal Medulla, the inner chiasm connects proximal Medulla, Lobula and Lobula plate; the two major populations of chiasm glia (XGO and XGI) are depicted in blue. **A.2.** Single coronal section ($1\mu\text{m}$) through the optic lobe; co-labeling of chiasm glia (green, 53H12-Gal4; UASmyrGFP), glial nuclei (blue, REPO) and neuronal nuclei (grey, ELAV). **B.1-2** Co-labeling of chiasm glia (magenta, 53H12-LexA; lexAop-myr-smGFP-V5) and generic ensheathing glia (green, 56F03-Gal4; UAS-myr-smGFP-HA) **B.1-2** Outer chiasm and the neighboring ensheathing glial populations of the proximal Lamina and distal Medulla. **B.1** Frontal view, maximum density projection, $15\times 1\mu\text{m}$ sections. **B.2** Coronal view, maximum density projection, $4\times 1\mu\text{m}$ sections. **C.1-5** Individual cell morphologies of outer chiasm glia, as visualized by the chiasm glial (53H12-) Gal4 driving multicolor-flpout reporters (5 min hs). **C.1** Oblique coronal view, maximum density projection, $30\times 1\mu\text{m}$ sections. **C.2-3** Single sagittal section ($0.5\mu\text{m}$) showing glia (**C.2**, blue, green magenta) and co-

labeling of neuronal tracts (**C.3**, 22C10, grey). Neuronal tracts are enveloped by chiasm glia (open arrows). **C.4-5** 3D reconstruction of **C.1 C.4** View from medial Medulla into chiasm. **C.5** Oblique coronal view onto Lamina portion of chiasm. Different fibers crossing the chiasm at perpendicular angles can be ensheath by one and the same chiasm glia cell. **D.1-4** Individual cell morphologies of inner chiasm glia, as visualized by the chiasm glial (53H12-) Gal4 driving multicolor-flpout reporters (10 min hs) **D.1** Oblique coronal view, maximum density projection, 93x1 μ m sections. A single inner chiasm glia cell may extend its sheath-like processes along the entire coronal plane of the inner chiasm and fills it. **D.2** Coronal view, maximum density projection, 117x0.5 μ m sections. Inner chiasm glia send many long protrusions (open white arrows) into all three neighboring neuropiles (Medulla, Lobula, Lobula plate). Chiasm glial cell body lies outside the chiasm (filled white arrow). **D.3-4** 3D reconstruction of the projection in **D.1**. View of the dorso-ventral axis of the chiasm. **D.4** Sagittal cut through **D.3** Inner chiasm glia (turquoise) envelop neuronal tracts (red). Scale bar = 10 μ m in all images.

6.2.4 *Glia in the Lobula complex*

The Lobula complex comprises the Lobula plate, which is involved in motion processing (Borst et al., 2010), and the Lobula, which is involved in higher order color processing (Morante and Desplan, 2008). Trans-neurons connect Medulla to Lobula and/or Lobula plate, and Lobula and Lobula plate. Both Lobula and Lobula plate contain large dendritic arborizations of visual projection neurons. Astrocyte-like glia enter the Lobula and Lobula plate predominantly from the outer margins (medial/anterior margin of Lobula plate, lateral/anterior margin of the Lobula) and only rarely from the inner chiasm (Figure 23B.1-4). Multi-color mosaic experiments reveal that astrocyte-like glia in the Lobula complex show greater variation in shape than those of Lamina and Medulla; however, the glia that invade the Lobula from the anterior margin show a more columnar organization (Figure 23B.4). Not infrequently, the glia form two branches, which may invade two of the three neighboring neuropiles (Lobula/ Lobula plate/ Medulla) (Figure 23B.3). All astrocyte-like glia in the Lobula complex look spongy / show a high structural density.

Ensheathing glia send large projections from the outer margins into Lobula and Lobula plate (Figure 23C.1, open white arrow, columnar structure, open red arrow, tubular structure), while inner chiasm glia send fine protrusions from the inner margins into all three neighboring neuropiles (Medulla, Lobula, Lobula plate) (Figure 23, open red arrow, columnar structure). In both Lobula and Lobula plate, multi-color mosaics show that ensheathing glia form columnar processes perpendicular to the neuropile margin (Figure 23C.1, open white arrow), as well as tangential processes parallel to the margin (Figure 23C.1, open red arrow, Figure 23C.2-3). Higher magnification and co-labeling of neuronal processes reveal complex three-dimensional networks of branches (Figure 23C.2-3), in which ensheathing glia enclose neuronal processes (Figure 23C.4-6).

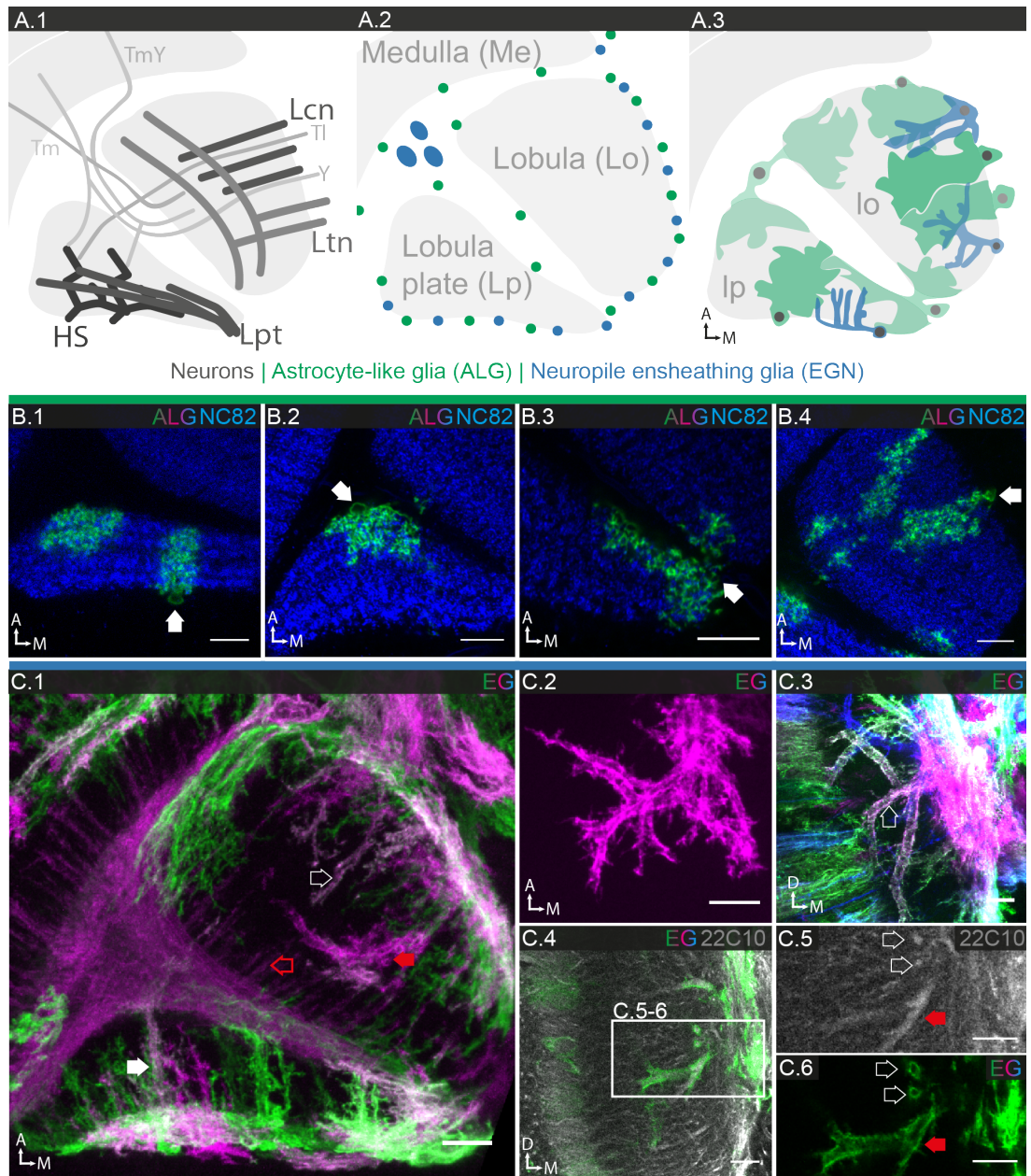


Figure 23: Glial cell morphologies in the Lobula complex.

A.1 Schematic depicting the main features of the two major glial subtypes, astrocyte-like glia (green) and ensheathing glia (blue), that populate the Lobula complex, consisting of Lobula and Lobula plate. **A.2** Schematic depicting the location of astrocyte-like (green) and ensheathing (blue) glial cell bodies. Note the large inner chiasm/ensheathing glia cell bodies located between proximal Medulla and Lobula complex. **A.3** Schematic depicting the major neuronal projections into and out of the Lobula complex. Trans-neurons (light grey) connect Medulla to Lobula and/or Lobula plate, and Lobula and Lobula plate. Both Lobula and Lobula plate contain large dendritic arborizations of visual projection neurons (dark grey). **B.1-4** Individual cell morphologies of astrocyte-like glia in the Lobula complex, as visualized by the astrocyte-like glial (86E01-) Gal4 driving multicolor-flpout reporters (6 min hs), co-labeling of synaptic regions (blue, nc82). In both Lobula and Lobula plate, astrocyte-like glia take on various shapes and sizes and can send branches into both Lobula and Lobula plate (arrow in **B.3**) Astrocyte-like glia entering the Lobula from the anterior margin show a (loosely) columnar organization (**B.4**). **C.1-6** Individual cell morphologies of ensheathing glia in Lobula and Lobula plate, as visualized by EG and EG22C10 staining. EG (green) and EG22C10 (magenta) staining of ensheathing glia in Lobula and Lobula plate. EG (green) and EG22C10 (magenta) staining of ensheathing glia in Lobula and Lobula plate. EG (green) and EG22C10 (magenta) staining of ensheathing glia in Lobula and Lobula plate.

Lobula plate, as visualized by the ensheathing glial (56F03-) Gal4 driving multicolor-flpout reporters (5-8 min hs). **C.1** Coronal view, maximum density projection, 25x0.5 μ m sections. Visible are column-like processes (white and red open arrows, white filled arrow) perpendicular to the margin, as well as tangential processes (red filled arrow) parallel to the margin. **C.2** Coronal view, maximum density projection, 21x0.5 μ m sections, **C.3** Frontal view, maximum density projection, 10x1 μ m sections, co-labeling of neural processes (22C10, grey). Ensheathing glia form a complex three-dimensional network of branches. **C.4-6** Single frontal section (0.5 μ m), co-labeling of neuronal processes (22C10, grey, **C.4-5**). Scale bar = 10 μ m in all images.

6.2.5 Summary

We have characterized the glia that we found in the visual system of *Drosophila* with respect to glial numbers, equivalency of the visual system specific glia and generic glial subtypes and morphology of single glial cells in relation to the entities they are associated with. We managed to (1) characterize all previously identified visual system glia at unprecedented resolution, (2) identify two previously unknown glial subtypes in the Lamina, (3) identify and characterize in detail a subpopulation of ensheathing glia in the Medulla, (4) show that ensheathing glia in the Medulla associate with the tracheal system, (5) provide evidence that the chiasm glia are in fact ensheathing glia and characterize all neuropile glia of the Medulla and Lobula complex with respect to astrocyte-like glia and ensheathing glia morphologies. Finally, demonstrating the close relationship of ensheathing glia and single neuronal-entities, we show that ensheathing glia form tube-like structures in the Lobula complex to ensheath large dendritic branches of a single neuron.

6.3 Characterization of glia in the olfactory system

Similar to the visual system, the olfactory system makes up a significant portion of the fly brain and has been studied in great detail anatomically and functionally (Aso et al., 2009; Gao et al., 2000; Hallem and Carlson, 2004a; Hallem et al., 2004; Ito et al., 1998; Laissue et al., 1999; Leiss et al., 2009; Stocker, 1994; Strausfeld et al., 2003; Tanaka et al., 2004; Turner et al., 2008). The glia of the olfactory system have been investigated in previous work in *Drosophila* (Doherty et al., 2009; Ito et al., 1997; Leiss et al., 2009; Oland et al., 2008; Sen et al., 2005; Sinakevitch et al., 2010) and other insects (Hahnlein and Bicker, 1996; Oland and Tolbert, 1989), but a comprehensive analysis and detailed characterization of single cell morphologies and equivalency of glial morphologies with the here described generic subtypes is still incomplete. In the following two sections, we will describe the glia employing our toolkit in different portions of the olfactory system, from the antennal lobe to the higher olfactory centers mushroom body and lateral horn. The neuronal architecture is well understood and excellent neuronal Gal4 drivers are available (including specific neuronal Gal4s for different parts of the olfactory neurons, also refer to Figure 24A.1, 4.4.4), which in combination with our newly generated glial LexA drivers allowed us to examine the interactions between glia and neurons in exquisite detail in different regions of the olfactory system.

6.3.1 *Glia in the Antennal lobe*

We sought to resolve the open questions regarding antennal lobe glial morphology which were (i) to determine if the entire antennal lobe neuropile is enclosed by ensheathing glia, (ii) if a single ensheathing glia cell associates with only one particular single glomeruli or randomly with multiple glomeruli (iii) if a single astrocyte-like glia cell associates with particular single glomeruli only or randomly with multiple glomeruli, (iv) to identify single cell morphology of ensheathing glia, (v) evaluate if those cells appear sheet-like or filamentous and if they percolate the glomeruli, and last, to describe the relationship between

astrocyte-like and ensheathing glia with respect to their location in the antennal lobe neuropile.

Approximately 1300 olfactory receptor neurons (ORNs) project from the antenna/maxillary palp onto 43 distinct glomeruli in the antennal lobe, which contain local interneurons (LNs) and 150-200 projection neurons (PNs). The PNs project their dendrites into specific glomeruli of the antennal lobe and send their axons to the higher olfactory centers (Figure 24A.1).

The cortex of the antennal lobe contains cortex glia, the neuropile is populated by both astrocyte-like and ensheathing glia (Figure 24A.2). However, in contrast to the visual system, we could not identify antennal lobe-specific drivers for any of the three glial subtypes in the JFRC Gal4 collection, and thus based our analysis on generic drivers and multicolor mosaic experiments. Similar to other regions in the brain, the cell bodies of ensheathing glia and astrocyte-like glia are found surrounding the surface of the antennal lobe but not within the neuropile (Figure 24A.3-4). Cortex glia populate the (anterior) cortical region of the antennal lobe and enclose the neuronal cell bodies of (LNs and) PNs (Figure 24B.1-3). Astrocyte-like glia show an evenly high density of extensions throughout the entire neuropile, without any significant differences between individual glomeruli (Figure 24B.1). Individual astrocyte-like glia are not confined to one glomerulus (Figure 24B.3-4) but rather spread out until they reach their astrocyte-like neighbors. High magnification views of individual astrocyte-like glia reveal a highly branched morphology, studded with locally increased densities (Figure 24B.2). Ensheathing glia cover the entire neuropile of the antennal lobe with a very thin sheet (Figure 24C.1); the small holes visible in the sheet likely provide the entry way for incoming neuronal projections (Figure 24C.2). Moreover, the ensheathing glia send extensions in between the glomeruli (Figure 24C.3). 3D reconstructions show that while the antennal lobe is covered by a nearly contiguous sheet, the individual glomeruli are not (Figure 24C.4). Many of these ensheathing glial extensions appear as tube-like structures (Figure 24C.6, C.8), and double labeling shows that these glial extensions strongly co-localize with neuronal/axonal processes (Figure 24C.5). Multicolor mosaic experiments using a

generic ensheathing glial driver (56F03) reveal that the glia are large, elongated cells of irregular shape. The cells do not physically overlap but frequently interweave with one another. Optical cross-sections through the lobe show that the extensions of individual ensheathing glia reach deep into the neuropile, often contacting several glomeruli (Figure 24C.7). Individual ensheathing glial cells display a lamellar morphology, with fine processes branching out into the glomeruli themselves (Figure 24C.8).

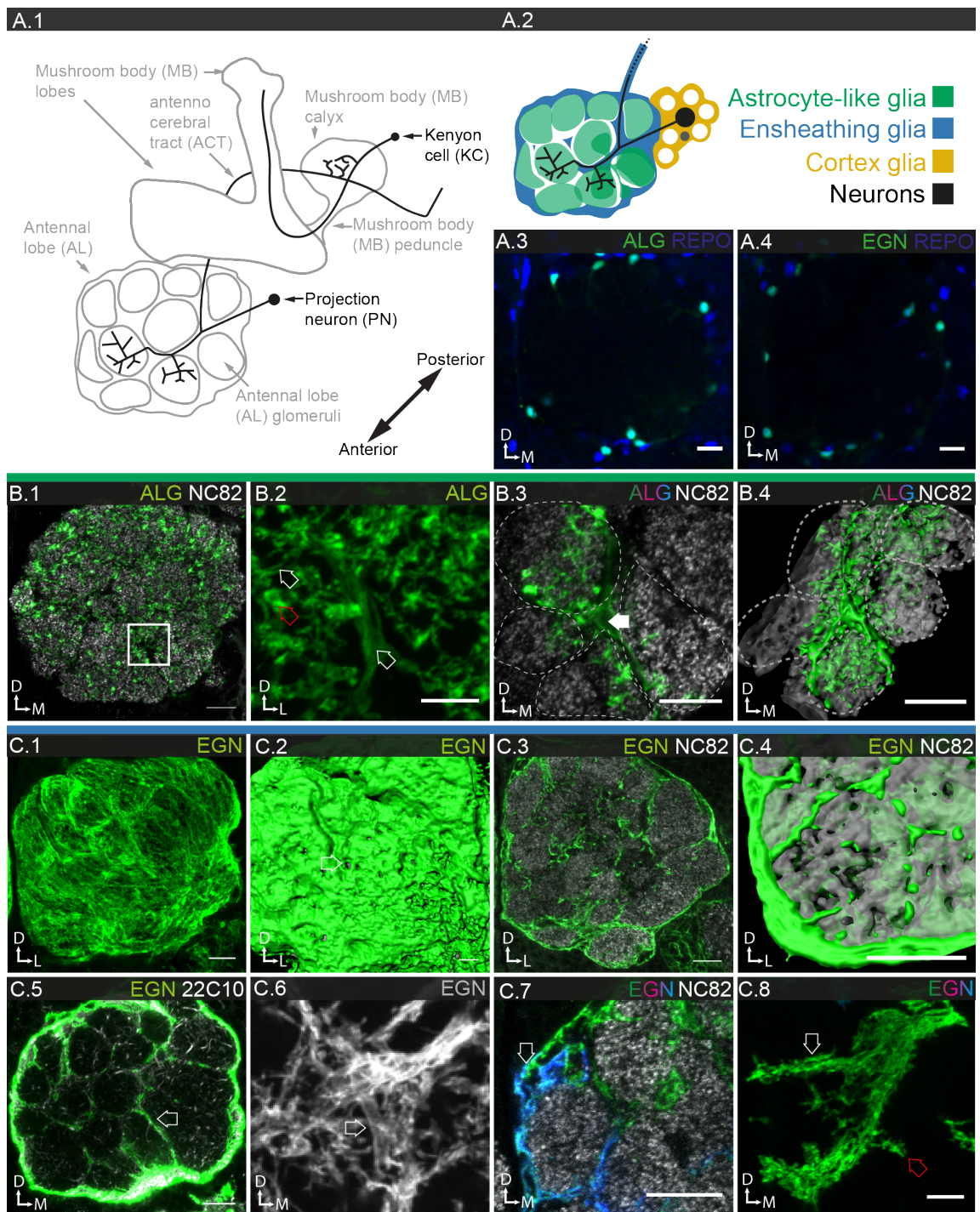


Figure 24: Characterization of the generic glia and glia-neuron interactions in the antennal lobe.

A.1 Schematic of the olfactory system and major neuronal projections. Olfactory receptor neurons (ORNs) detect olfactory cues in the antenna and maxillary pulp and relay olfactory information through the antennal nerve into the antennal lobe. They converge onto defined glomeruli. Projection neurons connect the antennal lobe with higher brain centers. The cell bodies of projection neurons are located in the cortex surrounding the antennal lobe; their dendritic (post-synaptic) compartments are located within the glomeruli of the antennal lobe (light green); the axonal projections run through the antenno-cerebral tract and terminate (pre-synaptic compartment) in two higher brain centers, the mushroom body calyx and the lateral horn. The predominant mushroom body intrinsic neuronal population are Kenyon cells. **A.2** Morphology of the antennal lobe and glial subtypes. Different subtypes of glia are associated with different compartments of the neurons. Astrocyte-like glia populate the neuropile regions; ensheathing glia ensheath the entire antennal lobe and protrude processes into the AL along the glomeruli boundaries; Cortex glia surround neuronal cell bodies of projection neurons and antennal lobe intrinsic neurons (not illustrated here) in the cortex region and enclose neuronal processes in the cortex region. **A.3** Localization of astrocyte-like glia cell bodies (86E01-Gal4; UAS-nls-GFP; green; REPO, blue)(single frontal section). Cell bodies are found surrounding the antennal lobe neuropile but not inside. **A.4** Localization of ensheathing glia cell bodies (56f03-Gal4; UAS-nls-GFP; green; REPO, blue)(single frontal section). Cell bodies are found surrounding the antennal lobe neuropile but not inside.

B.1-4 Astrocyte-like glia in the Antennal lobe. **B.1-2** General expression pattern (86E01-LexA; lexAop-myr-smGFP-V5; green; in **B.1**; nc82; grey) (**B.1**; single frontal section; **B.2**; frontal view, maximum density projection; 4x0.5um sections). The astrocyte-like glia processes protrude into different glomeruli without any evident anatomical registration. **B.2** Magnification of the boxed region in **B.1**. Note the large branches (open white arrow), fine processes (open red arrow) and occasional thickenings (red arrow). **B.3-4** Single cell morphology (86E01-Gal4; McFlip; hs= 10min; in **B.3**; nc82, grey) (**B.3**; single frontal section; **B.4**; reconstruction). **B.3** Single cells are not confined to single glomeruli (each surrounded by dashed line in **B.4**). **B.4** reconstruction of **B.3** Note the fine processes of one single cell that protrude into multiple glomeruli. **C.1-8** Ensheathing glia in the Antennal lobe. **C.1-6** Generic expression pattern (56F03-LexA; LexAop-myr-smGFP-V5; green; in **C.3**; nc82; grey; in **C.5**; 22C10, grey) (**C.1**; frontal view; maximum density projection; 7x0.5µm sections; **C.3**; single section; **C.5**; single frontal section; **C.6**; frontal view; maximum density projection; 7x0.5µm sections). **C.1** The surface of the lobe is covered by ensheathing glial processes. **C.2** Reconstruction of the glial sheath around the antennal lobe. Note the small holes (arrow) occasionally disrupting the otherwise continuous glial sheath. **C.3** Single glomeruli are not entirely enclosed by ensheathing glia. **C.4** Reconstruction of the ensheathing glia network inside the antennal lobe reveals discontinuity of the glial sheath around single antennal lobe glomeruli. This is likely due to ensheathing glia not forming continuous sheaths but wrap neuronal tracts running along the glomeruli boundaries. **C.5** Tracts enter the antennal lobe along the glomerular boundaries and are ensheathed by glial processes (green) (open white arrow). **C.6** Magnification of glomerular boundaries formed of ensheathing glia inside the antennal lobe reveals tube-like morphologies. **C.7-8** Single cell morphologies (56F03-Gal4; McFlip; hs= 7min; in **C.7**; nc82, grey) (**C.7**; single frontal section; **C.8**; frontal view; maximum density projection; 25x0.5µm sections) **C.7** Ensheathing glia cover discrete areas, in regions of contact they partially interdigitate. The overlap appears multilamellar (open white arrow). **C.8** Individual ensheathing glia are not confined to single glomeruli. From the main ensheathing glial processes along the glomerular boundaries (open white arrows), smaller branches project

perpendicularly into the glomeruli (open red arrows). Scale bar = 10 μ m in **A.3, 4, B.1,3, C.1-5**; 5 μ m in **B.2, C.7-8**.

6.3.2 *Glia in the mushroom body*

The higher order centers of the olfactory system, mushroom body and lateral horn, are innervated by 150-200 PNs via the inner antenno-cerebral tract. In the mushroom body, the PNs synapse onto Kenyon cells in a substructure called the calyx; in turn, the Kenyon cells send axonal projections through the peduncle into different lobes within the mushroom body and are thereby subdivided into three distinct subsets (α/β , α'/β' , γ) (Figure 24A.1) (for review: (Fiala, 2007)).

We aimed to resolve the open questions regarding mushroom body glial morphology which were (i) to elute the detailed composition of MB calyx glia from previously published observation (Leiss et al., 2009) in which all glia were labeled, (ii) describe the glial composition of the peduncle and the lobes, (iii) characterize the ensheathment and sub-compartmentalization of the peduncle and lobes, and (iv) comment on small invaginations that we found to enter the mushroom body lobes sub-regions.

As in other regions of the brain, the cortex of the mushroom body contains cortex glia, the neuropile regions are populated by both astrocyte-like and ensheathing glia. As in the case of the antennal lobe, we could not identify mushroom body-specific drivers for any of the three glial subtypes within the *Janelia Gal4* collection, and thus base our analysis on generic drivers, in particular glia-LexA/neuron-Gal4 co-labeling, and multicolor mosaic experiments. (Our description follows the mushroom body anatomy from distal to proximal.) Similar to other brain regions, the presence of astrocyte-like glia correlates with the presence of synapses, but the density of glial processes is anti-correlated with the density of synapses. The calyx is synapse-rich and pervaded by a low density of filligrane astrocyte-like processes (Figure 25B.1). Interestingly, the morphology of these glial processes is unlike that of other brain regions; the processes show thickenings at branch points, from whence thin dendritic processes emerge (Figure 25B.2-3). The peduncle is a tract region sparse in synapses that contains very few

astrocyte-like processes (Figure 25B.4-5). The lobes of the mushroom bodies, similar to the calyx, are rich in synapses and are pervaded by a low density of astrocyte-like processes; the density of glial processes is lower compared to that of neighboring brain regions (Figure 25B.6-7).

Ensheathing glia envelop the outer bounds of the calyx but, surprisingly, show a vast number of extensions that permeate its inner structure (Figure 25C.1.) Co-labeling of intrinsic Kenyon cells reveal that their projections are wrapped by ensheathing glia and that, thereby, different neuronal subpopulations are kept sequestered from the calyx onwards throughout the peduncle (Figure 25C.2-5). Ensheathing glia envelop the mushroom body lobes and permeate their inner structure with numerous extensions as well (Figure 25C.6, open red arrow). Multicolor mosaics confirm both these morphologic features, sheath formation as well as protrusions that wrap neuronal processes (Figure 25C.7).

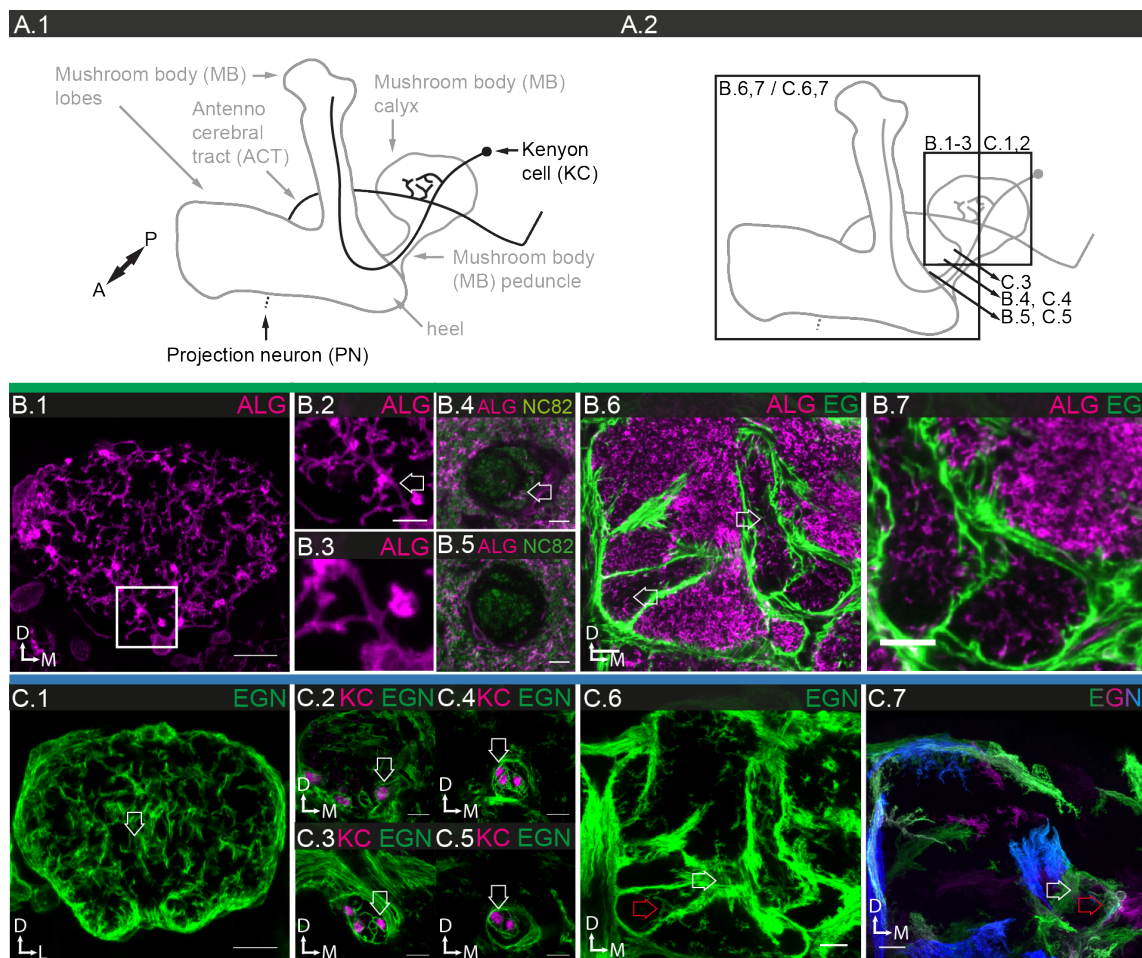


Figure 25: Characterization of the generic glia in the mushroom body.

A.1 Schematic of the olfactory neuronal projections in the mushroom body region. A detailed description of the neuropiles of the olfactory system as well as the major projections is given in the figure legend of Figure 13. **A.2** Schematic of the mushroom body neuropile and the focal planes represented in the panels below. **B.1-7** Astrocyte-like glia in the mushroom body. **B.1** Generic expression pattern (86E01-LexA; LexAop-myr-smGFP-V5; magenta (green in **B.4-5**); in **B.4-5**; nc82, green; in **B.6-7**; ensheathing glia; 56F03-Gal4; UAS-myr-smGFP-HA; green) (**B.1-3**, **6-7**; frontal views; maximum density projections; **B.1**; 11x0.5µm; **B.2-3** Magnifications of the boxed region in **B.1**; **B.4-5**; single frontal sections). **B.2-3** Star-shaped swellings (open white arrow), which were observed in other parts of the brain cannot be distinguished. Instead, astrocyte-like glia processes show thickenings at branching points from which thin dendritic processes branch out. **B.4** In the medial part of the peduncle, astrocyte-like glia processes are rarely found even in the proximity of synaptic regions (open white arrow). **B.5** In the transition zone from the anterior peduncle to the heel of the lobes, astrocyte-like glia processes emerge. **B.6-7** Low-density astrocyte-like glia processes characterize the mushroom body lobes neuropile. **C.1-6** Ensheathing glia in the mushroom body. **C.1-6** Generic expression pattern (56F03-LexA; LexAop-myr-smGFP-V5; green; in **C.2-5**; 17d-Gal4; magenta)(**C.1**; frontal view; maximum density projection; 10x0.5µm sections; **C.2-5**; single frontal sections; **C.6**; frontal view; maximum density projection; 20x0.5µm sections). **C.1** Ensheathing glia processes permeate the mushroom body calyx. **C.2** Anterior part of the mushroom body calyx; **C.3** Posterior peduncle; **C.4** Medial peduncle; **C.5** Anterior peduncle cross section. Note the sub-compartmentalization by ensheathing glia. This compartmentalization is maintained throughout the peduncle and gradually opens up in the transition zone between peduncle and calyx. Individual subpopulation of mushroom body intrinsic Kenyon cells (magenta) are enwrapped by ensheathing glia (open white arrow). **C.6** Beta and beta' lobe as well as gamma lobe are separated by a thin sheath of ensheathing glia (open white arrow); even within single subcompartments, there is subcompartmentalization (open red arrow). **C.7** Individual (single) cell morphologies of ensheathing glia in the mushroom body lobes (56F03-Gal4; McFlip; hs= 7 min)(frontal view; maximum density projection; 20x0.5µm sections). A single cell (blue) was labeled that separates alpha and alpha' lobes and a few cells in the region of the heel are shown which in part have a sheath like character but potentially also enwrap tracts within the peduncle (open white and red arrow). Scale bar = 10µm in **B.1-3**, **C.1-7**, **D.1**, **6-7**, **E.1-7**; 5µm in **D.2-5**.

6.3.3 *Neuron-glia interactions along olfactory projection neurons*

We examined the interaction between projection neurons and the different glial subtypes, from the antennal cortex to the mushroom body calyx, using neuron-Gal4/glia-LexA co-labeling. Cortex glia enwrap the cell bodies of PNs and accompany their projections toward the (antennal) neuropile region (Figure 26B.1-3). Ensheathing glia, which form a porous sheet around the glomeruli of the antennal lobe, take over and accompany neuronal projections until they enter the neuropile (Figure 26D.1-2). Astrocyte-like glia forms a sponge-like structure

surrounding the bushy post-synaptic compartment of PNs; interestingly, not all postsynaptic regions are in direct contact with the glia (Figure 26D.3-4).

In the inner antenno-cerebral tract, ensheathing glia completely enclose the projections of the PNs (Figure 26B.1-3) and accompany them to higher order olfactory centers. PN projections entering the mushroom body calyx are accompanied by ensheathing glia until they subdivide into different branches and terminate as PN boutons (Figure 26E.1-3). Astrocyte-like glial processes loosely intermingle with sites of synaptic connections but lack consistent/specific association with the pre-synaptic boutons/compartments (Figure 26E.4). Similarly, both astrocyte-like and ensheathing glia are found in the proximity of (AChR-positive) post-synaptic sites but lack a stereotyped specific association (Figure 26E.5-7).

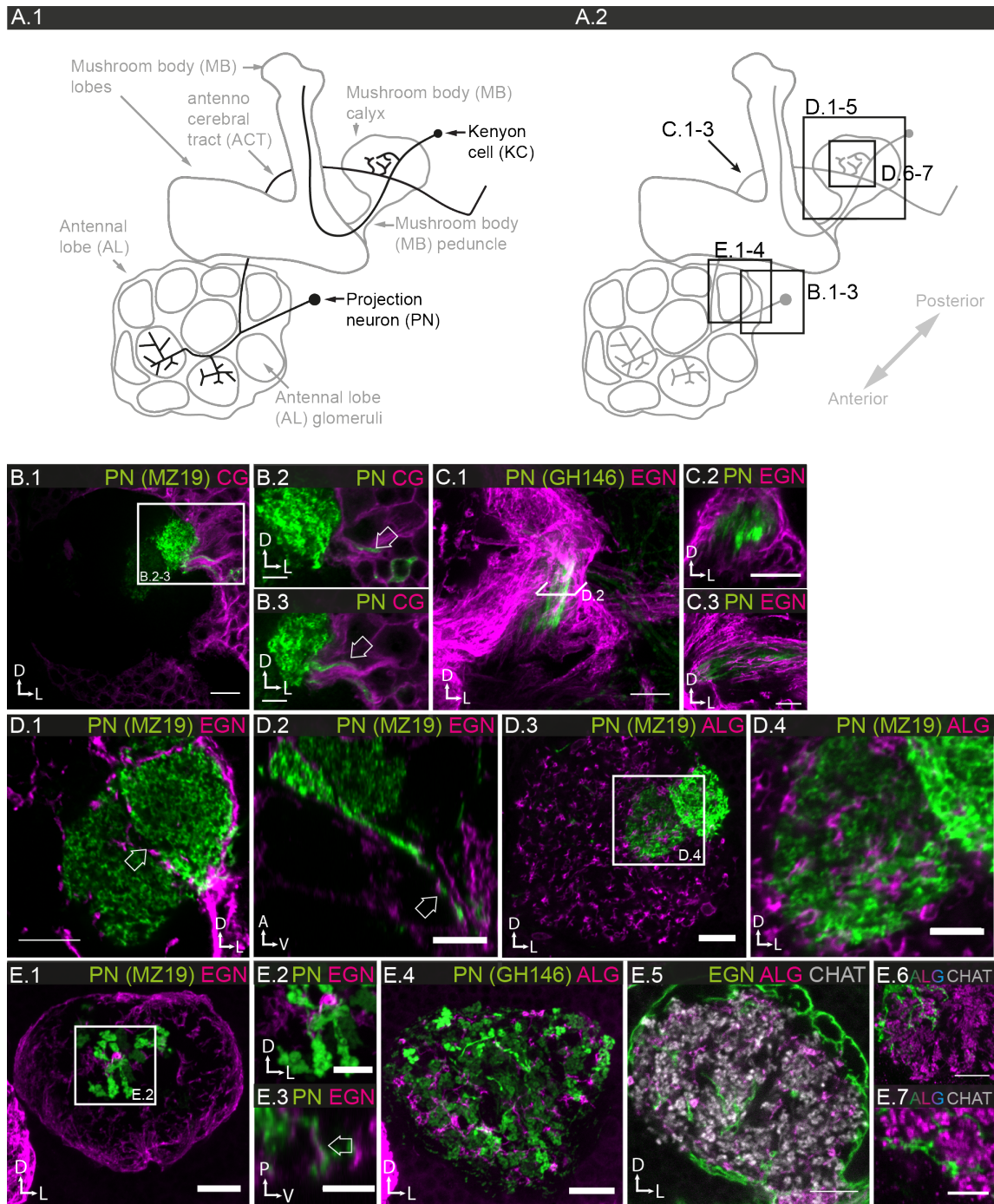


Figure 26: characterization of glia-neuron interactions in the olfactory system.

A.1 Schematic of the olfactory system and major neuronal projections. A detailed description of the neuropiles of the olfactory system as well as the major projections is given in the figure legend of Figure 13. The focal planes represented in the panels below are indicated. **B.1-3** Spatial relationship between the cell bodies of projection neurons (PN) and cortex glia (CG) in the antenna lobe cortex (PN; *mz19-Gal4*; *UAS-myrsGFP-HA*; green; CG; *77A03-LexA*; *lexAop-myrsGFP-V5*; magenta) (**B.1**; frontal view; maximum density projection; $4 \times 0.5 \mu\text{m}$ sections; **B.2-3**; single sections). Both the neuronal cell body (**B.2**, arrow) and the neuronal processes that project from the cell body to the neuropile region (**B.3**) are ensheathed by cortex glial extensions. **C.1-3** Projection neuron (PN) tracts within the antenno-cerebral tract (ACT) are wrapped by neuropile-ensheathing glia (PN; *GH146-Gal4*; *UAS-myrsGFP-HA*; green; EGN; *56F03-LexA*; *lexAop-myrs*

smGFP-V5; magenta) (**C.1**; frontal view; maximum density projection; 5x0.5 μ m sections; **B.2-3**; single sections). The tract is completely enclosed. **D.1-2** Ensheathing glia at the boundaries of single glomeruli in the antennal lobe (PN; mz19-Gal4; UAS-myr-smGFP-HA; green; EGN; 56F03-LexA; lexAop-myr-smGFP-V5; magenta) (**D.1**; frontal view; maximum density projection; 3x0.5 μ m sections; **D.2**; horizontal projection of **D.1**). **D.1** The glomeruli of the antennal lobe are ensheathed by a discontinuous layer (open white arrow) of neuropile-ensheathing glia. are shown at different magnifications. **D.2**, Ensheathing glia accompany neural tracts until they enter the neuropiles (open white arrows). **D.3-4** Astrocyte-like glia within single glomeruli in the antennal lobe (PN; mz19-Gal4; UAS-myr-smGFP-HA; green; ALG; 86E01-LexA; lexAop-myr-smGFP-V5; magenta) (**D.3**; frontal view; maximum density projection; 4x0.5 μ m sections; **D.4** Magnification of **D.3**). **D.1-2** In the glomeruli of the antennal lobe, the bushy postsynaptic compartment of projection neurons (green) is intertwined with astrocyte-like protrusions (magenta) but not all postsynaptic regions are directly in contact with the glia. **E.1-7** Spatial relationship of astrocyte-like and neuropile-ensheathing glia with the pre- and postsynaptic compartments in the mushroom body calyx. **E.1-3** Projection neuron presynaptic regions and association with neuropile-ensheathing glia in the mushroom body calyx (PN; mz19-Gal4; UAS-myr-smGFP-HA; green; EGN; 56F03LexA; lexAop-myr-smGFP-V5; magenta) (**E.1-2**; frontal view; maximum density projection; 5x0.5 μ m sections; **E.3**; horizontal projection of **E.1**). Neuropile-ensheathing glial processes wrap projection neuron extensions until they divide into different terminal regions. **E.4** Ensheathing and astrocyte-like glia in the region of postsynaptic compartments (labeled by cCHAT) (86E01-LexA; LexAop-myr-smGFP-V5; magenta; 56F03-Gal4; UAS-myr-smGFP-HA; green; CHAT; grey) (single section). **E.5-6** Single astrocyte-like glia in proximity to postsynaptic compartments (86E01-Gal4; McFlip; hs= 3min; CHAT; magenta)(**E.5**; frontal view; maximum density projection; 3x0.5 μ m; **E.6**; single section). **E.4-6** Both astrocyte-like and ensheathing glia are found in proximity to postsynaptic, acetylcholine receptor regions, but do not closely associate with them in a stereotypic manner. **E.7** Projection neuron presynaptic boutons and astrocyte-like glia in the mushroom body calyx (PN; GH146-Gal4; UAS-myr-smGFP-HA; green; 86E01-LexA; lexAop-myr-smGFP-V5; magenta)(frontal view; maximum density projection; 3x0.5 μ m sections). The density of astrocyte-like glial processes intermingle loosely with sites of synaptic connections but lack specific association with presynaptic compartments. Scale bar = 10 μ m in **B.1**, **C.1**, **D.1**, **D.3**, **E.1**, **E.4**; 5 μ m in **B.2-3**, **C.2-3**, **D.2**, **4**, **E.2-3**, **5-7**.

6.3.4 *Summary*

We have examined the glial components of the olfactory circuitry with respect to localization of the cells and special morphologic features. In addition, we characterized the interactions of the glia with the neuronal entities they associate with. In general, we found that glial morphologies and glia-neuron interactions follow the same principles found in other regions of the brain. Cortex glia populate the cortical regions of antennal lobe and mushroom body, single astrocyte-like and ensheathing glia are not confined to defined neuronal entities (i.e. single glomeruli in the AL) and neuronal processes are ensheath by ensheathing glia. However, we also find some remarkable differences to the other brain regions. First and foremost, the density of astrocyte-like glia processes in the mushroom body neuropile is the lowest found in the entire brain. Second, ensheathing glia extensively interweave the mushroom body calyx. Lastly, the neuronal processes of Kenyon cells projecting through the peduncle in the mushroom body lobes, are not individually ensheath by ensheathing glia, even though populations of Kenyon cell axons are separated from each other by thin ensheathing glial sheaths. Lastly, using the olfactory system as a role model, we investigated the interaction of different glia subtypes with pre- and postsynaptic compartments and found no obvious spatial association.

6.4 Discussion

Gal4 lines found within the Janelia Farm Gal4 collection were employed to characterize the different glial subtypes in unprecedented detail. In addition to having access to the largest Gal4 collection with expression in the adult brain, this was achieved by benefiting from several technical developments. A novel multi-color mosaic technique with highly sensitive immune-histochemical reporters permitted visualization of finest morphological details in individual cells. The use of two sensitive yet completely orthogonal expression systems facilitated the analysis of glia-glia and glia-neuron interaction. Finally, home-scripted image analysis tools allowed for a quantitative analysis of key morphological features. With these tools, we were able to corroborate earlier studies (Edwards and Meinertzhagen, 2010; Edwards et al., 2012) but also to extend very significantly the characterization of the different glial subtypes throughout the nervous system. This includes a high-resolution morphologic description of the glia themselves and their relationship with other glia and neuronal entities, revealing several fundamental rules governing these interactions. The clean sub-type specific drivers permitted a precise determination of cell numbers for the different glial subtypes, and, in conjunction with morphologic criteria, the driver line expression patterns helped assign glia to specific subtypes. Besides the fine-grained anatomical details uncovered here, these data enabled us for the first time to gain a simplistic view onto the glial realm in the adult *Drosophila* CNS. As a further consequence, it provides evidence for a common nomenclature.

We have used the generic Gal4 lines and their specific expression pattern as a tool to characterize glial anatomy. However, the definition of glial cell types and subdivision into different subtypes does not rely on their expression pattern. The cells' location, morphology and neuronal interaction are almost as important. When determining equivalency between region-specific and generic glial subtypes, as in the case of the Lamina, the drivers are simply used as cell type-specific markers. The finding that many driver lines exist in which specificity of expression coincides with specific glial cell subtypes suggests that marker

expression is an identifying feature of the cell type. The fact that region-specific lines are mostly found for the Lamina, which shows the most distinct morphologies for any of the generic subtype, further strengthens this argument. Thus, in conjunction with anatomical and morphological criteria expression patterns of driver lines *can* be and were used to define cell types.

Multiple aspects of our study lend strong support to a simple and unified nomenclature for the glia of the adult nervous system, which would have the added benefit of making *Drosophila* glia more accessible to both vertebrate and fly neurobiology communities. Using the generic driver lines, we have examined and compared the anatomy and cellular features of glial subtypes in different brain regions, in particular the different neuropiles of the visual and olfactory systems as well as many regions of the central brain and the ventral nerve chord. While within a given glial subtype differences and variation in morphological features are observed, they only reflect differences in the topology and organization of the neuronal entities with which the glia interact. For instance, perineurial and subperineurial glia, which adopt moderately different shapes in the brain, ventral nerve cord and the peripheral nervous system, show a distinct morphology at the interface between retina and Lamina. They accommodate the massive parallel entry of 800 retinula fibers forcing them into a distinct morphology while at the same time maintaining the usual two-layered structure of the surface glial layer.

Comparable situations are found for the region-specific characteristics of cortex and astrocyte-like glia in Lamina, central brain and ventral nerve chord. With respect to the name astrocyte-like glia for which other names have been suggested, we do not favor to change the existing name for the following reason. In vertebrates, two generic types of astrocytes have been characterized. Protoplasmic astrocytes are found in the grey matter where they associate with neuronal cell bodies; fibrous astrocytes populate the synapse-rich white matter. In *Drosophila*, the clear spatial segregation of neuronal cell bodies into cortical regions and of synaptic contacts into neuropile regions is also accompanied by a distinct separation of the glial populations. The cortex glia populate the cortical regions and the astrocyte-like glia populate the neuropiles. Thus they represent a

comparable subdivision of glial subtypes as has been observed for vertebrates even though with a much more obvious spatial separation. Despite these morphologic similarities (which are also accompanied by functional similarities (Melom and Littleton, 2013), renaming cortex glia into protoplasmic astrocytes and astrocyte-like glia into fibrous astrocytes would likely cause more confusion and not reflect the special anatomical characteristics of *Drosophila* CNS architecture. Furthermore, the definition of ensheathing glia has been discussed (Edwards and Meinertzhagen, 2010; Hartenstein, 2011). Within the population of ensheathing glial drivers, we observe the highest variation among all generic glial subtypes. We find driver lines, which associate with peripheral nerves, with tracts in the central brain and ventral nerve chord, with the chiasms and the neuropile regions. However, they all share the unifying feature to accompany single neuronal processes or neuronal bundles. The greater morphological variation we observe within this subtype is reflected in the fact that none of the ensheathing glial drivers is expressed in the entire subpopulation. The majority of drivers label both neuropile and tract associated glia in varying proportions, and there are only few drivers that are either neuropile- or tract-specific. In concordance with their morphologic features, all drivers for the inner chiasm also show expression in neuropile-ensheathing glia, while drivers for the outer chiasm also show expression in tract-ensheathing glia. Given these general common features, we suggest to maintain one generic umbrella term, ensheathing glia, and distinguish neuropile or tract/chiasm association when necessary. Overall, we suggest to maintain the previously suggested (Awasaki et al., 2008) nomenclature containing perineurial, subperineurial, cortex, astrocyte-like and ensheathing glia and, only in the case of region-specific expression pattern, specify the generic term with the specific region / subregion (i.e. tract-ensheathing glia).

Having settled on this unified nomenclature, we investigated the numbers of glia cells in the adult *Drosophila* CNS. Employing an algorithm that is robust against variation in expression level, we counted the total number of glia in the CNS using the pan-glial marker *REPO* as well as our set of subtype-specific Gal4 drivers. The two subtypes that form the surface sheath differ vastly in their numbers. The

subperineurial glia are few (300) and very large, while the perineurial glia are many (2250) and smaller. The subperineurial glia gain their large size through endoreplication (Unhavaithaya and Orr-Weaver, 2012), perineurial glia their large cell number through massive proliferation (Awasaki et al., 2008). Our data underline these findings. The population of cortex glia makes up 17%, underlining the general observation that cortex glia – with the exception of the Lamina cortex glia – are huge and cover large areas of the cortical areas of the central brain. The remaining number of glia distribute fairly evenly, astrocyte-like glia 30% and ensheathing glia 25%. The total number of (*REPO*-positive) glia is 15,700 cells (+/- 10%). Within the margin of error, our cell counts for the different subtypes at roughly 13,500 add up to the pan-glial cell count at 15,700, suggesting that our cell counting is reasonably reliable and that we have identified all existing glial subtypes. Since the number of neurons in the adult CNS is estimated at 150,000, glia make up about 10% of the cells in the adult brain, a number similar to that found for the embryonic ventral nerve cord (Ito et al., 1995). While cell counting has been carried out for different regions or subtypes (Edwards et al., 2012; Hartenstein, 2011), ours represents the first comprehensive assessment of *Drosophila* glial cell numbers.

As mentioned earlier, our analysis was based on excellent tools, which were developed just recently. While some of them (new JFRC Gal4s / cell counts / generic expression pattern with novel reporters) enabled us to complement/corroborate the existing knowledge about glia and their classification inside the *Drosophila* CNS, others (Gal4/LexAs / MulticolorFlpOuts) paved the way for studying the interactions of single cells of one subtype with one another as well as with neighboring glia cell populations or neurons. Those studies revealed new and exiting general features of all glial subtypes as follows: Our observations suggest that, within a given glial subtype, glia cells try to minimize the contact with other glia cells of the same type. For instance, perineurial and subperineurial glia show, compared to their size, only minimal overlap with other cells of their subtype. Depending on the specific brain region, one cortex glia cell ensconces a variable number of neuronal cell bodies, by internally forming a honey comb-like

structure. Their external morphology, however, is nearly spherical, minimizing the area of contact with neighboring cortex glia. The astrocyte-like glia of the neuropiles show the same neat tiling as the cortex glia; they cover confined areas with little to no overlap at the boundaries of the single cells. Finally, there are the ensheathing glia dedicated to accompanying both dendritic and axonal extensions, from individual fibers to large tracts and chiasms. Their macro-morphology is that of a sheet which adjusts to the topology of the neuronal entities, such as neuropiles, fiber tracts or chiasms. Their micro-morphology is defined by tube-like structures that protrude from the main sheet and ensheath one or few neuronal fibers. In the case of tract-ensheathing glia a flat basal sheet produces a multitude of extensions that form vertical stacks of tubes, in the case of neuropile-ensheathing glia a sheet hugging the curvature of the neuropile produces, often arborized, tubes that envelop neuronal processes as they enter the neuropile. Similar to cortex- and astrocyte-like glia, ensheathing glia also show little if any overlap with their immediate neighbors. Mechanistically, these new evidences suggest glia to generally minimize the contact with themselves, presumably to maximize the contact with neurons.

When we looked at the interactions between different glial populations we observed the following features: First, different glial populations do not populate the same region of the brain. With the exception of the surface glial layer (in which the different glial populations most likely take over very distinct functions), the different regions of the brain are populated by only one glial subtype. More precisely, different glial populations associate with distinct entities of the neurons: cortex glia predominantly with the neuronal cell bodies, ensheathing glia with the neurites (axons and dendrites) and astrocyte-like glia with the synaptic compartments. These examples may generally indicate that redundancy between glial function is low. However, at the interface between two glial populations, we frequently see shared functionalities, such as subperineurial glia helping cortex glia with enwrapping cell bodies at the surface of the cortex, or cortex glia ensheathing emerging axons before they leave the cortex and enter neuropiles or tract regions, where they are covered by ensheathing glia. Only between

ensheathing glia and astrocyte-like glia, no commonalities have been observed, indicating the two subtypes to serve different functionalities. Lastly, we observed that glia generate small areas of physical contact in particular with other glial subtypes. For example, cortex glia send small processes into the region of ensheathing glia; astrocyte-like glia frequently send small processes into the tract regions covered by ensheathing glia processes. Most strikingly, we even observed fine astrocyte-like glial processes ramifying through the ensheathing glial layer into the cortical region. Those mechanisms are likely to generate cohesion between the different regions of the brain, presumably to maintain the capacity to signal between each other without losing the glial cell subtype specific autonomy.

In our analysis, we find multiple evidence that all glial subtypes adapt macro- and micro-morphologies to meet region-specific demands of the particular neuropile regions.

Macroscopically, the perineurial and subperineurial glia form tubes around thin peripheral nerves but flat sheath-like cells with different shape around the CNS and VNC. The cortex glia vary remarkably in the number of neuronal cell bodies they enclose. While one single cortex glia cell in the central brain may ensconce up to one hundred neuronal cell bodies, the distal and proximal cortex glia in the Lamina only encapsulate 2-10 neuronal cell bodies; the structural integrity of the honeycomb-like meshwork remains untouched. Within the neuropile, if the neuropile has a columnar organization, the resident astrocyte-like and ensheathing glia will adapt a columnar morphology. Microscopically, the structural density of astrocyte-like glia branches is inversely correlated with the synaptic density, and this feature appears to be induced locally, since different regions of the cell can have different densities. Even more, we find that astrocyte-like glia processes can look spongy or filligrane independent from the overall structural density. One cell can perform both morphologic adaptations; this feature thus appears to be induced by local cues, too. Similarly, ensheathing glia adopt different shapes, depending on whether they wrap a neuropile, a tract or a

chiasm. These observations suggest mechanisms by which glial late-stage development is largely dictated by their local environment.

The investigation of the interaction of glial cells with neurons revealed evidence for two general mechanisms: First, the different glial subtypes seem to maximize the association with their corresponding neuronal counterpart. Cortex glia ensconce single neuronal cell bodies instead of populations of them; Ensheathing glia frequently enwrap individual neurons rather than bundles (also see (Stork et al., 2008)); astrocyte-like glia spread widely inside the synaptic region but do not overlap significantly with other, neighboring astrocyte-like glia cells. Second, our mosaic analysis shows that individual glial cells do not maintain a particular relationship with individual neurons or compartmental units. This can be illustrated in many contexts: Cortex glia in the Lamina do not associate with a specific set of cartridges, ensheathing glia do not wrap specific glomeruli in the antennal lobe and astrocyte-like glia invade more than one neuropile. Consequently, the number of neuronal units with which a glial cell interacts with can be quite variable. However, while true everywhere else, in the regions of synaptic contact, the close association between glia and neuron breaks down. These observations suggest that within a given glial subtype, functions are collectively served and do likely not depend on a particular registration between single neurons and glia.

Overall, glial cells populate all regions of the *Drosophila* brain and the different subtypes collaboratively associate with all major parts of a neuron. Our findings suggest a simple set of rules governing the morphogenesis of glia and their interaction with neuronal entities. The relationship between glia and neurons and with other glia can be summarized with the following: Glia generally seek to maximize their interaction with neurons and minimize their interaction with other glia of its subtype. At the same time, they generate small regions of overlap in particular with other glial subtypes. Glial cells thus appear to have optimized their morphology to serve the following functionalities to the CNS. First, they seem to provide the largest capacity of their functions to support the neuronal network. Second, glial cells are generalists; a single glial subtype is likely capable to

provide all functions to a particular brain region that it requires. It does not require any other glial cell type in this area. Third, different glial subtypes appear to generate cohesion between the different regions of the brain, likely to maintain glial-network intrinsic interaction / signaling. Lastly, by their broad distribution throughout the brain, all the glia *must* be important for the orchestrated homeostatic support of the nervous system.

7 Functional characterization of generic glia in the adult CNS

Glia cells take over important functions in the adult fly brain. However, due to missing glial specific drivers, missing suitable tools to obtain adult-specificity and the lack of a comprehensive understanding of glial cell anatomy, functional studies in *Drosophila* have mostly concentrated on investigating the functions of *all* glia throughout development (using the pan-glial driver repo-Gal4). Only few studies concentrated on specific functions of specific glial subtypes in the adult (Awasaki et al., 2011; Melom and Littleton, 2013; Ziegenfuss et al., 2012). They thus rather present proofs of principle than a comprehensive picture of glia subtype-specific functions in the homeostasis of the adult *Drosophila* CNS. In the Gaul lab, two screens have been performed to investigate glia specific functions (also see 4.2). Those screens provided further evidence for an underrated role of glia in the homeostasis of the adult *Drosophila* CNS.

Our preliminary analysis seeks to address the following questions: First, can adult-specific glial knockdowns be principally achieved in a setup using flippable versions of Gal4 drivers? Second, is there a role of adult glia in specific homeostatic mechanisms such as detoxification, nutrient supply, circadian rhythm, and neurotransmitter and ion homeostasis? Third, how specific or redundant are those functions within the different glial subtypes?

7.1 A preliminary adult-specific RNAi screen

To answer these questions, in collaboration with Sara Batelli, we combined glial-specific Gal4s (also see 5.2) with the previously introduced Flp/FRT system (also see 4.3.2, Figure 3, Figure 27) and RNAi (also see 4.3.5.) (Ito et al., 1997) to obtain adult-specific RNAi-mediated gene function knockdown. We designed a preliminary RNAi screen based on the design of previous screens done in the lab (also see 4.2). Therefore, we selected a number of RNAi lines as positive controls (specified in 7.1.3) to principally demonstrate successful adult-specific knock

downs and phenotypic monitoring within our setup. In addition, we selected 56 RNAi lines targeting key mechanisms in the detoxification, nutrient supply, circadian rhythm, and neurotransmitter and ion homeostasis machinery as well as negative controls (specified in 7.1.3) to investigate the glia specific function in adult *Drosophila* CNS homeostasis (a full list with all RNAi lines is provided in 7.1.2). To determine the effect of the knock downs, we decided to monitor for 3 month the survival as well as obvious behavioral alterations, which we determined by eye examination (also see 7.1.1).

7.1.1 Genetic constructs and screening strategy

Sara Batelli, generated flies in which she inserted a double ‘STOP cassette’ between the enhancer sequence and the Gal4 domain of the five generic glial drivers (also see 4.3.3 for details about the Flp/FRT system, Figure 27A). The general experiments strategy was the following:

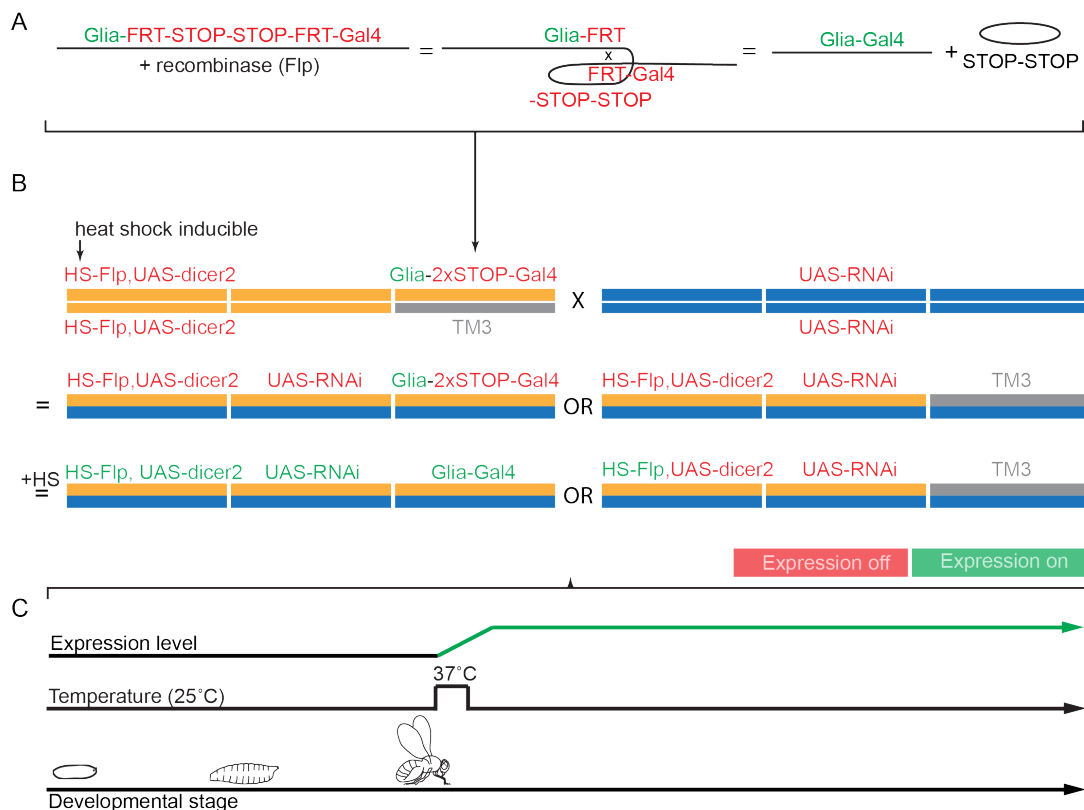


Figure 27: Schematic of an adult-specific, glial subtype-specific RNAi screen.

A Schematic of the excision of the double stop cassette through the Flippase. **B** Crossing scheme of the RNAi screen. Female flies carrying the heat-shock inducible Flippase, the UAS-dicer2 construct and the flippable

glial subtype specific Gal4 were crossed to RNAi line of interest. **C** The progeny was heat-shocked for 2h (2x 1h) at 37deg after 2-3 days after eclosion; dead flies were counted every two days.

We generated flies carrying a heat-shock inducible flippase and the ‘Glia-STOP-Gal4’. Upon crossing those flies to flies carrying the RNAi of interest under UAS control, their progeny was heat shocked 3-4 days after eclosion for 2h at 37°C (also see Figure 27C) (also see Supplemental figure 3 for details about heat shock times). The flies were then monitored for 3 months. Flies were flipped every 2-3 days and the number of dead flies was counted. Survival rate (viability) of flies was counted by the percentage of flies that survived until a given time point. In addition, we non-quantitatively investigated the flies for behavioral defects after banging the vial on the table (‘Banging assay’).

7.1.2 RNAi lines

RNAi lines were selected according to the following criteria: (1) Targeted genes had to be key players in one of the above-mentioned pathways and controls. For every homeostatic mechanism, five to ten RNAi lines were selected (full list in Table 8). (2) The targeted genes had to have a phenotype in the two screens performed previously. (3) A few RNAi lines were selected because of a previously published effect on adult survival.

Category	Gene name (CG number)
Nutrient supply	Glycogen phosphorylase (CG7254), Hexokinase A (CG3001), Phosphoglucose isomerase (CG8251), Aldolase (CG6058), Wollknaeuel (CG7870), COP9 complex homolog subunit 4 (CG8725), Calmodulin (CG8472), Phosphorylase kinase gamma (CG1830), Protein phosphatase V (CG12217), Carbonic anhydrase 1 (CG7820), Aldolase (CG6058), Foraging (CG10033), leucine import (CG12317), monocarboxylic acid transmembrane transporter activity (CG3456),
Circadian Rhythm	Clock (CG7391), Cycle (CG8727), Cyclin A (CG5940), Timeless (CG3234), PAR-domain protein 1 (CG17888), supernumerary limbs (CG3412), Casein kinase II beta subunit (CG15224), Casein kinase II beta2 subunit (CG8914), PDF receptor (CG13758), clockwork orange (CG17100), Twins (CG6235), Shaggy (CG2621), Widerborst (CG5643), Ebony (CG3331)
Neurotransmitter	glutamate transporter (CG3747), nicotinic- acetylcholine receptor beta 21C (CG11822), vesicular GABA transporter (CG8394), GABA _B receptor (CG6706), serotonin receptor 7 (CG12073), Neuropeptide Y receptor-like (CG5811), Neuropeptide F receptor (CG1147)
Detox/Redox	Superoxide dismutase 2 (Mn) (CG8905), Ferritin 1 heavy chain (CG2216), Ferritin 2 light chain (CG1469), Heat

	shock gene 67Ba (CG4167), Heat shock gene 67Bc (CG4190), Cytochrome p450-4g1 (CG3972), Thioredoxin-like (CG5495), Cytochrome p450-4e2 (CG2060), Formaldehyde dehydrogenase (CG6598)
Ionic Homeostasis	Innexin 2 (CG4590), Innexin 3 (CG1448), small conductance calcium-activated potassium channel (CG10706), Inwardly rectifying potassium channel 3 (CG10369), Inwardly rectifying potassium channel 2 (CG4370), Open rectifier K+ channel 1 (CG1615), Na pump a subunit (CG5670), transmembrane transport (CG4726), sodium:hydrogen antiporter activity (CG9256), phosphate transmembrane transporter activity (CG9090)
Housekeeping	Histone 4 (CG33871), Ribosomal protein 4 (CG5502), Small ribonucleoprotein particle protein SmF (CG16792), transcription elongation regulator activity (CG 7626), Ribosomal protein S30 (CG15697)
Negative Controls	zinc ion binding (CG17359), response to lipid hydroperoxide (CG12013), anti-apoptosis (CG6303)

Table 8: RNAi lines according to category.

RNAi lines were selected according to functional pathways (categories). Only pathways that could principally be important in glia were selected. Importance was rated by phenotype in either or both screens performed in the lab previously.

7.1.3 Controls and statistical analysis

We planned to introduce several kinds of controls. First, based on the design of the developmental RNAi screen done by Myrto Deligiannaki (also see 4.3.1), experimental flies were compared to control flies in which the ‘Glia-STOP-Gal4’ was replaced with a TM3 balancer (also see Figure 27). Those experiments aimed to obtain an ‘internal control’. Second, positive and negative control genes were selected according to their phenotype in previous screens. Positive control genes predominantly contained ‘Housekeeping’ genes, which were for example ribosomal proteins or histones that caused lethality in the developmental pan-glial screen. Negative control genes showed normal viability in the developmental RNAi screen.

For reasons, which will be further explained in the discussion, TM3 control flies as well as positive and negative controls could not be employed in the statistical analysis, because they showed inconclusive results (Figure 28). We thus tested if we could determine reduced viability within a given experiment by comparing it with the normal distribution of the values of all experiments that did not show an effect. However, due to the low number of experiments and flies, this approach

was also not suited. Therefore, we determined potential phenotypes by the rank of their survival in comparison to other experiments within the same glial subtype (also see Figure 27, for explanation of the analysis). We note that based on this analysis, we should not rely on the significance of observed effects and conclude phenotypes only when they are accompanied by behavioral alterations.

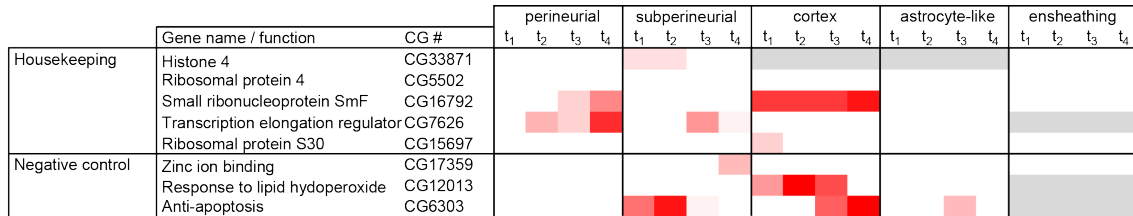


Figure 28: Effect of the knock down of positive and negative control gene function.

Housekeeping genes represent the positive control; negative control genes were selected according to their rank in the developmental screen where they had no effect (also see 4.2). The matrix is subdivided into categories according to the glial subtypes perineurial, subperineurial, cortex, astrocyte-like and ensheathing glia. For each category, four time points are plotted representing the survival rates after 2, 4, 6 and 8 weeks. Within the matrix, grey boxes represent values for which no data was retrieved, shades of red represent presumable phenotypes of the knockdown. Only those ranks were plotted that exceeded the 75th percentile of ranks of all the values for one glial subtype. The higher the intensity of red, the higher the rank of the death rate. Notably, the knockdown of positive control gene function did not lead to reduced viability in all glial subtypes. On the contrary, RNAi of negative control genes occasionally leads to reduced viability.

The analysis was performed as follows: First, the survival rate of each experiment (=single glial subtype crossed to one RNAi line) was determined as the percentage of flies that survived until that time point. Second, since experiments were started in batches at different time points, all experiments were adjusted to a common time frame to provide comparability between experiments. Third, four time points (t₁ - t₄, t₁=14days, t₂= 28days etc) were selected which were separated by 2 week intervals. Therewith the survival data for the first two month of the counting are covered. (The survival was originally monitored for three month, however, to avoid effects of the natural mortality rate, only the first two month were considered in the analysis). Fourth, for all values the percentile rank was determined by comparing all values from one glial subtype at all five time points (t₁ - t₄). Fifth, all values with a percentile rank above the 75th percentile were plotted as a matrix. Within this matrix, darker colors represent higher ranks (and

consequently more severely reduced viability) whereas light colors represent lower ranks.

7.1.4 *The glial subtype-specific role in CNS homeostasis*

We decided to investigate the role of glia in five important homeostatic mechanisms: Circadian rhythm, ionic homeostasis, neurotransmitter homeostasis, detoxification and nutrient supply. Circadian rhythms steer many elemental processes in the central nervous system. The molecular components of this machinery have been extensively studied, leading to the identification of the core ‘clock’ genes and regulatory mechanisms (for review: (Hardin, 2005; Jackson, 2011); nevertheless, we are only beginning to understand the cellular components and interactions. Aside their localization within neuronal components, oscillating levels of key circadian rhythm proteins were found in glia (Jackson, 2011) and lead to reduced viability and locomotor defects when knocked down (Suh and Jackson, 2007) suggesting an important role in the circadian machinery. Glia have furthermore been suggested to be involved in the regulation of finely adjusted electrochemical gradients built by varying concentrations of ions (ionic homeostasis). Many important functions such as action potential propagation and transport across cell membranes rely on such gradients. In addition, there is evidence that glia are involved in various aspects of neurotransmitter homeostasis (Anderson and Swanson, 2000; Araque et al., 2001; Karadottir and Attwell, 2007; Kastritsis and McCarthy, 1993; Newman, 2003; Stys, 2011). Those processes are of major importance for the homeostasis of adult organisms because the release, binding, reuptake and recycling of neurotransmitters governs the proper function of neuronal connections. Detoxification and maintenance of an equilibrated level of reactive oxygen within cells are functions to protect cells from accumulation of hazardous materials. In the previous screens performed in the lab (also see 4.2), genes involved in major detoxification pathways such as oxidative stress response and alcohol oxidation were also found to be upregulated or caused lethality when knocked down developmentally. Lastly, we wanted to test the glial role in nutrient supply of the adult CNS. The nutritive supply of the CNS is elemental for its performance. Glia ubiquitously populate all regions of the brain; simply by their

close association with all parts of the neurons, it seems likely they play a role in the nutrition of the neurons. It is debated whether glucose or lactate are the main energy metabolites in the brain, and if (and when) either or both are required for basal and upregulated neuronal activity (Aubert et al., 2005; Bak et al., 2006; Pellerin et al., 2007; Simpson et al., 2007). Multiple considerable hypotheses are currently discussed. Among those, the astrocyte-neuron lactate shuttle (ANLS) hypothesis proposed by Pellerin and Magistretti in 1994 grant astrocytes a major role in metabolizing glucose into lactate which would subsequently be transported into the neurons (Pellerin and Magistretti, 1994).

For the reasons mentioned, we strongly believe that different glial subtypes could play a major role in each of these mechanisms. Therefore, we systematically knocked down a small set of the major genes of these pathways specifically in each of the generic glial subtypes. The preliminary results are presented in Figure 29.

	Gene name / function	CG #	perineurial				subperineurial				cortex				astrocyte-like				ensheathing			
			t ₁	t ₂	t ₃	t ₄	t ₁	t ₂	t ₃	t ₄	t ₁	t ₂	t ₃	t ₄	t ₁	t ₂	t ₃	t ₄	t ₁	t ₂	t ₃	t ₄
Circadian rhythm	Clock	CG7391																				
	Cycle	CG8727																				
	Cyclin A	CG5940																				
	Timeless	CG3234																				
	PAR domain protein 1	CG17888																				
	supernumary limbs	CG3412																				
	Casein kinase II beta subunit	CG15224																				
	Casein kinase II beta2 subunit	CG8914																				
	clockwork orange	CG17100																				
	Ebony	CG3331																				
	Widerborst	CG5643																				
	Shaggy	CG2621																				
	Twins	CG6235																				
Ionic homeostasis	Innexin 3	CG1448																				
	Small cond. Ca-activ. K+-channel	CG10706																				
	Inward rectifying K+ channel 3	CG10369																				
	Open rectifier K+ channel 1	CG1615																				
	Na pump subunit	CG5670																				
	Phosphate:sodium transporter	CG4726																				
	Na:OH antiporter activity	CG9256																				
Phosphate:ion transporter	CG9090																					
Neuroransmitter homeostasis	glutamate transporter	CG3747																				
	nicotinic-Ach receptor beta 21C	CG11822																				
	vesicular GABA transporter	CG8394																				
	GABA _A receptor	CG6706																				
	serotonin receptor 7	CG12073																				
	Neuropeptide Y-like receptor	CG5811																				
	Neuropeptide F receptor	CG1147																				
Detoxification	Superoxide dismutase 2	CG8905																				
	Ferritin 1 heavy chain	CG2216																				
	Ferritin 2 light chain	CG1469																				
	Heat shock gene 67Ba	CG4167																				
	Heat shock gene 67Bc	CG4190																				
	Cytochrome p450-4g1	CG5495																				
	Thioredoxin-like protein	CG3972																				
	Cytochrome p450-4e2	CG2060																				
	Formaldehyde dehydrogenase	CG6598																				
Nutrient supply	Glycogen phosphorylase	CG7254																				
	Hexokinase A	CG3001																				
	Phosphoglucose isomerase	CG8251																				
	Aldolase	CG6058																				
	Wollknaeucl	CG7870																				
	COP9 complex homolog subunit 4	CG8725																				
	Calmodulin	CG8472																				
	Phosphorylase kinase gamma	CG1830																				
	Protein phosphatase V	CG12217																				
	Carbonic anhydrase 1	CG7820																				
	Foraging	CG10033																				
	Monocarbox acid transporter	CG3456																				
	Leucine importer	CG12317																				

Figure 29: Effect of the knock down of functions involved in different mechanisms of CNS homeostasis.

Genes potentially involved in circadian rhythm based on a previous developmental RNAi screen as well as published results (reviewed in (Hardin, 2005; Jackson, 2011)) were knocked down and the effect onto the survival of a population of flies was measured after 2, 4, 6 and 8 weeks. A detailed description of the matrix is provided in Figure 28. Boxes with black outline indicate experimental groups in which a behavioral phenotype was observed.

Circadian rhythm

In our experiments, we knocked down the molecular key components of the circadian machinery in all glial subtypes (Figure 29). We only observe behavioral phenotypes in the case of astrocyte-like glia (*Supernumerary limbs* (CG 3412), *Casein kinase II beta subunit* (CG 15224), *Casein kinase II beta2 subunit* (CG 8914)) and in a single case in ensheathing glia (*Casein kinase II beta subunit* (CG 15224)) (Figure XYZ). *Supernumerary limbs* is part of a complex that interacts with PER and accelerates its degradation (Ko et al., 2002). However, the degradation complex in which *supernumerary limbs* is involved could also have broader functions, which caused behavioral phenotypes upon RNAi mediated gene knock down in astrocyte-like glia. With respect to the strong effects we observe in astrocyte-like and ensheathing glia after knock down of *casein kinase II beta subunit*, we conclude the following: Within the circadian machinery, casein kinase II and its subunits have the function to destabilize PER and thus maintain its oscillating rhythms. However, ubiquitous functions of casein kinase II (based on *Drosophila* interaction database it has 381 protein-protein-interactions) leave room to hypothesize about its essential non-circadian function in different glia cell populations that cause the behavioral defects we observe in our experiments. Overall, these observations add to earlier observations. However, to fully understand the glial subtype specific roles in more detail, more genes of the circadian machinery (*doubletime*, *period* and others) will have to be tested using behavioral assays to monitor circadian rhythms and locomotor activity in more detail to detect even more subtle phenotypes.

Neurotransmitter and ionic homeostasis, detoxification and nutrient supply

The knock down of genes involved in neurotransmitter and ionic homeostasis, detoxification and nutrient supply did not reveal significant effects. In rare cases, we observe behavioral alterations, which are not accompanied by significantly reduced viability; in others, we see effects, which may indicate the potential involvement of specific glial subtypes in these processes. However, in the light of described difficulties with the internal, positive and negative control,

interpretation of these observations appears premature and conclusions on the glial subtype specific roles in these processes currently impossible.

7.2 Summary

We could demonstrate that the genetic approach of using flippable versions of generic glial subtype Gal4 drivers can be employed to study the function of different genes in specific phases of development (in our case, in the adult). We showed that RNAi-mediated gene knock down in glial subtypes leads to behavioral alterations which seem to be accompanied by reduced survival of the flies. However, due to low numbers of experiments, and more importantly, suitable controls, we cannot conclude about the glial subtype-specific functions in CNS homeostasis. These preliminary experiments thus predominantly thought us about the do's and don'ts of adult-specific RNAi screen design, and lay ground for future large scale studies to investigate adult glia function in *Drosophila*.

7.3 Discussion

The role of the different generic glia had not been systematically investigated with respect to their function in the CNS homeostasis, specifically of adult *Drosophila*. Here, we concentrated on the establishment of a screen design for genetic manipulations only in the adult fly. Having generated the genetic constructs and flies for those experiments, we employed them in a preliminary RNAi screen to look at the specific role of different glia subtypes in the adult. While we could principally show that adult-specific expression can be achieved with flippable Gal4 drivers, during the course of these experiments, we encountered problems with respect to screen design, proper controls and suitable readouts that made it difficult to draw functional conclusions. Therefore, in this discussion, I largely want to concentrate on the technical lessons learned and how those obstacles will have to be circumvented in future experiments.

The setup employed in our experiments relies on the complete initiation of expression of the Gal4 construct in dependence of the heat shock. Our experiments showed that when flies are raised at or below 25°C, there is no leakage of the flippase, and consequently no premature expression. Furthermore, we demonstrated that flies have to be heat-shocked for 2h to flip out the ‘Stop cassette’ in the majority of cells. Lastly, this heat shock period does not seem to cause temperature induced stress and significant death of the flies. This setup thus proved to be suitable for adult-specific expression of Gal4 drivers.

Nonetheless, we also encountered a few difficulties which will have to be considered in future experiments: First, the number of flies selected for each experiment was too low; second, the internal control unexpectedly showed a high variability of survival after twenty days; third, the positive and negative controls could not be employed and lastly, survival turned out to be too insensitive to monitor the defects induced in our experiments.

Initially, we had planned to normalize the survival curves of all experiments with their internal (TM3) control as well as positive and negative controls. In the developmental RNAi screen performed previously in the lab, TM3 balancer flies

were employed to compare the survival rate between experimental and control flies in which the Gal4 driver was replaced with a TM3 balancer. In our experiments, we sought to maintain the same screening procedure. However, we realized that survival within the TM3 group after twenty days is decreased and that the variance of survival is much higher compared to experimental groups. For these reasons, TM3 as an internal control does not seem to be suited in future experiments. Instead we plan to test the parental flies in parallel as controls with close genetic background. With respect to positive and negative controls, we assumed that the knockdown leads to dramatically reduced viability or normal viability, respectively. However, this could not be observed in the experiments. In fact, some of our negative controls lead to reduced survival when knocked down in the adult, suggesting that the adult-specific role of these genes is quite different than their role during development. Unfortunately, a suitable negative control such as an RNAi against an exogenous, non-existing gene like GFP is not available. For these reasons, we decided to exclude positive and negative control RNAis from the analysis; this led us with the lack of a suitable control to normalize our data. Nonetheless, we observed behavioral alterations in some of our experiments, which ultimately led to death of the flies. We are thus certain the experiments principally worked.

In our experiments, the effect of the gene knockdown was measured by means of survival of the flies. Only very clear phenotypes, which could be identified by eye by their abnormal behavior, were additionally registered. This approach was selected because it has the advantage of (i) providing comparability between experimental groups using relatively simple statistics and (ii) because it identifies the most serious phenotypes. However, at the same time, survival rate was identified as a limitation of our experimental setup. While some RNAi cause severe locomotion dysfunction followed by significantly earlier death of the flies, other RNAi (observably) weaken the flies without leading to reduced viability (and thus would not show up in our screen). In future experiments, we will use more sensitive readouts such as locomotion, sleep-wake cycle or geotaxis in combination with survival assays to obtain higher sensitivity. Additionally we

found that, when performing these experiments at 25°C, the flies age well and survive up to 3 month. Since temperature is likely to act as a stressor to the fly, has a significant effect onto the life expectancy of the flies and increases activity of the Gal4, we additionally intend to perform future experiments in a sensitized background at 29°C.

Overall, from this preliminary RNAi screen, we conclude that flippable Gal4 drivers are a suitable method to obtain adult-specific expression. Moreover, adult specific induction of RNAi-mediated gene knock down appears possible, even though at the expense of longer duration of experiments. Lastly, we identified potential drawbacks of the initial experimental setup and suggested various ways to optimize it, including higher number of experiments, higher number of flies per experiment, better-suited controls and behavioral readouts.

8 Outlook

In the current study, tools to investigate glial subtype specific function have been identified, morphologically characterized, modified for adult-specific expression and employed in a preliminary adult-specific RNAi screen. However, whilst this system now enables us to describe the generic glia subtypes in the adult *Drosophila* CNS in more detail, we suggest a few more methodological optimizations. Except for the generic subtype drivers, almost all glial drivers show little to significant neuronal background making them defective for functional experiments. To overcome these handicaps, we suggest first to continue the generation of enhancer fragments based on a biased selection of glial specific genes and second, to clean up unwanted co-expression in neurons by glial-specific FlpOuts using a yet to be generated repo-Flp or split-Gal4s. Those approaches are essential to investigate the role of region-specific glia subtypes for example in the lamina.

In the last part of this thesis, the generic glial subtype-specific drivers were optimized for adult-specific application and established in a preliminary RNAi screen. The combination of the knowledge about the anatomy of the glial components of the central nervous system with the tools to functionally manipulate them independently in all phases of development allow for an investigation of specific aspects of glial subtype function in the future. From our point of view, the next steps towards a comprehensive understanding of glial cell function in the developing and adult nervous system comprise to ask the following questions: In the developing nervous system, what generic function do the different glial subtypes serve and how does malfunction of those glia affect overall CNS development? Asking this question, it will be particularly interesting to see how region-specific glial populations for example in the optic lobe contribute to proper neuropile formation. In the mature nervous system, questions with respect to anatomy or function arose during this thesis. With respect to the anatomy of glial cells, one major question is the role of differently dense astrocyte-like glial processes in different brain regions and whether they can be linked to functional

specializations of these regions. Also, it will be exciting to investigate in more detail the role of ensheathment within different compartments and how this contributes to the performance of certain brain areas. Looking more globally at the functions of glial cells, one should ask what functions different generic glial subpopulations provide to the well being of the CNS and what happens when those are perturbed? In our preliminary study, we confirmed and newly identified glial subtype-specific functions. However, future investigations should probably start again with a detailed investigation of redundancy and differences between different glial subtypes on a larger scale. In addition, those studies will likely profit tremendously from more sensitive behavioral readouts as well as previously described optimization of the screen set up.

Those investigations will complement our recent understanding of glial subtype-specific functions and likely unravel novel aspects of glial contribution to the integrity of the brain. Given the relative comparability of glial subtypes between invertebrates and vertebrates, it appears not unlikely that *Drosophila* may ultimately serve important insights to understanding the principle mechanisms of vertebrate brain function.

9 Material and Methods

9.1 Fly strains and genetics

The expression patterns of the Janelia Farm Gal4 driver collection had previously been established using a membrane-tagged GFP reporter (UAS-mCD8-GFP) and confocal imaging of entire adult brains (Jenett et al., 2012; Pfeiffer et al., 2008). By screening through the maximum density projections of this image collection, we identified lines with putative glial expression. For further analysis, we selected lines, which showed specific expression in one or two glial subpopulations, no neuronal background or mosaicism of expression. A complete annotated list of Gal4 lines with glial expression will be available online. All Gal4 strains are available through the Bloomington Stock Center.

Glial expression of drivers was ascertained using a nuclear GFP reporter (UAS-nls-GFP) and co-labeling with the pan-glial marker REPO; these nuclear co-labelings were also used to determine the cell number of specific glial subpopulations and the entire glial population in the adult brain.

The morphology of individual cells and the relationship between neighboring cells was determined by multi-color mosaic experiments using a new technique developed by A. Nern and B. Pfeiffer (unpublished) (also see (Tuthill et al., 2013)). In these experiments, a series of three differently tagged reporters under UAS control is kept silent by FRT-flanked transcriptional terminators. Through a brief pulse of heat shock-induced Flippase expression, terminators are removed randomly in individual cells; expression occurs only in cells that also express a (glial) Gal4 driver. This leads to a (sparse) patchwork of differently colored cells of a given glial cell type (also see 4.3.4).

To study the relationship between two different cell populations (glia/glia or glia/neuron), LexA versions of the best glial drivers were generated. The two binary expression systems, Gal4-UAS (Brand and Perrimon, 1993; Fischer et al., 1988) and LexA-Leap (Lai and Lee, 2006; Pfeiffer et al., 2008; Pfeiffer et al., 2010), were then used to concurrently label two distinct cell populations with strong

well-defined reporters (UAS-myr-smGFP-HA, LexAOp-myr-sm-GFP-V5) (Pfeiffer et al., 2010) (Aljoscha Nern, Barret Pfeiffer, unpublished). All drivers used in this study are listed in Table 9. All reporters used in this study are listed in Table 10.

<i>General</i>	<i>Descriptor</i>	<i>Abbrev.</i>	<i>Specificity</i>	<i>Genotype</i>	<i>Source</i>	<i>Comment</i>
PNG	Perineurial glia	PNG	generic	85G01-Gal4 (attP2)	JFRC	
	Perineurial glia	PNG	generic	85G01-LexA (attP40)	JFRC	
	Lamina perineurial glia	L-PNG	Lamina	47G01-Gal4 (attP2)	JFRC	fenestrated glia
	Lamina chalice-like glia	L-cl-PNG	Lamina	27H11-Gal4 (attP2)	JFRC	
SPG	Subperineurial glia	SPG	generic	54C07-Gal4 (attP2)	JFRC	
	Subperineurial glia	SPG	generic	54C07-LexA (VK00027)	JFRC	
	Lamina subperineurial glia	L-SPG	Lamina	50A12-Gal4 (attP2)	JFRC	pseudo-cartridge glia
CG	Cortex glia	CG	generic	77A03-Gal4 (attP2)	JFRC	
	Cortex glia	CG	generic	77A03-LexA (attP40)	JFRC	
	Cortex glia	CG	generic	54H02-Gal4 (attP2)	JFRC	
	Lamina distal cortex glia	L-dCG	Lamina	53B07-Gal4 (attP2)	JFRC	distal satellite glia
	Lamina proximal cortex glia	L-pCG	Lamina	44B12-Gal4 (attP2)	JFRC	proximal satellite glia
	Lamina proximal cortex glia	L-pCG	Lamina	46H12-Gal4 (attP2)	JFRC	proximal satellite glia
ALG	Astrocyte-like glia	ALG	generic	86E01-Gal4 (attP2)	JFRC	
	Astrocyte-like glia	ALG	generic	86E01-LexA (VK00027)	JFRC	
	Lamina astrocyte-like glia	L-ALG	Lamina	55B03-Gal4 (attP2)	JFRC	epithelial glia
EG	Neuropile-ensheathing glia	EGN	generic	56F03-Gal4 (attP2)	JFRC	
	Neuropile-ensheathing glia	EGN	generic	56F03-LexA (VK00027)	JFRC	
	Tract-ensheathing glia	EGT	generic	75H03-Gal4 (attP2)	JFRC	
	Lamina	L-EGN	Lamina	60F04-Gal4 (attP2)	JFRC	marginal glia
	Lamina	L-EGN	Lamina	35E04-Gal4 (attP2)	JFRC	marginal glia
	Chiasm glia	XGO / XGI	chiasms	53H12-Gal4 (attP2)	JFRC	
	Chiasm glia	XGO / XGI	chiasms	53H12-LexA (attP40)	JFRC	
Neuronal	Kenyon cells			17d-Gal4		Hiromu Tanimoto, Manoli et al. 2005, Akalal et al. 2006
	Projection neurons	PN	few cells	mz19-Gal4		Bloomington
	Projection neurons	PN	many cells	GH146-Gal4		Bloomington

Table 9: Summary of drivers used in this thesis.

Flies for the mosaic experiments were grown at 18°C, heat-shocked 1 day after eclosion and dissected 2-3 days later. For all other experiments, flies were grown at 25°C and dissected 3-5 days after eclosion.

<i>Reporters</i>	<i>Descriptor</i>	<i>Genotype</i>	
	membrane tagged GFP	UAS-mCD8-GFP	JFRC
	membrane tagged GFP	UAS-myr-smGFP-V5	JFRC
	nuclearly expressed GFP	UAS-nls-GFP	Bloomington
	cytosolic expressed GFP	UAS-DM21-GFP-BP	JFRC
	Double labelings	UAS-myr-smGFP-HA / LexAop-myr-smGFP-V5	JFRC
	McFlip	HsFlpPestOpt; ; UAS-McFlip (UAS-STOP-smGFP-HA, UAS-STOP-smGFP-V5, UAS-STOP-smGFP-FLAG)	JFRC

Table 10: Summary of reporters used in this thesis.

9.2 Immunohistochemistry

9.2.1 Embryos

Embryos from 16 hours collection were transferred with a brush from the yeasted grape juice agar plates to a collection basket. They were rinsed 3 times in PBTx (1x PBS + 0.1 % Triton X-100) in order to remove rests of yeast and other impurities. They were dechorionated in 50 % bleach for 5 min and again rinsed in PBTx for three times. Afterwards, they were transferred into scintillation vials with 8 ml of 100 % Heptane, 0.5 ml of 4 % formaldehyde was added and the vials were put on the rotator for 20 minutes at room temperature (RT). The lower aqueous phase was then drawn off and 8 ml of 100 % Methanol (MeOH) were added. After shaking them for one more minute on the rotator, the settled embryos were drawn off and rinsed three times in 100 % MeOH. After the fixation, the embryos were stored at -20 °C until the preparation for the staining.

The embryos were rehydrated and washed with PBTw (1XPBS with 0.1 % Tween 20) and BBTw (PBTw with 0.1 % BSA). Then they were blocked in BBTw with 2.5 % normal goat serum (NGS) and 2.5 % normal donkey serum (NDS). After the blocking, the primary antibodies (ABs) were diluted to the appropriate concentrations in BBTw with 2.5 % NGS and 2.5 % NDS and incubated at 4 °C, overnight (o/n). On the next day, the ABs were drawn off and the embryos washed with BBTw. The secondary ABs were diluted in BBTw with 2.5 % NGS and 2.5 % NDS and added. Embryos were rocked for 2 hours at RT. After drawing off the secondary antibodies the samples were rinsed in PBTw several times. Antibodies were used at dilutions indicated below.

Embryos were washed in 50 % Glycerol (diluted in PBTw) and in 70 % Glycerol with 2.5 % DABCO antifading agent. They were mounted on a coverslip previously treated with 1 % Tween solution and imaged with a confocal microscope. Early stage 17 embryos were imaged. (DABCO antifading solution: 70 % Glycerol; 2.5 % DABCO; 10 mM Tris, pH 7.5).

9.2.2 *Adult and larval CNS*

Flies were anesthetized with CO₂ to select the desired genotype, washed in cold 70% ethanol (30''), then cold PBS (30'') and kept in cold ExpressFive™ cell culture medium™ (Invitrogen) before and during preparation. Brains were dissected immediately using forceps and transferred into cold fixative. All subsequent steps were performed on a nutator at room temperature in 200µl PCR tubes.

Brains were fixed in 2% paraformaldehyde (PFA, Electron Microscopy Sciences) in ExpressFive™ medium for 1h. After three or more washes (15' each) with adult brain washing solution (0.5% BSA (Sigma), 0.5% TX-100 (Sigma) in PBS), the tissues were blocked with blocking solution (3% normal goat serum (Jackson Laboratories), 3% normal donkey serum (Jackson Laboratories), 0.5% TX-100 in PBS) for 30'. Tissues were incubated with primary antibodies overnight, washed 3x1h in adult brain washing solution, incubated with secondary antibodies overnight, washed 3x1h in adult brain washing solution, followed by a final wash in PBS overnight. Tissues were mounted in VectaShield (Vector Laboratories) or 50:50 VectaShield and SlowFate™ Gold (Invitrogen).

Antibodies were obtained from the Developmental Studies Hybridoma Bank (DSHB), developed under the auspices of the NICHD and maintained by The University of Iowa, Department of Biology, Iowa City, IA 52242, as well as commercial sources. All antibodies used in this study are listed in Table 11.

<i>Antibodies</i>	<i>Descriptor</i>	<i>Target</i>	<i>Dilution</i>	<i>Host</i>	<i>Source</i>
primary	Neuropiles / Synapses	NC82	1:25	mouse	DSHB, Erich Buchner
	Glial cell bodies	REPO, 8D12	1:25	mouse	DSHB, Corey Goodman
	Neuronal cell bodies	ELAV	1:10	rat	DSHB, Gerald M. Rubin
	Axon tracts	22C10	1:10	mouse	DSHB, Seymour Benzer
	Photoreceptor neurons	24B10	1:25	mouse	DSHB, Seymour Benzer
	Acetylcholine transporter	CHAT	1:25	mouse	DSHB
	Antibody against GFP	GFP	1:500	rabbit	Invitrogen
	Antibody against HA tag	HA	1:500	rabbit	Cell signaling
	Antibody against FLAG tag	FLAG	1:100	rat	Novus Biologicals
conjugated	V5-tag:DyLight™-549	V5	1:200	mouse	AdSerotec
	HA-tag:DyLight™-488	HA	1:200	rabbit	Rockland
secondary	Pacific Blue	mouse	1:200	goat	Invitrogen
	AlexaFluor 488	rabbit	1:250	goat	Invitrogen
	DyLight 549	mouse	1:200	donkey	Jackson Laboratories
	AlexaFluor 568	rat	1:200	goat	Invitrogen
	DyLight 647	rat	1:100	donkey	Jackson Laboratories
	DyLight 649	mouse	1:100	donkey	Jackson Laboratories

Table 11: Summary of antibodies used in this thesis.

9.3 Confocal microscopy and image analysis

Stacks of serial confocal sections (0.32 μ m) were acquired using a Zeiss LSM 710 with 20x(air), 40x(water) and 63x(oil) objectives. An automated table and MultiTime2010 (Zeiss) allowed us to scan multiple locations automatically, in which case 40x (with halogen-free immersion medium, n=1.33) and 63x (n=1.52, oil) objectives were used.

Processing of confocal stacks included maximum density projections, substack projections, orthogonal views, rotations, changes in channel hue and adjustment of brightness and contrast. Confocal images were processed with ImageJ (Abramoff, 2004; Rasband, 1997-2012); 3D reconstructions were created in Imaris (Bitplane). All figures and illustrations were prepared in Adobe Illustrator CS5 version 15.0.0.

Counting of nuclei within confocal stacks was carried out as described in Figure 30 using a home-written Definiens XD 2.0 script. Subsequent statistical analysis was done in Excel and finished in GraphPadPrism. Considerations regarding coverage of single generic drivers and additional use of region-specific drivers to count the glial cells of one subtype in the entire brain are explained earlier (also see 6.1.1). The structure density of astrocyte-like glia and synapses in different brain regions was determined and correlated as described in Figure 31 using a home-written Definiens XD 2.0 script. To determine the average density of astrocyte-like glia density processes per brain neuropile, we manually rated the densities for every neuropile as is explained in Figure 32.

.

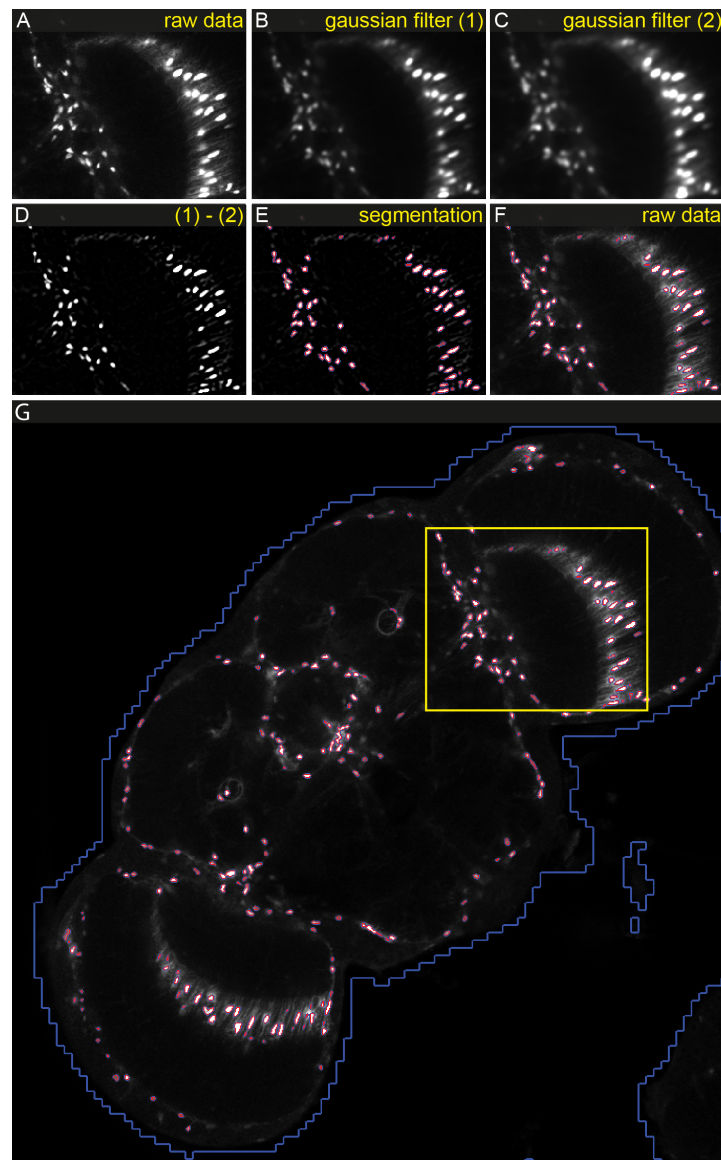


Figure 30: Automated counting of immune-histochemically labeled glial cell bodies.

Confocal stacks of brains, in which glial cell bodies were labeled using a nuclear GFP reporter (example here: 28A04Gal4; UASnls-GFP) and anti-REPO AB and neuronal cell bodies were co-labeled with anti-ELAV AB, were processed as follows: The contours of the brain were identified based on the ELAV signal in channel one, the entire set of glial cell bodies was identified based on the REPO signal in channel two, subtype specific glial cell bodies were identified based on the nuclear GFP signal in channel three. Counting was carried out in 3D, however, in order to avoid over-counting, cell bodies were only counted in the z-layer with the highest density. To detect cell bodies, we applied the following strategy. In the raw images (A), which have a size of 1024x1024 pixels with a resolution of 692 nm per pixel in xy and a z slice of 1 μ m, the signal intensity of GFP- and REPO-labeled nuclei bodies is high, but the considerable variation in background intensity makes a precise identification of cells difficult. Therefore, using a global threshold does not produce good segmentation. Instead, we developed a strategy based on background reduction. As a first step, we applied a 3D-Gaussian filter with a kernel size of 5x5x3 pixels (B, Gaussian filter (1)), then applied a second 3D-Gaussian filter, again with a kernel size of 5x5x3 pixels, (C, Gaussian Filter (2)), and then subtracted C from B, which resulted in the background subtracted image shown in D. As a last step, we applied a global

threshold and carried out segmentation using an algorithm implemented in the *Definiens XD 2.0* software platform, as shown in **E**. Briefly, the so-called Multi-Threshold Segmentation algorithm used splits the image domain and classifies the resulting image objects based on a defined pixel value threshold. **F** shows the segmentation patterns (magenta lines) superimposed on the raw data. Despite strong background heterogeneities, as seen on the right, cells are readily identified (**G**). The 3D segmentation patterns are displayed for an exemplary confocal plane of a full *Drosophila* brain. Finally, the data were exported and statistically evaluated in Microsoft Excel and GraphPathPrism.

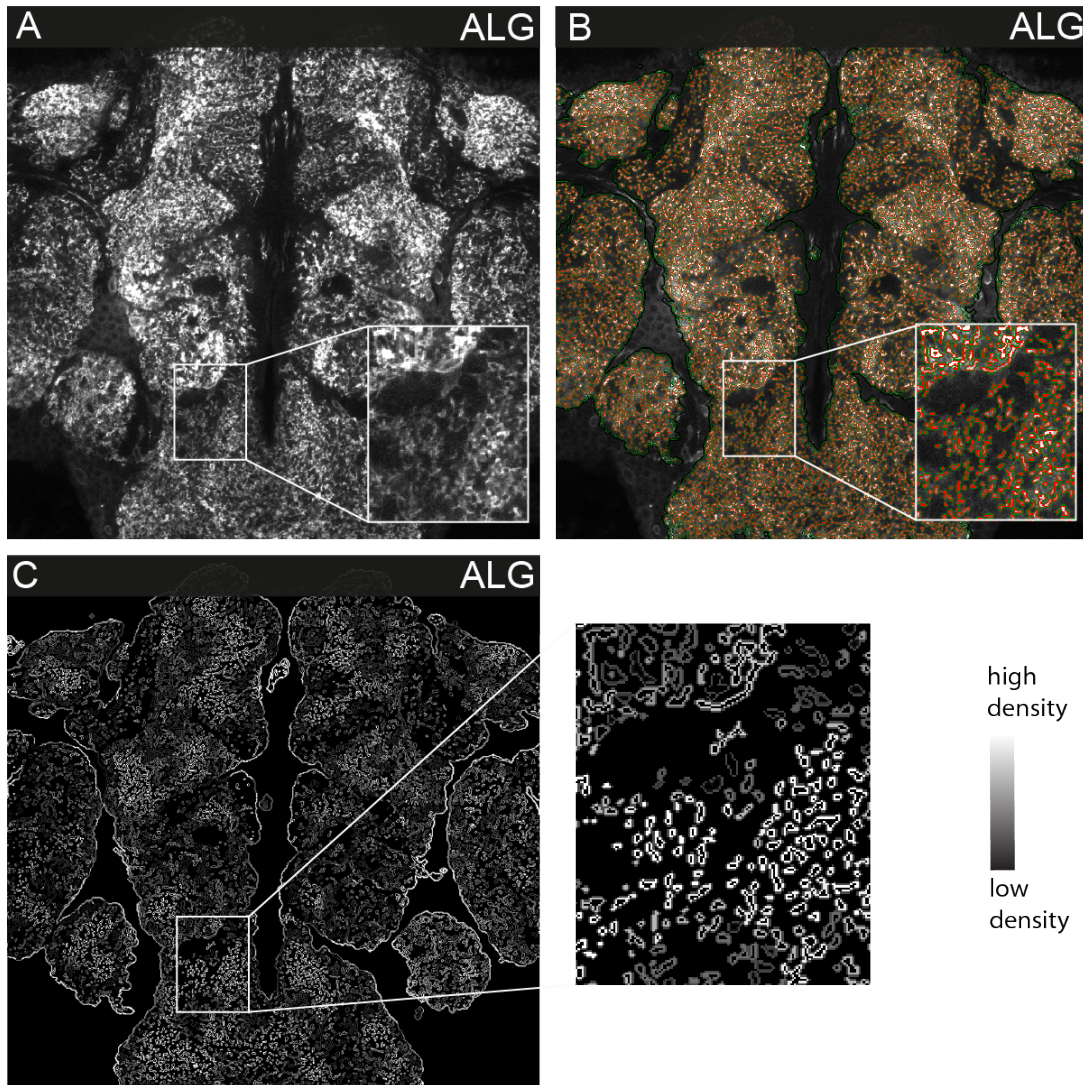


Figure 31: Automated analysis of the astrocyte-like glia-processes density.

The structure density of astrocyte-like glia processes (ALG channel) and synapses (nc82 channel) were determined and correlated using a home-written *Definiens XD 2.0* script. The analysis strategy is illustrated for the ALG channel. First, the astrocyte-like glia channel was segmented similarly to the procedure described in Figure 30. As a first step, we applied a 3D-Gaussian filter with a kernel size of 5x5x3 pixels (Figure 30B), then applied a second 3D-Gaussian filter, again with a kernel size of 5x5x3 pixels (Figure 30C), and then subtracted C from B, which resulted in a background subtracted image (Figure 30D). As a last step, we applied a global threshold and carried out segmentation using an algorithm implemented in the *Definiens XD 2.0* software platform. Briefly, the so-called Multi-Threshold Segmentation algorithm used splits the image domain and classifies the resulting image objects based on a defined pixel value threshold. A shows an exemplary confocal slice. The segmented patterns of the brain (in green) as well as of the astrocyte-like glia cells (in red) are superimposed in B. The astrocyte-like glia cell density was subsequently determined as illustrated in the insert of C. For each individual cell the total area of surrounding cells was used as a measurement of the local cell density. For each single image object of interest (in blue) we computed the total area in pixels (in yellow) of the neighboring objects present in a radius of 30 pixels around the center of mass of the image object of interest (region delimited by the blue circle). The image objects were then color-coded

according to their density (C), revealing regions with different ALG coverage. Finally, the procedure was reiterated with the nc82 channel.

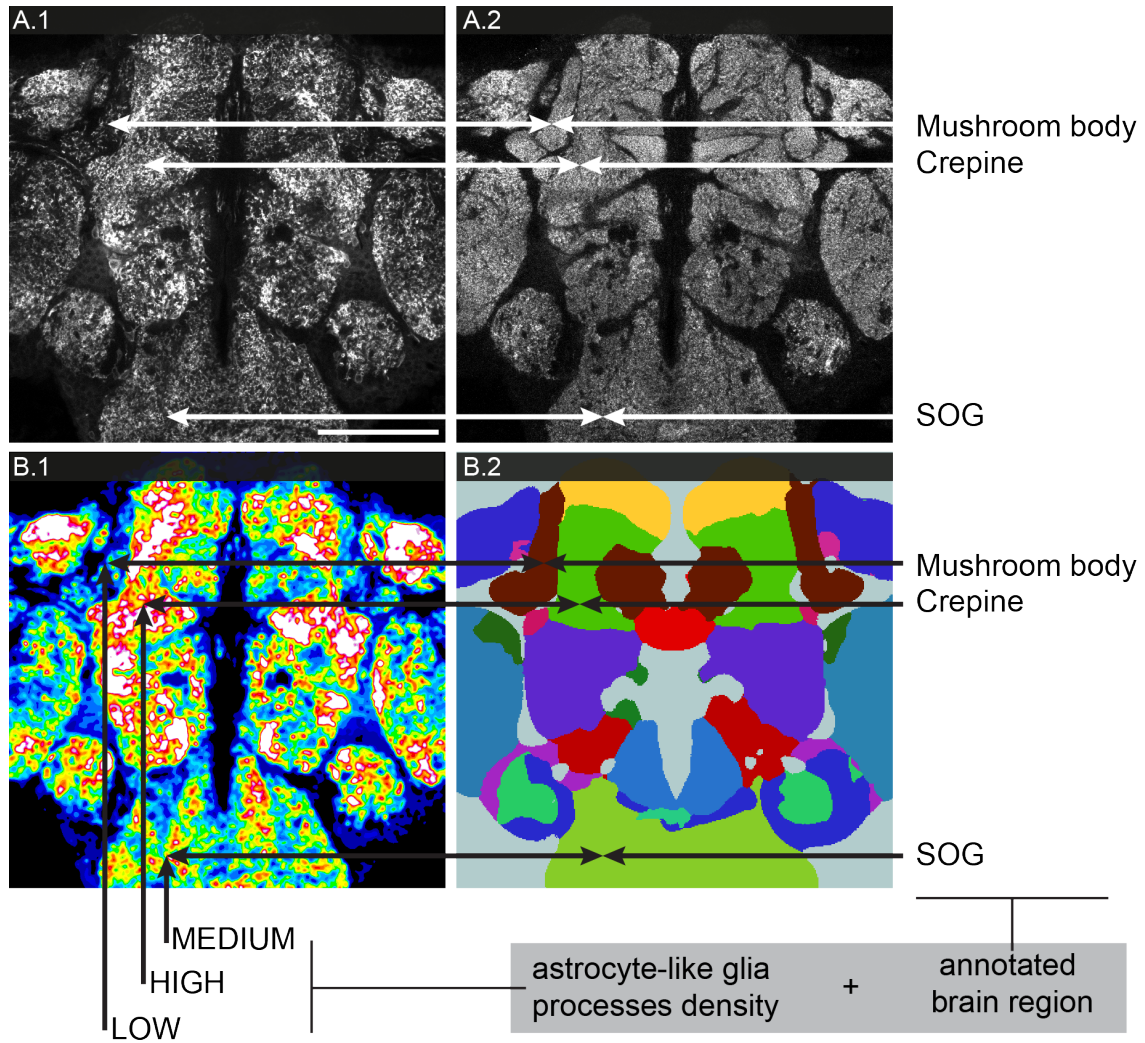


Figure 32: Annotation of astrocyte-like glia processes in different brain regions.

A.1 The density of astrocyte-like glia processes differs in different brain regions (single frontal section of the anterior protocerebrum). A.2 The density of NC82-labeled synapses differs in different brain regions. Within each brain regions, the variation in density level is low (single frontal section of the anterior protocerebrum). B.1 The density of astrocyte-like glia processes (A.1) was analyzed in Fiji as follows: The astrocyte-like glia signal was filtered using the 3D Gaussian blur filter function with a Kernel size of 4x4x4. Subsequently, the displayed greyscale image was transformed into a 16-color heat map (using the lookup table function) and analyzed. B.2 Previously defined brain regions (Insect Brain Name Working Group, unpublished data) were identified using the annotated mask kindly provided by Arnim Jenett, JFRC. B.1- 2 Matching between the brain region (identified in the annotation channel, B.2) and astrocyte-like glia processes density (A.1, B.1) was performed manually region by region and revealed the astrocyte-like glia densities per brain region shown in Table 2 in the main text. Scale bar = 50um in all images.

10 Summary of figures and tables

10.1 Figures

<i>Figure 1: Anatomy of the central nervous system (CNS) of adult Drosophila.</i>	16
<i>Figure 2: Binary transcription systems in Drosophila.</i>	18
<i>Figure 3: Schematic illustration of the heat-shock FlpOut-System.</i>	20
<i>Figure 4: Single and multicolor stochastic labelings of cells within a tissue of interest.</i>	23
<i>Figure 5: Development and proliferation of the different generic glial subtypes.</i>	29
<i>Figure 6: Glial populations found in the embryonic ventral nerve chord.</i>	30
<i>Figure 7: Schematic illustration of the anatomy of the optic lobes of adult Drosophila.</i>	34
<i>Figure 8: Glia in the Janelia Farm Gal4 collection.</i>	44
<i>Figure 9: Classification of glial Gal4 drivers into generic subtypes.</i>	45
<i>Figure 10: Triage of glial driver lines and classification of A-listed drivers into generic subtypes.</i>	47
<i>Figure 11: Anatomy of the Drosophila central nervous system and generic glial cell types</i>	49
<i>Figure 12: Illustration of the different region-specific expression pattern within each generic subclass.</i>	51
<i>Figure 13: Morphology of perineurial glia.</i>	63
<i>Figure 14: Morphology of subperineurial glia.</i>	65
<i>Figure 15: Morphology of cortex glia.</i>	67
<i>Figure 16: Morphology of astrocyte-like glia.</i>	70
<i>Figure 17: Morphology of ensheathing glia.</i>	75
<i>Figure 18: Characterization of glia-glia interactions.</i>	77
<i>Figure 19: Equivalency of Lamina-specific glial subtypes with generic glial subtypes.</i>	86
<i>Figure 20: Glial cell morphologies in the Lamina and interactions with neurons.</i>	88
<i>Figure 21: Glial cell morphologies in the Medulla and interactions with neurons.</i>	93
<i>Figure 22: The glia of the outer and inner chiasm.</i>	97
<i>Figure 23: Glial cell morphologies in the Lobula complex.</i>	100
<i>Figure 24: Characterization of the generic glia and glia-neuron interactions in the antennal lobe.</i>	106
<i>Figure 25: Characterization of the generic glia in the mushroom body.</i>	108
<i>Figure 26: characterization of glia-neuron interactions in the olfactory system.</i>	111
<i>Figure 27: Schematic of an adult-specific, glial subtype-specific RNAi screen.</i>	124
<i>Figure 28: Effect of the knock down of positive and negative control gene function.</i>	127
<i>Figure 29: Effect of the knock down of functions involved in different mechanisms of CNS homeostasis.</i>	130
<i>Figure 30: Automated counting of immune-histochemically labeled glial cell bodies.</i>	146
<i>Figure 31: Automated analysis of the astrocyte-like glia-processes density.</i>	148
<i>Figure 32: Annotation of astrocyte-like glia processes in different brain regions.</i>	150

10.2 Tables

<i>Table 1: Summary of generic reference lines and potential alternative drivers.</i>	50
<i>Table 2: Summary of drivers with region-specific expression pattern per generic subtype.</i>	52
<i>Table 3: Generic glial counts.</i>	60
<i>Table 4: Summary of astrocyte-like glia densities in the brain.</i>	72
<i>Table 5: Summary of Lamina-specific driver lines, cell counts per subtype and description of drivers.</i>	82
<i>Table 6: Summary of Medulla-specific driver lines, their cell counts and description of the drivers.</i>	91
<i>Table 7: Summary of chiasm-specific drivers, their cell counts and driver description.</i>	95
<i>Table 8: RNAi lines according to category.</i>	126
<i>Table 9: Summary of drivers used in this thesis.</i>	140
<i>Table 10: Summary of reporters used in this thesis.</i>	141
<i>Table 11: Summary of antibodies used in this thesis.</i>	144

10.3 Supplemental Figures

<i>Supplemental figure 1: Onset of expression of major generic glial drivers.</i>	156
<i>Supplemental figure 2: Generic glial subtype expression pattern in the larvae.</i>	159
<i>Supplemental figure 3: Heat shock conditions for adult-specific Gal4 FlpOuts.</i>	161

11 Abbreviations

CNS	– Central nervous system
GMC	– Ganglion mother cell
JFRC	– Janelia Farm Research Campus
PNG	– Perineurial glia
SPG	– Subperineurial glia
CG	– Cortex glia
ALG	– Astrocyte-like glia
EG	– Ensheathing glia
EGN	– Neuropile-ensheathing glia
EGT	– Tract-ensheathing glia
FACS	– Fluorescent activated cell sorting
EAAT	– Excitatory amino acid transporter
ACE	– Acetylcholine esterase
ROS	– Reactive oxygen species
VNC	– Ventral nerve chord
CB	– Central brain
RNAi	– RNA interference
GFP	– Green fluorescent protein
UAS	– Upstream activating sequence
JFRC	– Janelia Farm Research Center
TARGET	– Temporal and regional gene expression targeting
dsRNA	– double stranded RNA
mRNA	– messenger RNA
VDRC	– Vienna <i>Drosophila</i> Research Center
DRSC	– <i>Drosophila</i> RNAi Screening Center
HS	– Heat shock
GCM	– Glial cell missing
REPO	– Reverse polarity
TTK	– Tramtrack
Cbg	– Cell body glia
OL	– Optic lobe
GPC	– Glial precursor cell
Tm	– TransMedulla neurons
TmY	– TransMedulla Y neurons
VPN	– Visual projection neuron
OR	– Olfactory receptor
ORN	– Olfactory receptor neurons
AL	– Antennal lobe
PN	– Projection neuron
LN	– Local interneuron
MB	– Mushroom body
LH	– Lateral horn
ACT	– Antenno-cerebral tract
KC	– Kenyon cell

12 Supplemental material

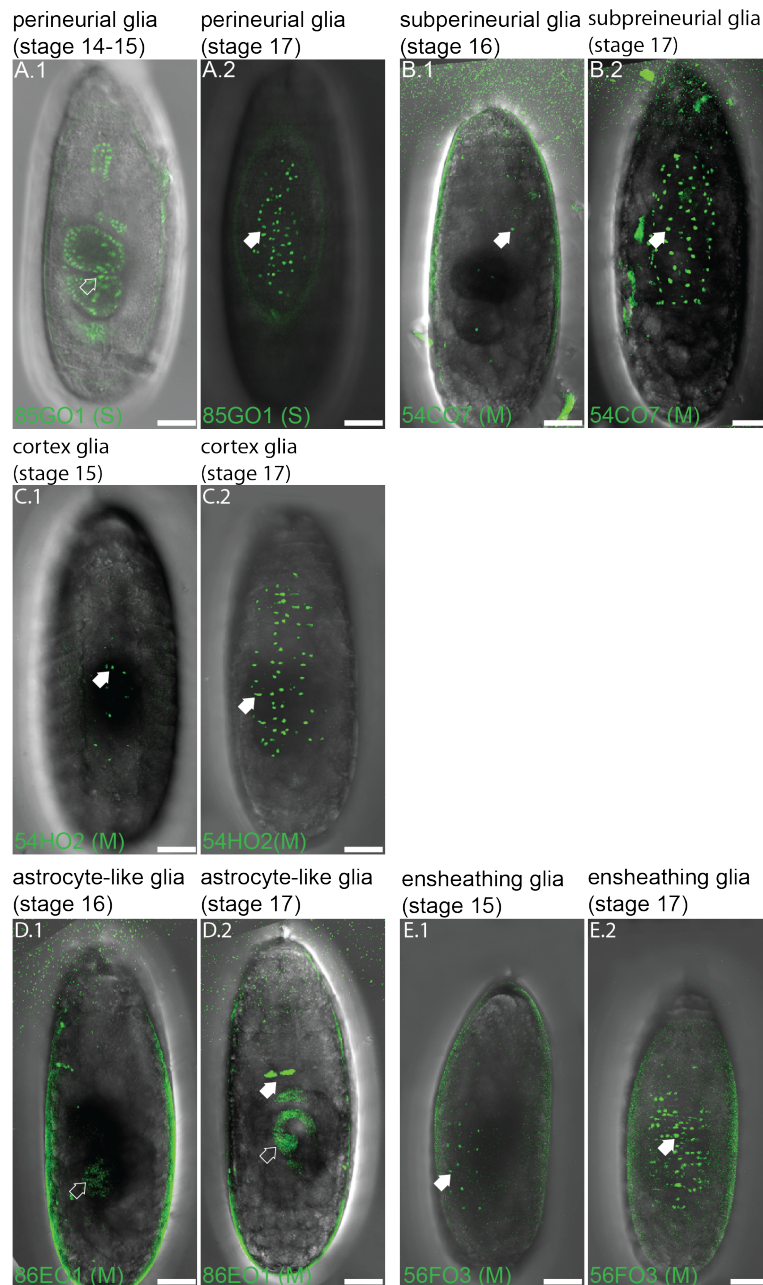
12.1 Expression pattern characteristics of generic glial drivers during development

12.1.1 Onset and glial identity of Gal4 'Reference' driver expression

The onset of expression is an important feature of Gal4 driver lines that requires consideration in most functional experiments. For this reason, together with an undergraduate student in the lab, Florian Simon, and a postdoc, Sara Batelli, we imaged all generic Gal4 driver lines driving a nuclearly-expressed GFP at different embryonic stages (Supplemental figure 1). Our goal was two-fold: We sought to first determine the onset of expression of the five generic driver lines we identified within the Janelia Farm Gal4 collection and second to investigate if they correspond to the glial populations which had been previously characterized in the embryo and larvae (Ito et al., 1995). To this end, we employed all five generic glial drivers to drive expression of either a nuclearly expressed GFP for onset of expression (Supplemental figure 1), to count cells (data not shown) or a membrane-tagged GFP to visualize the morphology of subpopulations (larvae: Supplemental figure 2).

In Supplemental figure 1, the onset of expression of the five different generic glial driver lines is shown. The earlier time point presents the onset of expression (Supplemental figure 1A-E.1) whereas the second time point (Supplemental figure 1A-E.2) represents the stage in which there is broad expression in *most* cells of one subtype. Our experiments revealed the following: The expression of the perineurial glia driver (*85CO1*) is first observed in early stage 16 embryos (Supplemental figure 1A.1) and augment up to stage 17 (Supplemental figure 1A.2). Additionally, co-expression in the gut region is observed. The expression of the subperineurial glia driver (*54CO7*) is first observed in stage 16 embryos (Supplemental figure 1B.1) and augments until stage 17 (Supplemental figure 1B.2). The expression of the cortex glia GAL4 driver (*54HO2*) is first observed in

the middle of stage 15 (Supplemental figure 1C.1) and augments up to stage 17 (Supplemental figure 1C2).



Supplemental figure 1: Onset of expression of major generic glial drivers.

Onset of the five different glia drivers determined by UAS-nuclear-GFP expression; the embryos are shown as single slices (S) and maximum density projections (M). Five embryos per genotype were imaged; **A.1** Intermediate stage 16 embryo with expression near the gut under the control of 85GO1; **A.2** Late stage 17 embryo under the control of 85GO1 with an increased expression compared to the earlier stage (data for expression around the gut not shown); **B.1** Intermediate stage 16 embryo with low expression under the

control of 54CO7; **B.2** Intermediate stage 17 embryo under the control of 54CO7 with an increased expression compared to the earlier stage; **C.1** Stage 15 embryo under the control of 54HO2; **C.2** Early stage 17 embryo under the control of 54HO2 with an increased expression compared to the earlier stage; **D.1** Intermediate stage 16 embryo under the control of 86EO1; **D.2** Intermediate stage 17 embryo with an increased expression compared to the earlier stage; **E.1** Late stage 15 embryo under the control of 56FO3; **E.2** Late stage 17 embryo with an increased expression compared to the earlier stage. Scale bar = 50 μ m. Images were kindly provided by Florian Simon and modified.

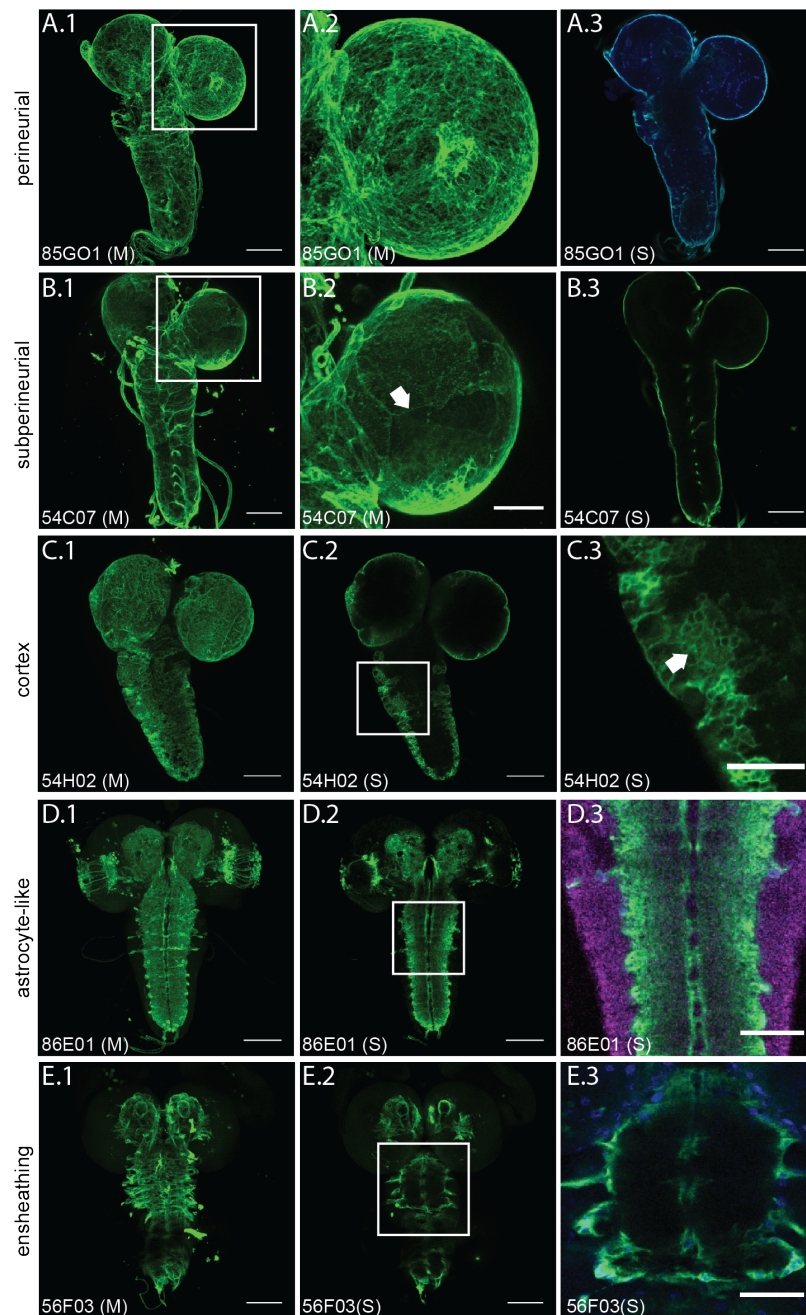
Additionally, a few cells are labeled around the gut region. The expression of the astrocyte-like glia driver (*86EO1*) is first observed in the middle of stage 17 (Supplemental figure 1D.2). However, we are not sure if the expression we observe is indeed glia (Supplemental figure 1D.2, filled arrow). Additionally, a few cells are been labeled around the gut (Supplemental figure 1D.1- 2, unfilled arrow). The expression of the ensheathing glia driver (*56FO3*) is first observed in the middle of stage 15 (Supplemental figure 1E.1) and augments up to stage 17 (Supplemental figure 1E.2).

We thus conclude that none of the drivers express in glia in embryonic stages earlier than 15. All driver lines start expression by stage 17 of embryonic development, with cortex and ensheathing glia expression been observed first followed by surface glia and (early larval stage) astrocyte-like glia expression.

12.1.2 Characterization of generic driver expression in third instar larvae

Having determined the expression pattern characteristics of the reference drivers in the embryo, we sought to confirm its subtype specific pattern also in third instar larvae. To this end, we used all five generic glial reference driver lines to drive expression of a membrane-tagged GFP and determined their expression pattern (Supplemental figure 2).

The perineurial (Supplemental figure 2A.1-3) and subperineurial glia (Supplemental figure 2B.1- 3) form a continuous layer around the nervous system. While the shape of single perineurial glia cells cannot be easily determined, subperineurial glia already show the square-shaped morphologies observed later in the adult CNS (compare to Figure 14). Cortex glia form a thick meshwork in the cortex region (Supplemental figure 2C.1- 2). The magnification of a single section reveals the fine mesh-like processes between neuronal cell bodies (Supplemental figure 2C.3). Astrocyte-like glia are located in the ventral nerve cord and in the medial portion of the two hemispheres (Supplemental figure 2D.1- 2). Ensheathing glia are found along the cortex-neuropile boundary (Supplemental figure 2E.1). In contrast to the ensheathing glia in the adult CNS (compared to Figure 17), they do not enter the neuropile regions themselves, however, they do ensheath (and presumably separate) single neuropile regions from one another (Supplemental figure 2E.1- 3).



Supplemental figure 2: Generic glial subtype expression pattern in the larvae.

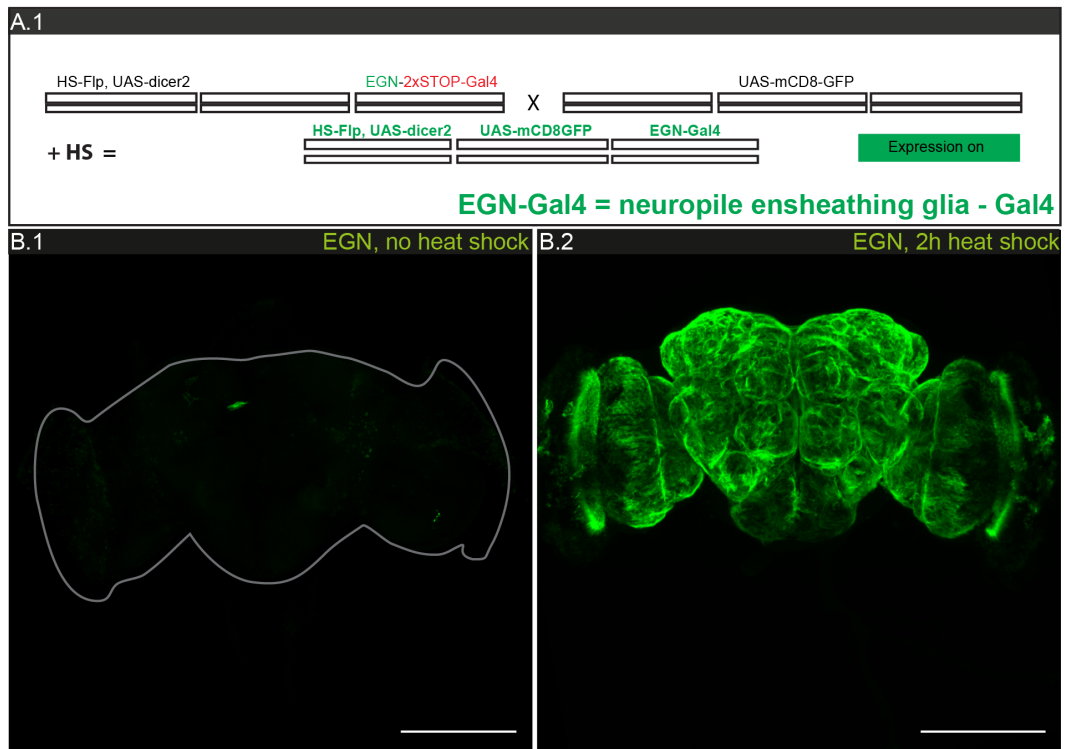
To determine the expression pattern of the different generic glial subtypes in the larvae, generic driver lines were employed to drive the expression of a membrane tagged GFP in all cells of a given subtype. **A** Perineurial glia. **B** Subperineurial glia. **C** Cortex glia. **D** Astrocyte-like glia. **E** Ensheathing glia. **A.1** Perineurial glia (85G01-Gal4; UAS-myr-smGFP-HA) enclose the entire CNS and PNS (frontal view; maximum density projection, $97 \times 1 \mu\text{m}$ sections). **A.2** Magnification of the boxed region in **A.1**. No obvious single cell shape can be observed, the cells rather form a continuous surface mesh. **A.3** Perineurial glia (85G01-Gal4; UAS-myr-smGFP-HA) enclose the entire CNS and PNS (frontal view; single section). The perineurial glia are exclusively

located around the CNS. **B.1** Subperineurial glia (54C07-Gal4; UAS-myr-smGFP-HA) enclose the entire CNS and PNS (frontal view; maximum density projection, 97x1µm sections). **B.2** Magnification of the boxed region in **B.1**. The arrow indicated the boundaries of a single cell. The cells have a square-like shape. **B.3** Subperineurial glia (54C07-Gal4; UAS-myr-smGFP-HA) enclose the entire CNS and PNS (frontal view; single section). The subperineurial glia are located around the CNS, occasionally, subperineurial glia (presumably remainders of the embryonic channel glia) are found along the central axis of the ventral nerve chord but not in the brain hemispheres. **C.1** Cortex glia (54H02-Gal4; UAS-myr-smGFP-HA) are located in the cortex regions of the entire CNS (frontal view; maximum density projection, 95x1µm sections). **C.2** The cortex glia populate the cortex region but not the neuropile region (frontal view, single section). **C.3** Magnification of the boxed region in **C.2**. The arrow indicates the characteristic mesh-like structure around the neuronal cell bodies. **D.1** Astrocyte-like glia (86E01-Gal4; UAS-myr-smGFP-HA) are located in the neuropile region of the entire CNS (frontal view; maximum density projection, 91x1µm sections). **D.2** Single section of **D.1**. **D.3** Magnification of the boxed region in **D.2**. Note the exclusive localization of the astrocyte-like glia to the neuropile (single section, neuronal cell bodies (cortex region) are labeled in magenta). **E.1** Ensheathing glia (56F03-Gal4; UAS-myr-smGFP-HA) are located along the neuropile-cortex border. In the brain, they delineate the boundaries of single neuropile regions, but in comparison to the adult ensheathing glia, they do not invade the neuropile regions quite as extensively (frontal view; maximum density projection, 87x1µm sections). **E.2** Single section of **E.1**. **E.3** Magnification of the boxed region in **E.2**. Note the exclusive localization of the ensheathing glia around the VNC and its peripheral nerves. Scale bar = 100µm in **A.1- 2, B.1, 3, C.1- 2, D.1- 2, E. 1- 2**; 50µm in **A.2, B.2, C.3, D.3, E.3**. Larval images were kindly provided by Florian Simon and modified.

12.1.3 Summary

All driver lines except for the astrocyte-like glia driver begin to express in the late (stage 15-17) embryo. The expression pattern found represent the glial subtype we expected to find based on the annotation in the adult. However, in the perineurial as well as the astrocyte-like glia driver line, we found co-expression in other tissue than glial cells. For all five driver lines, after the onset of expression, we observed continuous developmental and adult expression only in this particular single glial subtype indicating a consistent glial subtype-identity throughout development.

12.2 Optimization of heat shock conditions for adult specific FlpOuts



Supplemental figure 3: Heat shock conditions for adult-specific Gal4 FlpOuts.

A.1 Illustration of the fly genetics to investigate the length of required heat shock for adult-specific FlpOuts in all glial cells of one subtype. Flies carrying a heat-shock inducible flippase and flippable versions of neuropile ensheathing glia (EGN) were crossed with UAS-mCD8-GFP flies to label the cell membranes. **B.1-2** Different heat shock times were tested to evaluate the optimal time required to initiate Gal4 activation in *all* cells. **B.1** Without heat shock, almost no expression is observed. **B.2** Upon 2h of heat shock, expression is activated in almost all neuropile ensheathing glia (EGN).

13 Literature

- Abramoff, M.D., Magalhaes, P.J., Ram, S.J. (2004). Image Processing with ImageJ. *Biophotonics International* 11, 36-42.
- Alfonso, T.B., and Jones, B.W. (2002). gcm2 promotes glial cell differentiation and is required with glial cells missing for macrophage development in *Drosophila*. *Developmental biology* 248, 369-383.
- Allen, N.J., and Barres, B.A. (2009). Glia and Synapse Formation: An Overview. In *Encyclopedia of Neuroscience*, R.S. Editor-in-Chief: Larry, ed. (Oxford: Academic Press), pp. 731-736.
- Anderson, C.M., and Swanson, R.A. (2000). Astrocyte glutamate transport: review of properties, regulation, and physiological functions. *Glia* 32, 1-14.
- Araque, A., Carmignoto, G., and Haydon, P.G. (2001). Dynamic signaling between astrocytes and neurons. *Annual review of physiology* 63, 795-813.
- Aso, Y., Grubel, K., Busch, S., Friedrich, A.B., Siwanowicz, I., and Tanimoto, H. (2009). The mushroom body of adult *Drosophila* characterized by GAL4 drivers. *Journal of neurogenetics* 23, 156-172.
- Aubert, A., Costalat, R., Magistretti, P.J., and Pellerin, L. (2005). Brain lactate kinetics: Modeling evidence for neuronal lactate uptake upon activation. *Proc Natl Acad Sci U S A* 102, 16448-16453.
- Auld, V.J., Fetter, R.D., Broadie, K., and Goodman, C.S. (1995). Gliotactin, a novel transmembrane protein on peripheral glia, is required to form the blood-nerve barrier in *Drosophila*. *Cell* 81, 757-767.
- Awasaki, T., Huang, Y., O'Connor, M.B., and Lee, T. (2011). Glia instruct developmental neuronal remodeling through TGF-beta signaling. *Nature neuroscience* 14, 821-823.
- Awasaki, T., Lai, S.L., Ito, K., and Lee, T. (2008). Organization and postembryonic development of glial cells in the adult central brain of *Drosophila*. *J Neurosci* 28, 13742-13753.
- Bak, L.K., Schousboe, A., Sonnewald, U., and Waagepetersen, H.S. (2006). Glucose is necessary to maintain neurotransmitter homeostasis during synaptic activity in cultured glutamatergic neurons. *Journal of cerebral blood flow and metabolism : official journal of the International Society of Cerebral Blood Flow and Metabolism* 26, 1285-1297.
- Bate, M., and Arias, A.M. (1993). *The development of Drosophila melanogaster*, Vol 1 (Cold Spring Harbor Laboratory Press).
- Bear, M.F., Connors, B.W., and Paradiso, M.A. (2006). *Neuroscience: Exploring the brain* (Lippincott Williams & Wilkins).
- Bello, B.C., Izergina, N., Caussinus, E., and Reichert, H. (2008). Amplification of neural stem cell proliferation by intermediate progenitor cells in *Drosophila* brain development. *Neural development* 3, 5.
- Bilen, J., and Bonini, N.M. (2005). *Drosophila* as a model for human neurodegenerative disease. *Annual review of genetics* 39, 153-171.
- Boone, J.Q., and Doe, C.Q. (2008). Identification of *Drosophila* type II neuroblast lineages containing transit amplifying ganglion mother cells. *Developmental neurobiology* 68, 1185-1195.
- Borst, A. (2009). *Drosophila's* view on insect vision. *Current biology : CB* 19, R36-47.
- Borst, A., Haag, J., and Reiff, D.F. (2010). Fly motion vision. *Annu Rev Neurosci* 33, 49-70.

- Borycz, J., Borycz, J.A., Loubani, M., and Meinertzhagen, I.A. (2002). tan and ebony genes regulate a novel pathway for transmitter metabolism at fly photoreceptor terminals. *J Neurosci* 22, 10549-10557.
- Braitenberg, V. (1970). [Order and orientation of elements in the visual system of the fly]. *Kybernetik* 7, 235-242.
- Brand, A.H., and Perrimon, N. (1993). Targeted gene expression as a means of altering cell fates and generating dominant phenotypes. *Development* 118, 401-415.
- Cahoy, J.D., Emery, B., Kaushal, A., Foo, L.C., Zamanian, J.L., Christopherson, K.S., Xing, Y., Lubischer, J.L., Krieg, P.A., and Krupenko, S.A. (2008). A transcriptome database for astrocytes, neurons, and oligodendrocytes: a new resource for understanding brain development and function. *The Journal of Neuroscience* 28, 264-278.
- Campbell, G., Goring, H., Lin, T., Spana, E., Andersson, S., Doe, C.Q., and Tomlinson, A. (1994). RK2, a glial-specific homeodomain protein required for embryonic nerve cord condensation and viability in *Drosophila*. *Development* 120, 2957-2966.
- Cantera, R., and Trujillo-Cenoz, O. (1996). Glial cells in insect ganglia. *Microscopy research and technique* 35, 285-293.
- Carlson, S.D., Juang, J.L., Hilgers, S.L., and Garment, M.B. (2000). Blood barriers of the insect. *Annual review of entomology* 45, 151-174.
- Chalfie, M., Tu, Y., Euskirchen, G., Ward, W.W., and Prasher, D.C. (1994). Green fluorescent protein as a marker for gene expression. *Science* 263, 802-805.
- Chotard, C., Leung, W., and Salecker, I. (2005). glial cells missing and gcm2 cell autonomously regulate both glial and neuronal development in the visual system of *Drosophila*. *Neuron* 48, 237-251.
- Chotard, C., and Salecker, I. (2007). Glial cell development and function in the *Drosophila* visual system. *Neuron glia biology* 3, 17-25.
- Clandinin, T.R., and Zipursky, S.L. (2002). Making connections in the fly visual system. *Neuron* 35, 827-841.
- Coleman, M.P., and Freeman, M.R. (2010). Wallerian Degeneration, WldS, and Nmnat. *Annual Review of Neuroscience* 33, 245-267.
- Colonques, J., Ceron, J., and Tejedor, F.J. (2007). Segregation of postembryonic neuronal and glial lineages inferred from a mosaic analysis of the *Drosophila* larval brain. *Mechanisms of development* 124, 327-340.
- Crittenden, J.R., Skoulakis, E.M., Han, K.A., Kalderon, D., and Davis, R.L. (1998). Tripartite mushroom body architecture revealed by antigenic markers. *Learning & memory* 5, 38-51.
- Dearborn, R., Jr., and Kunes, S. (2004). An axon scaffold induced by retinal axons directs glia to destinations in the *Drosophila* optic lobe. *Development* 131, 2291-2303.
- del Valle Rodriguez, A., Didiano, D., and Desplan, C. (2012). Power tools for gene expression and clonal analysis in *Drosophila*. *Nature methods* 9, 47-55.
- Diamond, M.C., Krech, D., and Rosenzweig, M.R. (1964). The effects of an enriched environment on the histology of the rat cerebral cortex. *The Journal of Comparative Neurology* 123, 111-119.
- Dietzl, G., Chen, D., Schnorrer, F., Su, K.-C., Barinova, Y., Fellner, M., Gasser, B., Kinsey, K., Oppel, S., Scheiblauer, S., et al. (2007). A genome-wide transgenic RNAi library for conditional gene inactivation in *Drosophila*. *Nature* 448, 151-156.
- Doherty, J., Logan, M.A., Tasdemir, O.E., and Freeman, M.R. (2009). Ensheathing glia function as phagocytes in the adult *Drosophila* brain. *J Neurosci* 29, 4768-4781.
- Dubnau, J., Grady, L., Kitamoto, T., and Tully, T. (2001). Disruption of neurotransmission in *Drosophila* mushroom body blocks retrieval but not acquisition of memory. *Nature* 411, 476-480.

- Edenfeld, G., Stork, T., and Klambt, C. (2005). Neuron-glia interaction in the insect nervous system. *Curr Opin Neurobiol* 15, 34-39.
- Edwards, J.S., Swales, L.S., and Bate, M. (1993). The differentiation between neuroglia and connective tissue sheath in insect ganglia revisited: the neural lamella and perineurial sheath cells are absent in a mesodermless mutant of *Drosophila*. *J Comp Neurol* 333, 301-308.
- Edwards, T.N., and Meinertzhagen, I.A. (2010). The functional organisation of glia in the adult brain of *Drosophila* and other insects. *Prog Neurobiol* 90, 471-497.
- Edwards, T.N., Nuschke, A.C., Nern, A., and Meinertzhagen, I.A. (2012). The organization and metamorphosis of glia in the *Drosophila* visual system. *J Comp Neurol*.
- Eroglu, C., and Barres, B.A. (2010). Regulation of synaptic connectivity by glia. *Nature* 468, 223-231.
- Fellner, L., Jellinger, K., Wenning, G., and Stefanova, N. (2011). Glial dysfunction in the pathogenesis of α -synucleinopathies: emerging concepts. *Acta Neuropathol* 121, 675-693.
- Fiala, A. (2007). Olfaction and olfactory learning in *Drosophila*: recent progress. *Curr Opin Neurobiol* 17, 720-726.
- Fields, R.D. (2009). The other brain.
- Fields, R.D., and Stevens-Graham, B. (2002). New Insights into Neuron-Glia Communication. *Science* 298, 556-562.
- Fire, A., Xu, S., Montgomery, M.K., Kostas, S.A., Driver, S.E., and Mello, C.C. (1998). Potent and specific genetic interference by double-stranded RNA in *Caenorhabditis elegans*. *Nature* 391, 806-811.
- Fischbach, K.-F.D., A.P.M. (1989). The optic lobe of *Drosophila melanogaster*. I. A Golgi analysis of wild-type structure. *Cell Tissue Res*, 441-475.
- Fischbach, K.F., and Hiesinger, P.R. (2008). Optic lobe development. *Advances in experimental medicine and biology* 628, 115-136.
- Fischer, J.A., Giniger, E., Maniatis, T., and Ptashne, M. (1988). GAL4 activates transcription in *Drosophila*. *Nature* 332, 853-856.
- Freeman, M.R., and Doherty, J. (2006). Glial cell biology in *Drosophila* and vertebrates. *Trends Neurosci* 29, 82-90.
- Gao, Q., Yuan, B., and Chess, A. (2000). Convergent projections of *Drosophila* olfactory neurons to specific glomeruli in the antennal lobe. *Nature neuroscience* 3, 780-785.
- Gao, S., Takemura, S.Y., Ting, C.Y., Huang, S., Lu, Z., Luan, H., Rister, J., Thum, A.S., Yang, M., Hong, S.T., *et al.* (2008). The neural substrate of spectral preference in *Drosophila*. *Neuron* 60, 328-342.
- Golic, K.G., and Lindquist, S. (1989). The FLP recombinase of yeast catalyzes site-specific recombination in the *drosophila* genome. *Cell* 59, 499-509.
- Grandérath, S., and Klambt, C. (1999). Glia development in the embryonic CNS of *Drosophila*. *Curr Opin Neurobiol* 9, 531-536.
- Hadjieconomou, D., Rotkopf, S., Alexandre, C., Bell, D.M., Dickson, B.J., and Salecker, I. (2011). Flybow: genetic multicolor cell labeling for neural circuit analysis in *Drosophila melanogaster*. *Nature methods* 8, 260-266.
- Hahnlein, I., and Bicker, G. (1996). Morphology of neuroglia in the antennal lobes and mushroom bodies of the brain of the honeybee. *J Comp Neurol* 367, 235-245.
- Hallem, E.A., and Carlson, J.R. (2004a). The odor coding system of *Drosophila*. *Trends in genetics* : TIG 20, 453-459.
- Hallem, E.A., and Carlson, J.R. (2004b). The spatial code for odors is changed by conditioning. *Neuron* 42, 359-361.

- Hallem, E.A., Ho, M.G., and Carlson, J.R. (2004). The molecular basis of odor coding in the *Drosophila* antenna. *Cell* 117, 965-979.
- Halter, D.A., Urban, J., Rickert, C., Ner, S.S., Ito, K., Travers, A.A., and Technau, G.M. (1995). The homeobox gene *repo* is required for the differentiation and maintenance of glia function in the embryonic nervous system of *Drosophila melanogaster*. *Development* 121, 317-332.
- Han, D.D., Stein, D., and Stevens, L.M. (2000). Investigating the function of follicular subpopulations during *Drosophila* oogenesis through hormone-dependent enhancer-targeted cell ablation. *Development* 127, 573-583.
- Hardin, P.E. (2005). The circadian timekeeping system of *Drosophila*. *Current biology : CB* 15, R714-722.
- Hartenstein, V. (2011). Morphological diversity and development of glia in *Drosophila*. *Glia* 59, 1237-1252.
- Hatten, M.E. (1999). CENTRAL NERVOUS SYSTEM NEURONAL MIGRATION. *Annual Review of Neuroscience* 22, 511-539.
- Hausen, K., Wolburg-Buchholz, W., and Ribi, W.A. (1980). The synaptic organization of visual interneurons in the lobula complex of flies. A light and electron microscopical study using silver-intensified cobalt-impregnations. *Cell Tissue Res* 208, 371-387.
- Hofbauer, A., Campos-Ortega, JA (1990). Proliferation pattern and early differentiation of the optic lobes in *Drosophila melanogaster*. *Roux Arch Dev Biol* 198, 264-274.
- Hosoya, T., Takizawa, K., Nitta, K., and Hotta, Y. (1995). Glial cells missing: A binary switch between neuronal and glial determination in *drosophila*. *Cell* 82, 1025-1036.
- Hoyle, G. (1986). Glial cells of an insect ganglion. *J Comp Neurol* 246, 85-103.
- Ito, K., Awano, W., Suzuki, K., Hiromi, Y., and Yamamoto, D. (1997). The *Drosophila* mushroom body is a quadruple structure of clonal units each of which contains a virtually identical set of neurones and glial cells. *Development* 124, 761-771.
- Ito, K., Suzuki, K., Estes, P., Ramaswami, M., Yamamoto, D., and Strausfeld, N.J. (1998). The organization of extrinsic neurons and their implications in the functional roles of the mushroom bodies in *Drosophila melanogaster* Meigen. *Learning & memory* 5, 52-77.
- Ito, K., Urban, J., and Technau, G. (1995). Distribution, classification, and development of *Drosophila* glial cells in the late embryonic and early larval ventral nerve cord. *Development Genes and Evolution* 204, 284-307.
- Izergina, N., Balmer, J., Bello, B., and Reichert, H. (2009). Postembryonic development of transit amplifying neuroblast lineages in the *Drosophila* brain. *Neural development* 4, 44.
- Jackson, F.R. (2011). Glial cell modulation of circadian rhythms. *Glia* 59, 1341-1350.
- Jacobs, J.R. (2000). The Midline Glia of *Drosophila*: a molecular genetic model for the developmental functions of Glia. *Progress in neurobiology* 62, 475-508.
- Jefferis, G.S., Potter, C.J., Chan, A.M., Marin, E.C., Rohlfsing, T., Maurer, C.R., Jr., and Luo, L. (2007). Comprehensive maps of *Drosophila* higher olfactory centers: spatially segregated fruit and pheromone representation. *Cell* 128, 1187-1203.
- Jenett, A., Rubin, G.M., Ngo, T.T., Shepherd, D., Murphy, C., Dionne, H., Pfeiffer, B.D., Cavallaro, A., Hall, D., Jeter, J., et al. (2012). A GAL4-Driver Line Resource for *Drosophila* Neurobiology. *Cell reports* 2, 991-1001.
- Joesch, M., Schnell, B., Raghu, S.V., Reiff, D.F., and Borst, A. (2010). ON and OFF pathways in *Drosophila* motion vision. *Nature* 468, 300-304.
- Jones, B.W., Fetter, R.D., Tear, G., and Goodman, C.S. (1995). glial cells missing: a genetic switch that controls glial versus neuronal fate. *Cell* 82, 1013-1023.

- Kammerer, M., and Giangrande, A. (2001). Glide2, a second glial promoting factor in *Drosophila melanogaster*. *The EMBO journal* 20, 4664-4673.
- Kandel, E.R., Schwartz, J.H., and Jessell, T.M. (2000). Principles of neural science, Vol 4 (McGraw-Hill New York).
- Karadottir, R., and Attwell, D. (2007). Neurotransmitter receptors in the life and death of oligodendrocytes. *Neuroscience* 145, 1426-1438.
- Kastritsis, C.H., and McCarthy, K.D. (1993). Oligodendroglial lineage cells express neuroligand receptors. *Glia* 8, 106-113.
- Kettenmann, H. (1999). Physiology of glial cells.
- Klambt, C., and Goodman, C.S. (1991). The diversity and pattern of glia during axon pathway formation in the *Drosophila* embryo. *Glia* 4, 205-213.
- Klambt, C., Hummel, T., Menne, T., Sadlowski, E., Scholz, H., and Stollewerk, A. (1996). Development and function of embryonic central nervous system glial cells in *Drosophila*. *Developmental genetics* 18, 40-49.
- Ko, H.W., Jiang, J., and Edery, I. (2002). Role for Slimb in the degradation of *Drosophila* Period protein phosphorylated by Doubletime. *Nature* 420, 673-678.
- Krashes, M.J., Keene, A.C., Leung, B., Armstrong, J.D., and Waddell, S. (2007). Sequential use of mushroom body neuron subsets during *drosophila* odor memory processing. *Neuron* 53, 103-115.
- Kurant, E., Axelrod, S., Leaman, D., and Gaul, U. (2008). Six-microns-under acts upstream of Draper in the glial phagocytosis of apoptotic neurons. *Cell* 133, 498-509.
- Lai, S.L., and Lee, T. (2006). Genetic mosaic with dual binary transcriptional systems in *Drosophila*. *Nature neuroscience* 9, 703-709.
- Laisue, P.P., Reiter, C., Hiesinger, P.R., Halter, S., Fischbach, K.F., and Stocker, R.F. (1999). Three-dimensional reconstruction of the antennal lobe in *Drosophila melanogaster*. *J Comp Neurol* 405, 543-552.
- Leiss, F., Groh, C., Butcher, N.J., Meinertzhagen, I.A., and Tavosanis, G. (2009). Synaptic organization in the adult *Drosophila* mushroom body calyx. *J Comp Neurol* 517, 808-824.
- MacDonald, J.M., Beach, M.G., Porpiglia, E., Sheehan, A.E., Watts, R.J., and Freeman, M.R. (2006). The *Drosophila* cell corpse engulfment receptor Draper mediates glial clearance of severed axons. *Neuron* 50, 869-881.
- McGuire, S.E., Le, P.T., and Davis, R.L. (2001). The role of *Drosophila* mushroom body signaling in olfactory memory. *Science* 293, 1330-1333.
- McGuire, S.E., Le, P.T., Osborn, A.J., Matsumoto, K., and Davis, R.L. (2003). Spatiotemporal rescue of memory dysfunction in *Drosophila*. *Science* 302, 1765-1768.
- Meinertzhagen, I.A.a.H., T.E. (1993). The development of the optic lobe. In *The Development of Drosophila melanogaster*, M.a.M.-A. Bate, A., ed. (Cold Spring Harbor: Cold Spring Harbor Press), pp. 1363-1491.
- Melom, J.E., and Littleton, J.T. (2013). Mutation of a NCKX eliminates glial microdomain calcium oscillations and enhances seizure susceptibility. *J Neurosci* 33, 1169-1178.
- Morante, J., and Desplan, C. (2008). The color-vision circuit in the medulla of *Drosophila*. *Current biology : CB* 18, 553-565.
- Newman, E.A. (2003). New roles for astrocytes: regulation of synaptic transmission. *Trends Neurosci* 26, 536-542.
- Ng, F.S., Tangredi, M.M., and Jackson, F.R. (2011). Glial cells physiologically modulate clock neurons and circadian behavior in a calcium-dependent manner. *Current biology : CB* 21, 625-634.

- Ni, J.-Q., Liu, L.-P., Binari, R., Hardy, R., Shim, H.-S., Cavallaro, A., Booker, M., Pfeiffer, B.D., Markstein, M., Wang, H., *et al.* (2009). A *Drosophila* Resource of Transgenic RNAi Lines for Neurogenetics. *Genetics* 182, 1089-1100.
- Ni, J.-Q., Markstein, M., Binari, R., Pfeiffer, B., Liu, L.-P., Villalta, C., Booker, M., Perkins, L., and Perrimon, N. (2008). Vector and parameters for targeted transgenic RNA interference in *Drosophila melanogaster*. *Nat Meth* 5, 49-51.
- O'Kane, C.J., and Gehring, W.J. (1987). Detection in situ of genomic regulatory elements in *Drosophila*. *Proc Natl Acad Sci U S A* 84, 9123-9127.
- Oland, L.A., Biebelhausen, J.P., and Tolbert, L.P. (2008). Glial investment of the adult and developing antennal lobe of *Drosophila*. *J Comp Neurol* 509, 526-550.
- Oland, L.A., and Tolbert, L.P. (1989). Patterns of glial proliferation during formation of olfactory glomeruli in an insect. *Glia* 2, 10-24.
- Ormo, M., Cubitt, A.B., Kallio, K., Gross, L.A., Tsien, R.Y., and Remington, S.J. (1996). Crystal structure of the *Aequorea victoria* green fluorescent protein. *Science* 273, 1392-1395.
- Osterwalder, T., Yoon, K.S., White, B.H., and Keshishian, H. (2001). A conditional tissue-specific transgene expression system using inducible GAL4. *Proc Natl Acad Sci U S A* 98, 12596-12601.
- Otsuna, H., and Ito, K. (2006). Systematic analysis of the visual projection neurons of *Drosophila melanogaster*. I. Lobula-specific pathways. *J Comp Neurol* 497, 928-958.
- Pascual, A., and Preat, T. (2001). Localization of long-term memory within the *Drosophila* mushroom body. *Science* 294, 1115-1117.
- Pellerin, L., Bouzier-Sore, A.K., Aubert, A., Serres, S., Merle, M., Costalat, R., and Magistretti, P.J. (2007). Activity-dependent regulation of energy metabolism by astrocytes: an update. *Glia* 55, 1251-1262.
- Pellerin, L., and Magistretti, P.J. (1994). Glutamate uptake into astrocytes stimulates aerobic glycolysis: a mechanism coupling neuronal activity to glucose utilization. *Proc Natl Acad Sci U S A* 91, 10625-10629.
- Pereanu, W., Shy, D., and Hartenstein, V. (2005). Morphogenesis and proliferation of the larval brain glia in *Drosophila*. *Developmental biology* 283, 191-203.
- Pereanu, W., Spindler, S., Cruz, L., and Hartenstein, V. (2007). Tracheal development in the *Drosophila* brain is constrained by glial cells. *Developmental biology* 302, 169-180.
- Pfeiffer, B.D., Jenett, A., Hammonds, A.S., Ngo, T.T., Misra, S., Murphy, C., Scully, A., Carlson, J.W., Wan, K.H., Laverty, T.R., *et al.* (2008). Tools for neuroanatomy and neurogenetics in *Drosophila*. *Proc Natl Acad Sci U S A* 105, 9715-9720.
- Pfeiffer, B.D., Ngo, T.T., Hibbard, K.L., Murphy, C., Jenett, A., Truman, J.W., and Rubin, G.M. (2010). Refinement of tools for targeted gene expression in *Drosophila*. *Genetics* 186, 735-755.
- Pfrieger, F.W. (2010). Role of glial cells in the formation and maintenance of synapses. *Brain Research Reviews* 63, 39-46.
- Pfrieger, F.W., and Barres, B.A. (1995). What the fly's glia tell the fly's brain. *Cell* 83, 671.
- Poeck, B., Fischer, S., Gunning, D., Zipursky, S.L., and Salecker, I. (2001). Glial cells mediate target layer selection of retinal axons in the developing visual system of *Drosophila*. *Neuron* 29, 99-113.
- Potter, C.J., Tasic, B., Russler, E.V., Liang, L., and Luo, L. (2010). The Q system: a repressible binary system for transgene expression, lineage tracing, and mosaic analysis. *Cell* 141, 536-548.
- Ramon y Cajal, S. (1909). *Histologie du systeme nerveux de l'homme et des vertebres*. Maloine, Paris, 774-838.
- Rasband, W.S. (1997-2012). ImageJ (Bethesda, Maryland, USA: U. S. National Institutes of Health).

- Richardt, A., Kemme, T., Wagner, S., Schwarzer, D., Marahiel, M.A., and Hovemann, B.T. (2003). Ebony, a novel nonribosomal peptide synthetase for beta-alanine conjugation with biogenic amines in *Drosophila*. *The Journal of biological chemistry* 278, 41160-41166.
- Richardt, A., Rybak, J., Stortkuhl, K.F., Meinertzhagen, I.A., and Hovemann, B.T. (2002). Ebony protein in the *Drosophila* nervous system: optic neuropile expression in glial cells. *J Comp Neurol* 452, 93-102.
- Rival, T., Soustelle, L., Strambi, C., Besson, M.T., Iche, M., and Birman, S. (2004). Decreasing glutamate buffering capacity triggers oxidative stress and neuropil degeneration in the *Drosophila* brain. *Current biology : CB* 14, 599-605.
- Rizzuto, R., Brini, M., De Giorgi, F., Rossi, R., Heim, R., Tsien, R.Y., and Pozzan, T. (1996). Double labelling of subcellular structures with organelle-targeted GFP mutants in vivo. *Current biology : CB* 6, 183-188.
- Sánchez, D.S. (1935). Contribution a l'étude de l'origine et de l'évolution de certains types de neuroglie chez les insectes. *Trab Lab Rech Biol Univ Madrid* 30, 299-353.
- Sanes, J.R., and Zipursky, S.L. (2010). Design principles of insect and vertebrate visual systems. *Neuron* 66, 15-36.
- Schmid, A., Chiba, A., and Doe, C.Q. (1999). Clonal analysis of *Drosophila* embryonic neuroblasts: neural cell types, axon projections and muscle targets. *Development* 126, 4653-4689.
- Schmidt, H., Rickert, C., Bossing, T., Vef, O., Urban, J., and Technau, G.M. (1997). The embryonic central nervous system lineages of *Drosophila melanogaster*. II. Neuroblast lineages derived from the dorsal part of the neuroectoderm. *Developmental biology* 189, 186-204.
- Schrier, B.K., and Thompson, E.J. (1974). On the Role of Glial Cells in the Mammalian Nervous System: UPTAKE, EXCRETION, AND METABOLISM OF PUTATIVE NEUROTRANSMITTERS BY CULTURED GLIAL TUMOR CELLS. *Journal of Biological Chemistry* 249, 1769-1780.
- Schwabe, T., Bainton, R.J., Fetter, R.D., Heberlein, U., and Gaul, U. (2005). GPCR signaling is required for blood-brain barrier formation in *drosophila*. *Cell* 123, 133-144.
- Schwaerzel, M., Heisenberg, M., and Zars, T. (2002). Extinction antagonizes olfactory memory at the subcellular level. *Neuron* 35, 951-960.
- Scott, E.K., Raabe, T., and Luo, L. (2002). Structure of the vertical and horizontal system neurons of the lobula plate in *Drosophila*. *J Comp Neurol* 454, 470-481.
- Sen, A., Shetty, C., Jhaveri, D., and Rodrigues, V. (2005). Distinct types of glial cells populate the *Drosophila* antenna. *BMC developmental biology* 5, 25.
- Shaw, S.R., and Varney, L.P. (1999). Primitive, crustacean-like state of blood-brain barrier in the eye of the apterygote insect *Petrobius* (Archaeognatha) determined from uptake of fluorescent tracers. *Journal of neurobiology* 41, 452-470.
- Simpson, I.A., Carruthers, A., and Vannucci, S.J. (2007). Supply and demand in cerebral energy metabolism: the role of nutrient transporters. *Journal of cerebral blood flow and metabolism : official journal of the International Society of Cerebral Blood Flow and Metabolism* 27, 1766-1791.
- Sinakevitch, I., Grau, Y., Strausfeld, N.J., and Birman, S. (2010). Dynamics of glutamatergic signaling in the mushroom body of young adult *Drosophila*. *Neural development* 5, 10.
- Soustelle, L., and Giangrande, A. (2007). Novel gcm-dependent lineages in the postembryonic nervous system of *Drosophila melanogaster*. *Developmental dynamics : an official publication of the American Association of Anatomists* 236, 2101-2108.
- Spindler, S.R., and Hartenstein, V. (2010). The *Drosophila* neural lineages: a model system to study brain development and circuitry. *Dev Genes Evol* 220, 1-10.
- Stocker, R.F. (1994). The organization of the chemosensory system in *Drosophila melanogaster*: a review. *Cell Tissue Res* 275, 3-26.

- Stork, T., Engelen, D., Krudewig, A., Silies, M., Bainton, R.J., and Klambt, C. (2008). Organization and function of the blood-brain barrier in *Drosophila*. *J Neurosci* 28, 587-597.
- Strausfeld, N.J., Sinakevitch, I., and Vilinsky, I. (2003). The mushroom bodies of *Drosophila melanogaster*: an immunocytochemical and golgi study of Kenyon cell organization in the calyces and lobes. *Microscopy research and technique* 62, 151-169.
- Stys, P.K. (2011). The axo-myelinic synapse. *Trends Neurosci* 34, 393-400.
- Suh, J., and Jackson, F.R. (2007). *Drosophila* ebony activity is required in glia for the circadian regulation of locomotor activity. *Neuron* 55, 435-447.
- Szeligo, F., and Leblond, C.P. (1977). Response of the three main types of glial cells of cortex and corpus callosum in rats handled during suckling or exposed to enriched, control and impoverished environments following weaning. *The Journal of Comparative Neurology* 172, 247-263.
- Tanaka, N.K., Awasaki, T., Shimada, T., and Ito, K. (2004). Integration of chemosensory pathways in the *Drosophila* second-order olfactory centers. *Current biology : CB* 14, 449-457.
- Tanaka, N.K., Tanimoto, H., and Ito, K. (2008). Neuronal assemblies of the *Drosophila* mushroom body. *J Comp Neurol* 508, 711-755.
- Taylor, T.D., Robichaux, M.B., and Garrity, P.A. (2004). Compartmentalization of visual centers in the *Drosophila* brain requires Slit and Robo proteins. *Development* 131, 5935-5945.
- Ting, C.Y., and Lee, C.H. (2007). Visual circuit development in *Drosophila*. *Curr Opin Neurobiol* 17, 65-72.
- Tix, S., Eule, E., Fischbach, K.F., and Benzer, S. (1997). Glia in the chiasms and medulla of the *Drosophila melanogaster* optic lobes. *Cell Tissue Res* 289, 397-409.
- Tsien, R.Y. (1998). The green fluorescent protein. *Annual review of biochemistry* 67, 509-544.
- Turner, G.C., Bazhenov, M., and Laurent, G. (2008). Olfactory representations by *Drosophila* mushroom body neurons. *J Neurophysiol* 99, 734-746.
- Tuthill, J.C., Nern, A., Holtz, S.L., Rubin, G.M., and Reiser, M.B. (2013). Contributions of the 12 neuron classes in the fly lamina to motion vision. *Neuron* 79, 128-140.
- Udolph, G., Rath, P., and Chia, W. (2001). A requirement for Notch in the genesis of a subset of glial cells in the *Drosophila* embryonic central nervous system which arise through asymmetric divisions. *Development* 128, 1457-1466.
- Unhavaithaya, Y., and Orr-Weaver, T.L. (2012). Polyploidization of glia in neural development links tissue growth to blood-brain barrier integrity. *Genes & development* 26, 31-36.
- Varon, S.S., and Bunge, R.P. (1978). Trophic Mechanisms in the Peripheral Nervous System. *Annual Review of Neuroscience* 1, 327-361.
- Venken, K.J., Simpson, J.H., and Bellen, H.J. (2011). Genetic manipulation of genes and cells in the nervous system of the fruit fly. *Neuron* 72, 202-230.
- Vincent, S., Vonesch, J.L., and Giangrande, A. (1996). Glide directs glial fate commitment and cell fate switch between neurones and glia. *Development* 122, 131-139.
- Virchow, R. (1858). Cellular pathology. As based upon physiological and pathological histology. Lecture XVI--Atheromatous affection of arteries.
- Wagner, S., Heseding, C., Szlachta, K., True, J.R., Prinz, H., and Hovemann, B.T. (2007). *Drosophila* photoreceptors express cysteine peptidase tan. *J Comp Neurol* 500, 601-611.
- Winberg, M.L., Perez, S.E., and Steller, H. (1992). Generation and early differentiation of glial cells in the first optic ganglion of *Drosophila melanogaster*. *Development* 115, 903-911.
- Xiong, W., and Montell, C. (1993). tramtrack is a transcriptional repressor required for cell fate determination in the *Drosophila* eye. *Genes & development* 7, 1085-1096.

- Xiong, W.C., and Montell, C. (1995). Defective glia induce neuronal apoptosis in the repo visual system of *Drosophila*. *Neuron* *14*, 581-590.
- Yamaguchi, S., Wolf, R., Desplan, C., and Heisenberg, M. (2008). Motion vision is independent of color in *Drosophila*. *Proc Natl Acad Sci U S A* *105*, 4910-4915.
- Yao, Y., Wu, Y., Yin, C., Ozawa, R., Aigaki, T., Wouda, R.R., Noordermeer, J.N., Fradkin, L.G., and Hing, H. (2007). Antagonistic roles of Wnt5 and the Drl receptor in patterning the *Drosophila* antennal lobe. *Nature neuroscience* *10*, 1423-1432.
- Younossi-Hartenstein, A., Salvaterra, P.M., and Hartenstein, V. (2003). Early development of the *Drosophila* brain: IV. Larval neuropile compartments defined by glial septa. *J Comp Neurol* *455*, 435-450.
- Yu, D., Akalal, D.B., and Davis, R.L. (2006). *Drosophila* alpha/beta mushroom body neurons form a branch-specific, long-term cellular memory trace after spaced olfactory conditioning. *Neuron* *52*, 845-855.
- Zars, T., Fischer, M., Schulz, R., and Heisenberg, M. (2000). Localization of a short-term memory in *Drosophila*. *Science* *288*, 672-675.
- Zhu, B., Pennack, J.A., McQuilton, P., Forero, M.G., Mizuguchi, K., Sutcliffe, B., Gu, C.J., Fenton, J.C., and Hidalgo, A. (2008). *Drosophila* neurotrophins reveal a common mechanism for nervous system formation. *PLoS biology* *6*, e284.
- Ziegenfuss, J.S., Doherty, J., and Freeman, M.R. (2012). Distinct molecular pathways mediate glial activation and engulfment of axonal debris after axotomy. *Nature neuroscience* *15*, 979-987.
- Ziegler, A.B., Brusselbach, F., and Hovemann, B.T. (2012). Activity and co-expression of *Drosophila* Black with Ebony in fly optic lobes reveals putative cooperative tasks in vision that evade ERG detection. *J Comp Neurol*.

